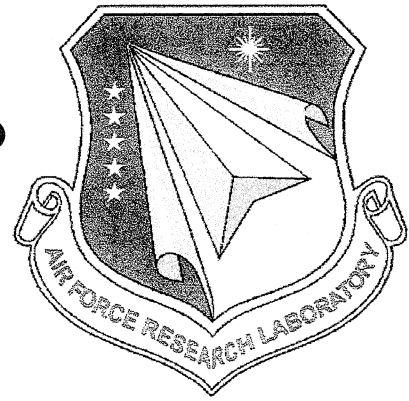


**AFRL-PR-WP-TR-2001-2083**

**COAL-BASED FUEL FORMULATION AND  
ENGINEERING**



**A. BOEHMAN  
P. HATCHER  
H. SCHOBERT  
C. SONG**

**Energy Institute and Department of Mechanical and Nuclear Engineering  
The Pennsylvania State University  
University Park, PA 16802-2320**

**FEBRUARY 2000**

**FINAL REPORT FOR PERIOD 01 NOVEMBER 1997 – 01 DECEMBER 1999**

**Approved for public release; distribution unlimited.**

**PROPULSION DIRECTORATE  
AIR FORCE RESEARCH LABORATORY  
AIR FORCE MATERIEL COMMAND  
WRIGHT-PATTERSON AIR FORCE BASE, OH 45433-7251**

Report Documentation Page		
<b>Report Date</b> 00012000	<b>Report Type</b> N/A	<b>Dates Covered (from... to)</b> -
<b>Title and Subtitle</b> Coal-Based Fuel Formulation and Engineering	<b>Contract Number</b>	
	<b>Grant Number</b>	
	<b>Program Element Number</b>	
<b>Author(s)</b>	<b>Project Number</b>	
	<b>Task Number</b>	
	<b>Work Unit Number</b>	
<b>Performing Organization Name(s) and Address(es)</b> Energy Institute and Department of Mechanical and Nuclear Engineering The Pennsylvania State University University Park, PA 16802-2320	<b>Performing Organization Report Number</b>	
<b>Sponsoring/Monitoring Agency Name(s) and Address(es)</b>	<b>Sponsor/Monitor's Acronym(s)</b>	
	<b>Sponsor/Monitor's Report Number(s)</b>	
<b>Distribution/Availability Statement</b> Approved for public release, distribution unlimited		
<b>Supplementary Notes</b>		
<b>Abstract</b>		
<b>Subject Terms</b>		
<b>Report Classification</b> unclassified	<b>Classification of this page</b> unclassified	
<b>Classification of Abstract</b> unclassified	<b>Limitation of Abstract</b> UU	
<b>Number of Pages</b> 126		

## NOTICE

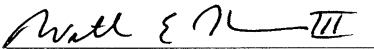
USING GOVERNMENT DRAWINGS, SPECIFICATIONS, OR OTHER DATA INCLUDED IN THIS DOCUMENT FOR ANY PURPOSE OTHER THAN GOVERNMENT PROCUREMENT DOES NOT IN ANY WAY OBLIGATE THE US GOVERNMENT. THE FACT THAT THE GOVERNMENT FORMULATED OR SUPPLIED THE DRAWINGS, SPECIFICATIONS, OR OTHER DATA DOES NOT LICENSE THE HOLDER OR ANY OTHER PERSON OR CORPORATION; OR CONVEY ANY RIGHTS OR PERMISSION TO MANUFACTURE, USE, OR SELL ANY PATENTED INVENTION THAT MAY RELATE TO THEM.

THIS REPORT IS RELEASABLE TO THE NATIONAL TECHNICAL INFORMATION SERVICE (NTIS). AT NTIS, IT WILL BE AVAILABLE TO THE GENERAL PUBLIC, INCLUDING FOREIGN NATIONS.

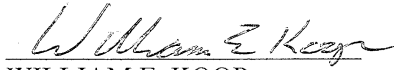
THIS TECHNICAL REPORT HAS BEEN REVIEWED AND IS APPROVED FOR PUBLICATION.



CYNTHIA OBRINGER  
Fuels Branch  
Turbine Engine Division  
Propulsion Directorate



WILLIAM E. HARRISON III  
Chief, Fuels Branch  
Turbine Engine Division  
Propulsion Directorate



WILLIAM E. KOOP  
Chief of Technology  
Turbine Engine Division  
Propulsion Directorate

IF YOUR ADDRESS HAS CHANGED, IF YOU WISH TO BE REMOVED FROM OUR MAILING LIST, OR IF THE ADDRESSEE IS NO LONGER EMPLOYED BY YOUR ORGANIZATION PLEASE NOTIFY AFRL/PRTG BLDG 490, 1790 LOOP ROAD N. WRIGHT-PATTERSON AFB, OH 45433-7103 TO HELP MAINTAIN A CURRENT MAILING LIST.

Do not return copies of this report unless contractual obligations or notice on a specific document requires its return.

REPORT DOCUMENTATION PAGE				Form Approved OMB No. 0704-0188	
<p>The public reporting burden for this collection of information is estimated to average 1 hour per response, including the time for reviewing instructions, searching existing data sources, gathering and maintaining the data needed, and completing and reviewing the collection of information. Send comments regarding this burden estimate or any other aspect of this collection of information, including suggestions for reducing the burden, to Department of Defense, Washington Headquarters Services, Directorate for Information Operations and Reports (0704-0188), 1215 Jefferson Davis Highway, Suite 1204, Arlington, VA 22202-4302. Respondents should be aware that notwithstanding any other provision of law, no person shall be subject to any penalty for failing to comply with a collection of information if it does not display a currently valid OMB control number.</p> <p><b>PLEASE DO NOT RETURN YOUR FORM TO THE ABOVE ADDRESS.</b></p>					
1. REPORT DATE (DD-MM-YYYY) February 2000		2. REPORT TYPE Final Report		3. DATES COVERED (From - To) 11/01/1997 – 12/01/1999	
4. TITLE AND SUBTITLE Coal-Based Fuel Formulation and Engineering			5a. CONTRACT NUMBER F33615-98-D-2802		
			5b. GRANT NUMBER		
			5c. PROGRAM ELEMENT NUMBER 62203F		
6. AUTHOR(S) A. Boehman, P. Hatcher, H. Schobert, C. Song			5d. PROJECT NUMBER 3048		
			5e. TASK NUMBER 05		
			5f. WORK UNIT NUMBER EX		
7. PERFORMING ORGANIZATION NAME(S) AND ADDRESS(ES) Energy Institute and Department of Mechanical and Nuclear Engineering The Pennsylvania State University University Park, PA 16802-2320				8. PERFORMING ORGANIZATION REPORT NUMBER D.O. 0003	
9. SPONSORING/MONITORING AGENCY NAME(S) AND ADDRESS(ES) Propulsion Directorate Air Force Research Laboratory Air Force Materiel Command Wright-Patterson AFB, OH 45433-7251 POC: Cynthia Obringer, AFRL/PRTG, 937-255-6390				10. SPONSOR/MONITOR'S ACRONYM(S) AFRL/PRTG	
				11. SPONSOR/MONITOR'S REPORT NUMBER(S) AFRL-PR-WP-TR-2001-2083	
12. DISTRIBUTION/AVAILABILITY STATEMENT Approved for Public Release, Distribution Unlimited.					
13. SUPPLEMENTARY NOTES					
14. ABSTRACT The potential coal based feedstocks that could produce or co-produce in a conventional petroleum refinery for use as blending stocks for the production of candidate JP-900 fuels were evaluated. The oxidative and pyrolytic stability of candidate coal based feedstocks were evaluated in both batch and flow reactors.					
15. SUBJECT TERMS Jet Fuel, Coal Derived Fuel, Thermal Stability, High Temperature Fuels, Pyrolytic Instability, Co-Coking, Coal Tar Blending					
16. SECURITY CLASSIFICATION OF:			17. LIMITATION OF ABSTRACT  SAR	18. NUMBER OF PAGES  122	19a. NAME OF RESPONSIBLE PERSON Cynthia Obringer
a. REPORT unclassified	b. ABSTRACT unclassified	c. THIS PAGE unclassified			19b. TELEPHONE NUMBER (Include area code) (937) 255-6390





## Table of Contents

1.0 BP SUBCONTRACT.....	1
2.0 HYDROGENATION CATALYSTS IN BATCH TESTS.....	2
2.1 Introduction.....	2
2.2 Experimental.....	3
2.3 Results .....	4
2.4 Conclusion .....	8
3.0 THERMAL STABILITY TESTING OF COPROCESSED LIQUIDS .....	17
3.1 Introduction.....	17
3.2 Experimental.....	18
3.3 Results and Discussion .....	19
3.4 Conclusion .....	25
4.0 CO-COKING OF PETROLEUM RESIDUE AND COAL.....	35
4.1 Aims .....	35
4.2 Introduction.....	35
4.3 Feedstocks Used.....	36
4.4 Co-coking Studies .....	37
4.5 Fluidity Studies .....	44
4.6 Study of Coke Quality and Morphology .....	48
4.7 Conclusions and Recommendations for Future Work .....	59
5.0 BLENDING OF COAL-TAR-PITCH DISTILLATES WITH SUITABLE REFINERY STREAMS.....	62
5.1 Aims .....	62
5.2 Introduction.....	62
5.3 Experimental.....	63
5.4 Results and Discussion .....	65
5.5 Conclusions and Future Recommendations.....	76
6.0 ENHANCING STABILITY OF THE PETROLEUM AND COAL-DERIVED COMPONENT.....	77
6.1 Thermal-Stability Testing of Naphthenic Liquids .....	77
6.2 Summary.....	80
7.0 CONFORMATIONAL ISOMERIZATION OF CYCLOALKANES.....	81
7.1 Introduction.....	81
7.2 Experimental.....	82
7.3 Results and Discussion .....	83
7.4 Conclusions.....	93

8.0 CARBON SKELETAL ISOMERIZATION .....	94
8.1 Introduction.....	94
8.2 Experimental .....	97
8.3 Results and Discussion .....	98
8.4 Conclusions.....	109
<b>9.0 REFERENCES.....</b>	<b>110</b>

## List of Figures

<b>Figure 3.1</b> Changes in chemical composition during hydrotreatment and dearomatization for the light cycle oil.....	26
<b>Figure 3.2</b> Differences in the chemical composition of the petroleum-derived jet fuel JP8P and the coal-derived JP8C.....	26
<b>Figure 3.3</b> GC-MS traces of the DA/HT LCO (top) and JP8P (bottom). ....	27
<b>Figure 3.4</b> Changes in gas and solid yields during stressing of DA/HT LCO at 450 °C under 100 psi N <sub>2</sub> . ....	27
<b>Figure 3.5</b> Variation in gas yield for DA/HT LCO, HT LCO, JP8P, and JP8C at 480°C (900F). ....	28
<b>Figure 3.6</b> Differences in the solid deposition formation for DA/HT LCO, HT LCO, JP8P, and JP8C at 480 °C. ....	29
<b>Figure 3.7</b> The solution-state <sup>13</sup> C NMR spectrum of the coal-derived jet fuel, JP8C, showing the general peak assignment. ....	29
<b>Figure 3.8</b> Changes in the main functional groups for DA/HT LCO as the residence time at 480 °C is increased from 30 minutes to 2 hours.....	30
<b>Figure 3.9</b> Changes in the aromatic content for the four jet fuels, DA/HT LCO, HT LCO, JP8P, and JP8C, stressed at 480 °C with residence times of up to 2 hours. ....	31
<b>Figure 3.10</b> Comparison of the ratio of the non-protonated aromatic-carbon content for the four jet fuels, DA/HT LCO, HT LCO, JP8P, and JP8C, with residence times up to 2 hours at 480°C.....	31
<b>Figure 3.11</b> Comparison of the CH <sub>2</sub> /CH <sub>3</sub> ratio for the four jet fuels, DA/HT LCO, HT LCO, JP8P, and JP8C, at 480 °C with residence times of up to 2 hours. ....	32
<b>Figure 3.12</b> Distillation plot for linear alkanes and boiling ranges for cycloalkanes generally found in DA/HT LCO fuel. ....	32
<b>Figure 3.13</b> GC traces of original severely hydro-treated light cycle oil (DA/HT LCO, bottom), the cut-point below 250 °C (middle), and the cut-point above 250 °C (top). ....	33
<b>Figure 3.14</b> Differences in the chemical composition of the original severely hydro-treated light cycle oil (DA/HT LCO, back) and the cut-point below 250 °C (B250, front).....	33
<b>Figure 3.15</b> Comparison of the gas product and the solid residue formed during stressing of the B250 fraction of DA/HT LCO at 480 °C with time.....	34

<b>Figure 4.1</b> Effect of temperature on the yields in the different boiling ranges.....	41
<b>Figure 4.2</b> Effect of feed on boiling ranges of the products of co-coking at 465°C .....	42
<b>Figure 4.3</b> Comparison of the thermoplastic profiles of coal/resid blends for the Powellton and Upper Banner seam coals.....	46
<b>Figure 4.4</b> Comparison of the thermoplastic profiles of coal/resid blends of Pittsburgh and Illinois #6 seam coals.....	47
<b>Figure 4.5</b> Change in Reflectance and Anisotropy of Coker Feed with Temperature.....	51
<b>Figure 4.6</b> Distribution of Carbon Textures with Carbonization Temperature of Coker Feed ...	52
<b>Figure 4.7</b> Distribution of Carbon Textures with Carbonization Temperature, Volatile- Derived Free Basis .....	55
<b>Figure 4.8</b> Distribution of coal-and Coker Feed-Derived Carbon Textures at 465 C .....	56
<b>Figure 4.9</b> Distribution of Coker Feed Carbon Textures in Coker Feed/Coal Blends.....	57
<b>Figures 5.1 and 5.2</b> The comparison of hydrogen-to-carbon ratio between different feedstocks, mixtures and reactions .....	69
<b>Figures 5.3 and 5.4</b> The comparison of jet-fuel fractions between different feedstocks, mixtures and reactions .....	69
<b>Figures 5.5 and 5.6</b> GC-MS of refined chemical oil and light cycle oil before (top) and after (bottom) reaction.....	72
<b>Figures 5.7, 5.8, and 5.9</b> GC-MS spectra of RCO and deeply hydrotreated LCO.....	74
<b>Figures 5.10, 5.11, and 5.12.</b> GC-MS of RCO at various pressures and temperatures .....	75
<b>Figure 6.1</b> Carbon-deposition and wetted-wall temperature versus axial distance for two kerosene runs. Furnace temperature, 700 °C; pressure, 700 psig; flow rate, 12 mL/min; duration, 7 hours. ....	77
<b>Figure 6.2</b> Carbon deposition and wetted-wall temperature profiles for kerosene run on improved reactor. Furnace temperature, 700 °C; pressure, 700 psig; flow rate, 10 mL/min; duration, 7 hours. ....	79
<b>Figure 7.1</b> Conversion to trans-DeHN vs. temperature.....	85
<b>Figure 7.2</b> Selectivity vs temperature.....	86

<b>Figure 7.3</b> Conversion to trans-DeHN achieved by different pressures .....	87
<b>Figure 7.4</b> Selectivity to trans-DeHN versus pressure.....	88
<b>Figure 8.1</b> Conversion of CH over 0.5Pt/CBV30A and 0.5Pd/CBV30A .....	100
<b>Figure 8.2</b> Selectivity to MCP over 0.5Pt/CBV30A and 0.5Pd/CBV30A.....	101
<b>Figure 8.3</b> Conversion vs pressure over 0.5Pt/CBV740 and 0.5Pd/CBV740 at 330 °C.....	106
<b>Figure 8.4</b> Selectivity vs pressure over 0.5Pt/CVB740 and 0.5Pd/CBV740 at 330 °C. ....	106
<b>Figure 8.5</b> Conversion vs pressure over 0.5Pt/CBV740 and 0.5Pd/CBV740 at 370 °C.....	107
<b>Figure 8.6</b> Selectivity vs pressure over 0.5Pt/CBV740 and 0.5Pd/CBV740 at 370 °C. ....	107

## List of Tables

<b>Table 2.1</b> Proximate analysis of subbituminous C coal (DECS-8) and hv A bituminous coal (DECS-12). .....	8
<b>Table 2.2</b> Ultimate analysis of subbituminous C coal (DECS-8) and hv A bituminous coal (DECS-12). (dmmf basis).....	8
<b>Table 2.3A</b> Effect of temperature for Molyvan L catalyst for coal conversion and product yield for DECS-8. ....	9
<b>Table 2.3B</b> Effect of temperature for Molyvan L catalyst on coal conversion and product yield for DECS-12. ....	9
<b>Table 2.4A</b> Effect of temperature and sample size on coal conversion and product yield for DECS-8 for nickel 2-ethylhexanoate. ....	9
<b>Table 2.4B</b> Effect of temperature and sample size on coal conversion and product yield for DECS-12 for nickel 2-ethylhexanoate. ....	10
<b>Table 2.5A</b> Effect of temperature on coal conversion and product yield for DECS-8 for cobalt naphthenate. ....	10
<b>Table 2.5B</b> Effect of temperature on coal conversion and product yield for DECS-12 for cobalt naphthenate. ....	10
<b>Table 2.6A</b> Effect of temperature on coal conversion and product yield for DECS-8 for cobalt/nickel (naphthenate and 2-ethylhexanoate) binary mixture. ....	10
<b>Table 2.6B</b> Effect of temperature on coal conversion and product yield for DECS-12 for cobalt/nickel (naphthahenate and 2-ethylhexanoate) binary mixture. ....	11
<b>Table 2.7A</b> Effect of temperature on coal conversion and product yield for DECS-8 for nickel/molybdenum chlorides binary mixture. ....	11
<b>Table 2.7B</b> Effect of temperature on coal conversion and product yield for DECS-12 for nickel/molybdenum chlorides binary mixture. ....	11
<b>Table 2.8A</b> Effect of temperature on coal conversion and product yield for DECS-8 for cobalt/nickel chlorides binary mixture. ....	12
<b>Table 2.8B</b> Effect of temperature on coal conversion and product yield for DECS-12 for cobalt/nickel chlorides binary mixture. ....	12
<b>Table 2.9A</b> Effect of temperature on coal conversion and product yield for DECS-8 for molybdenum/nickel (2-ethylhexanoate/naphthenate) binary mixture.....	12
<b>Table 2.9B</b> Effect of temperature on coal conversion and product yield for DECS-12 for molybdenum/nickel (2-ethylhexanoate/naphthenate) binary mixture.....	13
<b>Table 2.10A</b> Effect of temperature and sample size on coal conversion and product yield for DECS-8 for non-catalyzed samples. ....	13
<b>Table 2.10B</b> Effect of temperature and sample size on coal conversion and product yield for DECS-8 for non-catalyzed samples. ....	13
<b>Table 2.11</b> Effect of temperature and sample size on product yield for atmospheric residue.....	14
<b>Table 2.12A</b> Gaseous products from liquifaction reaction for DECS-8 coal. ....	14
<b>Table 2.12B</b> Gaseous products from reaction of DECS-12 coal. ....	15

<b>Table 3.1</b> Distribution of the chemical composition for DA/HT LCO and JP8P on the basis of initial amount, both original and stressed at 480 °C for 45 min under 100 psi N <sub>2</sub> .	25
<b>Table 4.1</b> Analysis of project coals.	36
<b>Table 4.2</b> Percent yields of different fractions.	38
<b>Table 4.3</b> Compound distribution of co-coking products.	43
<b>Table 4.4</b> Compound-distribution yield in the hexane-soluble fraction.	43
<b>Table 4.5a</b> Substituted-compound distribution and yield for the hexane-soluble fraction.	44
<b>Table 4.5b</b> Substituted-compound distribution and yield for the hexane-soluble fraction.	44
<b>Table 4.6</b> Elemental analysis of co-coking feedstocks (C, H, N reported on d.a.f. basis).	58
<b>Table 4.7</b> Elemental analysis of THF-insoluble products from co-coking runs and heat-treated resid coker feed at 450 °C.	58
<b>Table 4.8</b> Elemental analysis of THF-insoluble products from co-coking runs and heat-treated resid coker feed at 465 °C.	58
<b>Table 4.9</b> Elemental analysis of THF-insoluble products from co-coking runs and heat-treated resid coker feed at 475 °C.	59
<b>Table 4.10</b> Elemental analysis of THF-insoluble products from co-coking runs and heat-treated resid coker feed at 500 °C.	59
<b>Table 5.1</b> Feedstock chemical analysis.	64
<b>Table 5.2</b> Level of desulfurization in mixtures of coal-tar pitch and kerosene.	65
<b>Table 5.3</b> Properties and analyses of kerosene, 100%.	66
<b>Table 5.4</b> Properties and analyses of carbon-black oil, 100%.	66
<b>Table 5.5</b> Properties and analyses of 50% kerosene and 50% carbon-black oil (no filtration).	66
<b>Table 5.6</b> Properties and analyses of 50% kerosene and 50% carbon-black oil (with filtration)	66
<b>Table 5.7</b> Properties and analyses of deeply hydrogenated light cycle oil (LCO <sup>o</sup> ).	67
<b>Table 5.8</b> Properties and analyses of 50% LCO <sup>o</sup> and 50% CBO (no filtration).	67
<b>Table 5.9</b> Properties and analyses of refined chemical oil (RCO) and its 50% mixture with light cycle oil (LCO <sup>o</sup> ).	68
<b>Table 5.10</b> Properties and analyses of refined chemical oil (RCO) using a CoMo catalyst and reaction temperature of 350 °C.	68
<b>Table 5.11</b> Properties and analyses of a refined chemical oil (RCO) and light cycle oil (LCO <sup>o</sup> ) mixture reacted at 350 °C using a CoMo catalyst.	70



<b>Table 5.12</b> Analyses of hydrogenated products from refined chemical oil (RCO) under varying conditions.....	71
<b>Table 5.13</b> Analyses of hydrogenated products from the blends of refined chemical oil (RCO) and deeply hydrotreated light cycle oil (LCO <sup>o</sup> ) under varying conditions.....	73
<b>Table 5.14</b> Analyses of different LCO: RCO mixtures, 1000 psig H <sub>2</sub> pressure and 350°C.....	73
<b>Table 7.1</b> Typical properties of zeolites used. ....	83
<b>Table 7.2</b> Feed conditions used for conformational isomerization of cycloalkanes. ....	83
<b>Table 7.3</b> GC analysis programs used for liquid products. ....	83
<b>Table 7.4</b> Conformational isomerization of cis-1,4-DMCH over 0.5Pd/USY40 and 0.5Pd/HM30A.....	90
<b>Table 7.5</b> Conformational Isomerization of cis-1,3-DMCH over 0.5Pd/USY40 and 0.5Pd/HM30A.....	91
<b>Table 7.6</b> Conformational isomerization of cis-1,2-DMCH over Pd-loaded catalysts. ....	92
<b>Table 8.1</b> Typical properties of zeolites used. ....	97
<b>Table 8.2</b> GC analysis program used for product analysis. ....	97
<b>Table 8.3</b> Reaction conditions used for the effects of pressure. ....	98
<b>Table 8.4</b> Skeletal isomerization of cyclohexane over 0.5Pt/LZ-Y62 and 0.5Pd/LZ-Y62. ....	99
<b>Table 8.5</b> Reaction conditions used at 370 °C. ....	101
<b>Table 8.6</b> Cyclohexane isomerization by pressure change.....	102
<b>Table 8.7</b> Reaction conditions used at 300 °C. ....	103
<b>Table 8.8</b> CH isomerization over Pt- or Pd-loaded CBV30A with pressure change at 300 °C. ....	103
<b>Table 8.9</b> Reaction conditions used at 370 °C with different H <sub>2</sub> pressures. ....	104
<b>Table 8.10</b> CH isomerization over Pt- or Pd-loaded LZ-Y62 at 370 °C with pressure change. ....	104
<b>Table 8.11</b> Reaction conditions used with 0.5Pt/CBV740 and 0.5Pd/CBV740. ....	105
<b>Table 8.12</b> Reaction conditions used for different feedstock loadings. ....	108
<b>Table 8.13</b> Isomerization results for cyclohexane using 0.5Pt/CBV30A and 0.5Pd/CBV30A. ....	108

## **1.0 BP SUBCONTRACT**

As part of this Delivery Order, we had planned to establish a new subcontract with BP Oil to obtain further samples of refinery streams—kerosene and light cycle oil—and, more importantly, to investigate further the hydrotreating and dearomatization of the LCO. Unfortunately, events totally beyond our control resulted in this subcontract never being executed. As a result of the BP-Amoco merger, the following events took place: (a) our original technical contact at BP Oil was reassigned, and the Jet Fuel Project was handed to a different staff member; (b) the Warrensville, Ohio research facility, which had been the point of contact and locus of some of the work was closed; (c) the new technical contact was laid off; and (d) the staff member who had supervised most of the hydrotreating work at BP's Sunbury (U.K.) facility took early retirement. Despite repeated phone calls and letters from the Jet Fuel Project's principal investigator, from the Energy Institute's administrative assistant, from the College of Earth and Mineral Sciences' research accounting office, and from Penn State's Office of Sponsored Programs, it was rarely possible to get even a response from the cognizant BP staff, let alone establish a formal subcontract. Consequently, we gave up in frustration. Despite efforts from the Jet Fuel Project's principal investigator, from the Energy Institute's administrative assistant, from the College of Earth and Mineral Sciences' research accounting office, and from Penn State's Office of Sponsored Programs, it was not possible to establish a formal subcontract. New subcontracting arrangements, not part of this Delivery Order, have now been established with PARC Technical Services, Harmerville, PA.

## 2.0 HYDROGENATION CATALYSTS IN BATCH TESTS

### 2.1 Introduction

The main objective of this subtask is to explore the coprocessing of coal and petroleum resid for the production of oils that can then be upgraded for the subsequent production of advanced thermally stable jet fuels. Coprocessing of coal and petroleum resid has some advantages over direct coal liquefaction. The coexistence of coal and petroleum resid allows for the conversion processing of two difficult-to-refine heavy materials. The coal residue and coal ash can help in the removal of metal species from petroleum resid. The presence of coal in the coal/resid mixture can also facilitate the hydrogen transfer to the liquid products.

Based on the existing information on coal/resid coprocessing, we explored two types of catalyst: hydrogen catalysts (subtask 1.1.1) that are based on *in situ*-generated metal sulfides of Mo, Co, and Ni and their combinations, and hydrocracking catalysts (subtask 1.1.2) that are based on Lewis-acidic chlorides of Mo, Co, and Ni and their combinations. Because both types of catalysts were tested and compared with many common control experiments, we have combined the results for both types in this final report.

Whereas detailed results are provided below, the overall trend appears to be that the hydrogenation-type catalysts using oil-soluble precursors are superior to the Lewis-acid type hydrocracking catalysts. Although our model-compound tests have revealed such compounds to be active, it appears that the oil-soluble catalyst precursors (to the hydrogenation-type catalysts) can be better dispersed onto coal thus providing a more intimate contact with the surface for active hydrogen transfer. Another trend is that certain combinations of two metal species are more effective under some specific conditions for oil production in coal/resid coprocessing. These important general trends suggest that our future work should be directed toward more conversion studies using suitable combinations of oil-soluble precursors for coal/resid coprocessing. Specific details for the experiments and results are provided below.

## 2.2 Experimental

### Materials

#### *Coals*

Two coals were used in the investigation. One was DECS-8, subbituminous C, coal from the Smith-Rolland seam in Campbell County, Wyoming. The other was DECS-12 an hv A bituminous from the Pittsburgh seam in Greene County, Pennsylvania. Proximate and ultimate analysis of these as-received coals are listed in Tables 2.1 and 2.2. [1].

#### *Atmospheric Oil Residue*

An atmospheric oil residue (AR) from the Marathon Oil Company was used. The term “atmospheric residue” or “resid” describes the crude-oil product from the bottom of the atmospheric distillation tower having a boiling point higher than 340 °C. Elemental analysis of the AR is as follows: C-84.64; H-11.14; S-3.87; N-0.23; O (by diff.)-0.12 wt% [2].

#### *Gases*

Ultra-High Purity (UHP) hydrogen was used.

#### *Catalysts*

The following catalysts and their binary mixtures were used: Molyvan L, molybdenum and nickel 2-ethylhexanoate, cobalt naphthenate and nickel, cobalt and molybdenum chlorides. Molyvan L, is a stable, organic, completely oil-soluble liquid product from the R.T. Vanderbilt Company, Inc., containing 8.1% Mo, 6.4% P, and 6.4% S. The nickel and molybdenum 2-ethylhexanoates and cobalt naphthenate contain 8%, 15%, and 6% of metal, respectively. These catalysts are produced by the Mooney Chemicals Company of Cleveland, OH. Nickel, molybdenum, and cobalt chlorides are produced by the Aldrich Chemical Company.

### Procedure

Reactors consisting of a 25-mL capacity horizontal-tubing bomb were used to investigate coal and atmospheric residue hydroprocessing under an initial hydrogen pressure of 6.9 MPa . As-received coal was impregnated with a catalyst and was dried for 2 hrs under vacuum. The catalyst, a single component or binary mixture of two metals, was diluted with water and/or

THF. Usually, the amount of added water and/or THF was normalized per unit weight of dmmf coal,  $((0.33\text{g H}_2\text{O} + \text{THF})/\text{g C})$ . Such impregnated coals were placed into the reactors and AR oil was added. After closing the reactors, hydrogen was added, and the system was tested for leaks. The total hydrogen pressure was the same for all experiments and equalled 6.9 MPa. A sand bath fluidized-bed reactor was used in the studies. The total reaction time, after reaching a desired reaction temperature, was 1 hr. Usually, about 3 min was needed to reach the final temperature after inserting the reactors into the fluidized-bed sand bath. Most experiments were done isothermally at 375, 400, and 425 °C; however, in some cases the linear temperature increase from 375 to 425 °C was studied. As a rule, the total reaction time was 1 hr. In some cases of linear temperature increase, the reaction started at 375 °C and was kept at this temperature for 15 min. Then the temperature was increased at a heating rate of 1.6 °C/min (30 min) to 425 °C and kept at this final temperature for an additional 15 min. In addition, some low-temperature pretreatment at 200 °C was included in the routine procedure to investigate its influence on hydroprocessing behavior. After the reaction, the reactors were quenched in water for fast reaction termination and the products were separated by first removing the gases. The non-volatile slurry was removed from the reactor to a weighed ceramic thimble and then separated by Soxhlet extraction using hexane, toluene, and THF in series. The fractions were classified as oil, asphaltene, and preasphaltene for the hexane solubles, toluene solubles and THF solubles, respectively. The gaseous products were analyzed by GC. The coal conversion and the asphaltene and preasphaltene yields were normalized per dmmf of the coal. Gas yield was normalized per sum of dmmf coal plus oil. The oil fraction was calculated by the difference.

## 2.3 Results

Listed in Tables 2.1 and 2.2, the proximate and ultimate analysis shows more moisture and oxygen but less fixed carbon for the lower-rank coal (DECS-8) than for the higher-rank coal (DECS-12).

The experimental data for conversion and product yield are listed in tabular form. In the “A” tables, the data for DECS-8 coal are listed while the “B” tables contain data for DECS-12 coal. The data are listed in similar form to facilitate a comparison among different catalysts.

### Molyvan L

Tables 2.3A and 2.3B list the data for the Molyvan L catalyst. For this catalyst only 3-g samples were under investigation. The maximum conversion for DECS-8 coal was observed for the experiment carried out at 400 °C (54.5%) and for the experiment using a linear-temperature ramp of 375-425 °C (51.7%). For DECS-12 coal, the conversion was even greater than for the lower-rank coal, which is rather unusual. For experiments at 425 °C, the conversions were ca. 65 and 69%. For the experiment with a linear temperature increase of 375-425°C, the conversion was 69.5%. The asphaltene and preasphaltene fractions were lower for the lower-rank coal DECS-8 than for the higher-rank DECS-12. Both coals were in the range 3-10%, with gases less than 5%.

### Nickel 2-ethylhexanoate

For the nickel 2-ethylhexanoate catalyst (Tables 2.4A and 2.4B), the maximum conversion for DECS-8 coal was observed in the experiments at 425 °C and using a linear-temperature ramp of 375-425 °C with 1-g sample. The conversions were 76.6 and 75.5%, respectively. Similar behavior was observed for DECS-12 coal, and the conversions were 85.3 and 68.4% for experiments at 425 °C and using a linear-temperature ramp of 375-425 °C, respectively. For larger sample sizes, the conversion using the same experimental conditions was lower than for a smaller sample weight. The gaseous fraction was also less than 5%. The asphaltene and preasphaltene fractions were greater than those for the Molyvan L catalyst.

### Cobalt Naphthenate

For this catalyst the data are listed in Tables 2.5A and 2.5B. The maximum conversion was observed for both coals at 425 °C. For 1-g samples, the conversions were 68.8 and 75.1% for DECS-8 and DECS-12, respectively. This cobalt catalyst was less active than nickel 2-ethylhexanoate, as previously reported.

### Cobalt/nickel (Naphthenate and 2-ethylhexanoate) Binary Mixture

Tables 2.6A and 2.6B list the data for the cobalt-nickel binary mixture. The mixture of these two catalysts produced a conversion similar to that produced by single metals. The maximum conversion was in the range of 72-76% for DECS-8 coal. It was observed in experiments at 425

°C with pretreatment to 200 °C and also in the linear-temperature experiment, 375-425 °C, with a similar pretreatment to 200 °C. For DECS-12 coal, the highest conversion was observed over a much broader temperature range, 400-450 °C, and also with the linear temperature increase with and without pretreatment. The highest conversion was ca. 85% for DECS-8 and 83.3% for DECS-12 (exp. 32A and 32B).

#### Nickel/molybdenum Chloride Binary Mixture

The data for this binary mixture are listed in Tables 2.7A and 2.7B. The cobalt molybdenum chloride binary mixture produced a lower conversion than that previously reported for a Co/Ni oil-soluble catalyst. In the Ni/Mo case, the maximum conversion at 450 °C was 71.3% for DECS-8 coal and 69.3% for DECS-12 coal. The asphaltene and preasphaltene fractions were greater than those for the Molyvan L catalyst.

#### Cobalt Nickel Chloride Binary Mixture

The data for cobalt/nickel binary mixture are listed in Tables 2.8A and 2.8B. For this catalyst mixture, the experiments were done only at 425 °C. The cobalt/nickel binary mixture of chlorides was also used to compare their catalytic activity with that of the other catalysts. The conversion values were 71-73% for DECS-8 coal and 68-77% for DECS-12 coal.

#### Molybdenum/nickel (2-ethylhexanoate/naphthenate) Binary Mixture

Finally, the oil-soluble binary mixture studied in this investigation was the molybdenum-nickel catalyst. The data are listed in Tables 2.9A and 2.9B. For DECS-8 coal, a maximum conversion of 70-75% was observed in the 425 °C experiments. For DECS-12 coal, a maximum conversion of 70-75% was observed both for the 400-425 °C experiments and for the linear temperature increase (375-425 °C) experiment.

#### Noncatalyzed Process

The experimental data for noncatalyzed hydrogenation are listed in Tables 2.10A and 2.10B. Comparing this data with results from experiments performed under similar reaction conditions using catalyzed samples, the noncatalyzed hydroprocessing was never as effective. The highest conversion in such cases was observed for 425 and 450 °C, and was never greater than 45%.

### Atmospheric Residue Hydrogenation

In addition to the coal- and oil-slurry hydrogenation, a similar investigation was undertaken to observe the behavior of atmospheric residue alone. The experimental data for the effort are shown in Table 2.11. Noncatalyzed and catalyzed experiments using only a single-metal precursor of nickel 2-ethylhexanoate, cobalt naphthenate, or nickel chloride were undertaken. The main objective of the study was to obtain the percentage of the gaseous fraction. The gaseous fraction of the coal and oil resid hydrogenation was normalized on the total-dmmf coal and resid oil taken into the reaction. This study was undertaken to show that the effect of oil hydrogenation on the gaseous-product yield is not negligible. The asphaltene and preasphaltene fractions were small and, in most cases, not greater than a few percent. The gaseous fraction is usually in the range of 3-7%.

### Effect of Sample Weight

In addition to the above-described effect of temperature, for some selected samples the use of different sample weights of coal was also investigated. (Because the ratio of coal to oil was kept at 1:1, increasing the amount of coal in the sample also required an increase in the amount of oil resid.) Because the size of the reactor in all experiments was the same, increasing the amounts solid and liquid reaction components caused the ratio of hydrogen to coal and oil to change. In decreasing this ratio, it is reasonable to expect that the efficiency of hydrogenation may be lower. As observed in Table 2.4, where such cases are listed, the conversion was usually lower for larger coal samples under investigation. Comparing the conversions for DECS-8 coal for experiments listed in these tables, 2.9A with 2.10A, 2.11A with 2.12A, and 2.13A with 2.14A; and also 2.9B with 2.10B, 2.11B with 2.12B, and 2.13B with 2.14B, we find that in all these cases the lower the sample size the higher the conversion.

### Gas Analysis

The gas-chromatography technique was used to analyze gaseous products from the reaction. Product distributions for DECS-8 and DECS-12 coals are listed in Tables 2.12A and 2.12B, respectively. Usually light hydrocarbons of  $C_1$ - $C_4$ , in addition to CO and  $CO_2$ , were detected.  $CH_4$  and  $CO_2$  were the main products of the reaction; however, in some cases ethane and propane were also observed in higher percentages, greater than 10 or even 20%. Usually the total



percentage of CO and CO<sub>2</sub> for DECS-8 was higher than the corresponding quantity for DECS-12. This is what one might expect because the oxygen content in subbituminous coals (DECS-8) is higher than that in bituminous coals (DECS-12).

## 2.4 Conclusion

Seven catalyst precursors of molybdenum, nickel, and cobalt metals were investigated. Catalyst activity was narrowed to the temperature range 375-450 °C and a hydrogen partial pressure of 6.9 MPa (cold). The maximum conversions for the catalysts studied are as follows: Molyvan L - 54.5% at 400 °C for DECS-8 coal and 69.5% with 375-425°C for DECS-12 coal; nickel 2-ethylhexanoate - 76.6% for DECS-8 coal and 85.3% for DECS-12 coal, both at 425 °C; cobalt naphthenate - 68.8% for DECS-8 coal and 75.1% for DECS-12 coal, both at 425 °C; cobalt/nickel (naphthenate and 2-ethylhexanoate) mixture - 84.9% for DECS-8 coal and 83.3% for DECS-12 coal, both at 450 °C; nickel/molybdenum chloride mixture - 71.3% for DECS-8 coal and 69.3% for DECS-12 coal, both at 540 °C; cobalt/nickel chloride - 73.0% for DECS-8 coal and 75-77% for DECS-12 coal; molybdenum/nickel (2-ethylhexanoate and naphthenate) mixture - 75.0% for DECS-8 coal and 78.5% for DECS-12 coal, both at 425 °C.

Noncatalyzed coals resulted in much lower conversion levels, at best, which never exceeded 45%.

**Table 2.1** Proximate analysis of subbituminous C coal (DECS-8) and hv A bituminous coal (DECS-12).

	subbitC coal (DECS-8)	Hvbituminous (DECS-12)
% Moisture	28.42	2.40
% Ash	9.90	10.00
Vol. Matter	32.38	35.16
Fixed Carbon	29.30	52.44

**Table 2.2** Ultimate analysis of subbituminous C coal (DECS-8) and hv A bituminous coal (DECS-12). (dmmf basis)

	subbit. C coal (DECS-8)	hv bituminous (DECS-12)
%Carbon	74.43	83.32
%Hydrogen	5.24	4.97
%Nitrogen	1.00	1.20

%total Sulfur	0.85	1.23
Oxygen (diff.)	18.48	9.28

**Table 2.3A** Effect of temperature for Molyvan L catalyst for coal conversion and product yield for DECS-8.

Exp.No	Catalyst	Sample Weight (g)	Temp. (C)	Conv. dmmf wt%	Gas wt%	Oil dmmf wt%	Asph. dmmf wt%	Preasph dmmf wt%
A1	1% Mo	3	375	43.9	4.3	31.5	5.2	2.9
A2	1% Mo	3	375	45.0	4.7	28.1	7.2	5.0
A3	1% Mo	3	400	54.5	4.2	40.0	4.1	6.2
A4	1% Mo	3	425	49.2	3.8	35.2	4.2	6.0
A5	1% Mo	3	425	46.3	3.5	32.6	4.4	5.8
A6	1% Mo	3	375-425	51.7	4.1	38.5	5.2	3.9

**Table 2.3B** Effect of temperature for Molyvan L catalyst on coal conversion and product yield for DECS-12.

Exp. No	Catalyst	Sample Weight (g)	Temp. (C)	Conv. dmmf wt%	Gas wt%	Oil dmmf wt%	Asph. dmmf wt%	Preasph. dmmf wt%
B1	1% Mo	3	375	46.4	2.1	36.0	5.2	3.1
B2	1% Mo	3	375	37.8	1.8	28.0	4.7	3.3
B3	1% Mo	3	400	49.9	2.9	38.3	4.9	3.8
B4	1% Mo	3	425	68.7	3.3	46.8	9.7	8.9
B5	1% Mo	3	425	64.7	3.2	43.7	9.5	8.3
B6	1% Mo	3	375-425	69.5	3.8	48.8	9.7	7.2

**Table 2.4A** Effect of temperature and sample size on coal conversion and product yield for DECS-8 for nickel 2-ethylhexanoate.

Exp. No	Catalyst	Sample Weight (g)	Temp. (C)	Conv. dmmf wt%	Gas wt%	Oil dmmf wt%	Asph. dmmf wt%	Preasph. dmmf wt%
A8	1% Ni	3	375	44.1	3.6	27.6	6.8	6.1
A9	1% Ni	3	400	50.3	3.7	32.1	8.9	5.6
A10	1%Ni	1	400	57.2	4.0	37.2	9.3	6.7
A11	1%Ni	3	425	40.0	3.3	29.4	4.9	2.4
A12	1%Ni	1	425	76.6	4.5	63.0	7.3	1.8
A13	1% Ni	3	375-425	47.6	3.8	30.9	8.9	4.0
A14	1%Ni	1	375-425	75.5	4.8	52.7	12.3	5.7

**Table 2.4B** Effect of temperature and sample size on coal conversion and product yield for DECS-12 for nickel 2-ethylhexanoate.

Exp. No	Catalyst	Sample Weight (g)	Temp. (C)	Conv. dmmf wt%	Gas wt%	Oil dmmf wt%	Asph. dmmf wt%	Preasph. dmmf wt%
B8	1% Ni	3	375	38.6	1.9	19.2	6.6	10.9
B9	1% Ni	3	400	47.4	2.3	25.4	10.8	8.9
B10	1%Ni	1	400	67.3	3.7	46.9	8.9	7.8
B11	1%Ni	3	425	53.5	2.9	36.7	9.4	4.5
B12	1%Ni	1	425	85.3	4.5	73.8	5.5	1.5
B13	1% Ni	3	375-425	49.5	2.4	28.2	10.5	8.4
B14	1% Ni	1	375-425	68.4	3.0	36.6	18.3	10.5

**Table 2.5A** Effect of temperature on coal conversion and product yield for DECS-8 for cobalt naphthenate.

Exp. No	Catalyst	Sample Weight (g)	Temp. (C)	Conv. dmmf wt%	Gas wt%	Oil dmmf wt%	Asph. dmmf wt%	Preasph. dmmf wt%
A16	1%Co	1	375	34.2	3.2	12.5	8.3	1.0
A17	1%Co	1	400	52.9	4.3	31.3	11.2	6.1
A18	1%Co	1	425	68.8	4.9	42.4	13.1	8.4
A19	1%Co	1.5	425	58.1	4.5	43.3	9.3	1.0
A20	1%Co	1	375-418	48.8	3.9	25.9	12.6	6.4
A21	1%Co	1	375-425	55.6	4.2	32.7	13.3	5.4

**Table 2.5B** Effect of temperature on coal conversion and product yield for DECS-12 for cobalt naphthenate.

Exp. No	Catalyst	Sample Weight (g)	Temp. (C)	Conv. dmmf wt%	Gas wt%	Oil dmmf wt%	Asph. dmmf wt%	Preasph. dmmf wt%
B16	1% Co	1	375	39.0	3.4	26.0	6.7	2.9
B17	1% Co	1	400	52.8	4.2	32.8	9.3	6.5
B18	1% Co	1	425	75.1	5.0	44.1	18.2	7.8
B19	1%Co	1.5	425	59.4	4.2	37.2	9.5	8.5
B20	1%Co	1	375-418	61.8	4.4	35.2	13.7	9.5
B21	1%Co	1	375-425	66.8	4.5	37.9	13.1	11.3

**Table 2.6A** Effect of temperature on coal conversion and product yield for DECS-8 for cobalt/nickel (naphthenate and 2-ethylhexanoate) binary mixture.

Exp. No	Catalyst	Sample Weight (g)	Temp. (C)	Conv. dmmf wt%	Gas wt%	Oil dmmf wt%	Asph. dmmf wt%	Preasph. dmmf wt%
A25	1%Co/Ni	1	425	65.4	2.8	43.8	16.1	2.7
A27	1%Co/Ni	1	375	38.8	1.3	23.2	11.5	2.9
A28	1%Co/Ni	1	400	63.8	3.2	31.6	19.1	9.9
A29	1%Co/Ni	1	375-425	72.6	3.8	54.6	11.9	2.3
A30	1%Co/Ni	1	200-375-425	72.1	3.9	46.8	16.5	4.9
A31	1%Co/Ni	1	200-425	76.5	4.3	49.9	12.7	9.6

A32	1%Co/Ni	1	425	69.4	3.5	46.1	13.6	6.2
A33	1%Co/Ni	1	450	84.9	3.8	71.6	8.7	0.8
A35	1%Co/Ni	1	430	76.2	3.3	55.1	12.3	5.5
A36	1%Co/Ni	1	450	79.5	5.3	63.8	7.8	2.6

**Table 2.6B** Effect of temperature on coal conversion and product yield for DECS-12 for cobalt/nickel (naphthahenate and 2-ethylhexanoate) binary mixture.

Exp. No	Catalyst	Sample Weight (g)	Temp. (C)	Conv. dmmf wt%	Gas wt%	Oil dmmf wt%	Asph. dmmf wt%	Preasph. dmmf wt%
B25	1%Co/Ni	1	425,	66.6	3.3	33.4	21.4	8.6
B27	1%Co/Ni	1	375	46.8	2.5	27.9	13.0	3.3
B28	1%Co/Ni	1	400	72.1	4.2	36.7	18.7	12.5
B29	1%Co/Ni	1	375-425	73.6	4.3	34.8	24.7	9.8
B30	1%Co/Ni	1	200 375-425	73.4	4.4	30.9	25.7	12.4
B31	1%Co/Ni	1	200 425	71.0	4.6	25.8	25.4	15.2
B32	1%Co/Ni	1	425	82.7	3.2	56.2	15.5	7.8
B33	1%Co/Ni	1	450	83.3	3.6	67.9	9.9	1.9
B35	1%Co/Ni	1	430	75.8	3.7	31.6	17.9	10.5
B36	1%Co/Ni	1	450	80.5	4.8	54.6	0.4	0.2

**Table 2.7A** Effect of temperature on coal conversion and product yield for DECS-8 for nickel/molybdenum chlorides binary mixture.

Exp. No	Catalyst	Sample Weight (g)	Temp. (C)	Conv. dmmf wt%	Gas wt%	Oil dmmf wt%	Asph. dmmf wt%	Preasph. dmmf wt%
A41	10% Ni/Mo	425	1	60.0	4.2	35.6	11.3	8.9
A42	1% Ni/Mo	425	1	63.3	4.8	31.5	12.8	14.2
A43	1% Ni/Mo	400	1	66.0	8.5	34.5	13.9	9.1
A44	1% Ni/Mo	450	1	71.3	15.5	43.9	8.6	3.3

**Table 2.7B** Effect of temperature on coal conversion and product yield for DECS-12 for nickel/molybdenum chlorides binary mixture.

Exp. No	Catalyst	Sample Weight (g)	Temp. (C)	Conv. dmmf wt%	Gas wt%	Oil dmmf wt%	Asph. dmmf wt%	Preasph. dmmf wt%
B41	10% Ni/Mo	1	425	49.9	3.2	25.2	9.5	12.0
B42	1% Ni/Co	1	425	68.6	3.2	41.9	14.5	9.0
B43	1% Ni/Mo	1	400	68.5	3.5	39.1	16.4	9.5
B44	1% Ni/Mo	1	450	69.3	12.5	45.5	8.7	2.6

**Table 2.8A** Effect of temperature on coal conversion and product yield for DECS-8 for cobalt/nickel chlorides binary mixture.

Exp. No	Catalyst	Sample Weight (g)	Temp. (C)	Conv. dmmf wt%	Gas wt%	Oil dmmf wt%	Asph. dmmf wt%	Preasph. dmmf wt%
A47	1% Ni/Co	1	425	71.0	12.0	32.9	14.7	11.4
A49	1% Co/Ni	1	425	71.3	10.0	42.7	10.5	9.8
A50	1% Co/Ni	1	425	73.0	10.2	43.9	9.4	6.6

**Table 2.8B** Effect of temperature on coal conversion and product yield for DECS-12 for cobalt/nickel chlorides binary mixture.

Exp. No	Catalyst	Sample Weight (g)	Temp. (C)	Conv. dmmf wt%	Gas wt%	Oil dmmf wt%	Asph. dmmf wt%	Preasph. dmmf wt%
B47	1% Ni/Co	1	425	77.3	9.5	49.4	11.3	7.1
B49	1% Co/Ni	1	425	75.4	6.0	45.2	16.1	8.1
B50	1% Co/Ni	1	425	67.4	5.0	43.1	11.1	7.9

**Table 2.9A** Effect of temperature on coal conversion and product yield for DECS-8 for molybdenum/nickel (2-ethylhexanoate/naphthenate) binary mixture.

Exp. No	Catalyst	Sample Weight (g)	Temp. (C)	Conv. dmmf wt%	Gas wt%	Oil dmmf wt%	Asph. dmmf wt%	Preasph. dmmf wt%
A57	1% Mo/Ni	1	425	70.0	8.5	37.4	16.7	7.4
A58	1% Mo/Ni	1	425	75.0	9.5	47.5	13.0	5.0
A59	1% Mo/Ni	1	400	65.8	7.5	33.3	17.6	7.4
A60	1% Mo/Ni	1	400	65.3	8.2	28.6	18.2	10.3
A61	1% Mo/Ni	1	425	72.6	9.3	40.0	16.7	6.6
A62	1% Mo/Ni	1	425	74.9	9.6	45.8	17.0	2.5
A63	1% Mo/Ni	1	375-425	72.0	9.4	39.0	19.9	3.6
A64	1% Mo/Ni	1	425	70.6	8.8	37.4	20.2	4.2
A65	1% Mo/Ni	1	400	67.6	8.3	37.6	12.9	8.8
A66	1% Mo/Ni	1	375	47.2	7.1	22.1	11.6	6.4

**Table 2.9B** Effect of temperature on coal conversion and product yield for DECS-12 for molybdenum/nickel (2-ethylhexanoate/naphthenate) binary mixture.

Exp. No	Catalyst	Sample Weight (g)	Temp. (C)	Conv. dmmf wt%	Gas wt%	Oil dmmf wt%	Asph. dmmf wt%	Preasph. dmmf wt%
B57	1% Mo/Ni	1	425	78.5	6.0	42.4	20.3	9.8
B58	1% Mo/Ni	1	425	73.3	5.5	33.1	25.2	9.5
B59	1% Mo/Ni	1	400	69.3	4.5	22.1	29.4	13.3
B60	1% Mo/Ni	1	400	71.4	4.7	20.1	29.0	17.6
B61	1% Mo/Ni	1	425	71.4	5.0	35.0	26.8	4.6
B62	1% Mo/Ni	1	425	75.1	5.3	44.0	22.0	3.8
B63	1% Mo/Ni	1	375-425	71.8	4.9	31.5	9.9	4.9
B64	1% Mo/Ni	1	425	70.8	4.6	37.0	23.7	5.5
B65	1% Mo/Ni	1	400	65.2	3.9	30.8	22.6	7.9
B66	1% Mo/Ni	1	375	46.4	3.1	20.8	16.0	6.5
B67	1% Mo/Ni	1	375	48.3	3.2	9.9	19.8	15.4

**Table 2.10A** Effect of temperature and sample size on coal conversion and product yield for DECS-8 for non-catalyzed samples.

Exp.No	Catalyst	Sample Weight	Temp. (C)	Conv. wt%	Gas wt%	Oil wt%	Asp. wt%	Preasph wt%
A7	no cat.	3	425	37.9	3.1	25.4	4.8	4.6
A15	no cat.	1	425	39.9	3.1	28.4	6.1	2.3
A22	no cat.	2	425	26.7	2.9	12.0	7.2	4.6
A40	no cat.	1	450	42.7	6.0	19.2	9.9	7.6

**Table 2.10B** Effect of temperature and sample size on coal conversion and product yield for DECS-8 for non-catalyzed samples.

Exp.No	Catalyst	Sample Weight	Temp. (C)	Conv. wt%	Gas wt%	Oil wt%	Asp. wt%	Preasph wt%
B7	no cat.	3	425	23.6	1.7	15.8	3.0	3.1
B15	no cat.	1	425	42.6	1.9	33.1	3.3	4.3
B22	no cat.	2	425	27.3	3.1	11.6	8.2	4.4
B40	no cat.	1	450	23.5	2.1	10.9	5.2	5.3

**Table 2.11** Effect of temperature and sample size on product yield for atmospheric residue.

Exp.No	Catalyst	Sample Weight	Temp. (C)	Conv. wt%	Gas wt%	Oil wt%	Asp. wt%	Preasph wt%
A26	no cat.	2	425	98.9	4.3	91.5	3.0	0.2
A34	no cat.	2	425	98.5	3.5	87.8	6.8	0.4
B26	no cat.	4	425	99.0	4.3	91.5	3.0	0.2
B34	no cat.	3	425	98.7	3.3	86.0	9.0	0.4
A48	1%Co(2)	1	425	98.7	9.0	84.7	4.1	0.9
B48	1%Co(2)	2.5	425	97.5	7.0	82.7	6.6	1.2
A51	1% Ni(2)	1.7	375-425	97.9	5.2	88.8	3.4	0.5
B51	1%Ni(2)	2.5	375-425	98.9	3.5	92.7	2.3	0.4
A52	1% Ni(2)	1	425	98.5	6.7	80.8	9.2	1.8
B52	1%Ni(2)	2.5	425	96.7	3.5	85.7	7.1	0.4
A54	1%Ni(1)	1.8	450	93.0	6.7	78.8	0.6	6.9
B54	1%Ni(1)	2	450	91.6	7.7	76.9	1.1	5.9
A53	1%Ni(1)	1.7	425	98.6	4.5	90.5	2.8	0.8
B53	1%Ni((1)	2.5	425	97.8	5.4	87.3	2.9	2.2

Legend:

Ni(1)- nickel 2-ethylhexanoate

Ni(2) -nickel chloride

Co(2)- cobalt chloride

**Table 2.12A** Gaseous products from liquifaction reaction for DECS-8 coal.

Exp. No.	CO	CH <sub>4</sub>	CO <sub>2</sub>	C <sub>2</sub> H <sub>6</sub>	C <sub>3</sub> H <sub>8</sub>	C <sub>4</sub> H <sub>10</sub>
A1	22.8	6.0	62.2	5.5	4.0	0.0
A2	2.7	7.1	78.6	5.1	4.5	2.0
A3	10.6	10.6	63.5	7.2	5.8	2.4
A4	0.1	17.9	57.2	12.0	8.9	4.0
A5	0.2	18.1	58.8	11.5	8.7	2.8
A6	0.5	12.3	60.5	9.5	11.7	6.0
A7	2.9	13.7	67.1	10.2	11.6	2.3
A8	0.2	18.6	41.1	26.1	4.2	9.9
A9	9.0	4.0	79.8	7.3	0.6	2.1
A10	6.2	12.4	55.2	10.9	11.2	3.9
A11	7.1	13.6	48.7	11.2	13.9	5.4
A12	12.9	14.3	40.2	13.4	14.3	4.7
A13	2.1	17.1	63.4	12.5	1.7	2.8
A14	2.6	18.9	65.2	10.8	1.9	0.5
A15	2.9	26.2	25.6	21.1	18.9	5.1
A16	0.4	16.1	63.3	12.2	4.9	2.8
A17	5.9	7.7	75.0	7.3	1.9	2.2
A18	8.2	13.5	45.0	13.2	15.5	4.1
A19	12.9	14.3	52.4	16.6	1.1	2.7
A20	11.4	18.6	37.1	15.4	12.7	2.8
A21	10.9	15.0	48.8	13.2	3.7	2.5
A22	10.6	37.3	13.0	28.8	4.2	6.0
A25	2.4	18.2	57.7	13.3	5.4	3.0
A26	0.0	78.3	0.0	12.5	5.4	3.7
A27	3.9	17.7	61.8	9.3	4.1	3.2
A28	3.3	16.5	55.2	12.3	7.9	4.8
A29	4.8	18.5	50.4	15.5	6.5	4.4

A30	6.6	15.9	51.1	12.3	8.7	5.4
A31	6.6	18.7	55.3	12.0	5.1	2.3
A32	2.7	17.2	37.5	20.8	17.3	4.5
A33	3.3	16.1	28.9	22.1	23.5	7.1
A34	0.1	28.8	0.2	29.2	26.5	9.8
A35	0.1	15.1	53.9	14.4	11.8	3.5
A36	2.0	22.2	38.5	18.2	14.6	4.3
A37	9.3	21.6	31.8	19.7	14.1	3.5
A38	9.8	22.2	34.8	16.5	13.1	3.6
A39	9.2	19.9	32.4	22.7	12.5	3.3
A40	6.5	20.0	41.9	15.6	12.0	4.1
A41	6.6	14.2	54.9	11.5	9.9	2.7
A42	3.9	12.5	58.2	11.7	10.1	3.4
A43	0.0	7.8	72.5	6.8	5.9	7.0
A44	11.5	5.7	49.1	7.3	25.3	1.1
A45	0.6	16.7	54.5	13.2	11.2	3.8
A46	6.0	7.2	73.1	6.2	5.7	1.7
A47	5.4	11.8	63.0	9.8	7.6	2.2
A48	0.0	35.4	0.0	35.3	29.3	0.0
A49	6.6	14.8	49.3	14.7	14.0	0.1
A50	8.6	17.9	47.1	13.6	9.7	2.9
A51	1.5	37.3	3.9	30.0	27.4	0.2
A52	7.6	27.2	18.2	24.1	22.5	0.2
A53	20.9	29.8	5.0	23.4	20.9	0.0
A54	5.4	46.3	1.8	25.3	21.2	0.0
A55	22.8	3.6	26.0	9.5	27.5	10.6
A56	20.3	3.6	30.0	9.2	26.2	10.6
A57	8.9	12.7	58.0	12.7	9.9	2.9
A58	10.8	13.3	57.5	9.3	5.9	3.2
A59	26.0	23.6	26.8	18.9	4.8	0.0
A60	22.1	27.3	33.2	13.2	3.1	1.1
A61	18.0	29.3	38.2	7.2	3.5	3.8
A62	17.6	30.3	36.2	6.9	6.3	2.7
A63	15.5	26.3	43.7	8.9	3.3	2.3
A64	13.3	28.9	49.6	3.9	2.9	1.4
A65	16.9	20.6	55.6	3.9	1.2	1.8
A66	10.2	19.5	33.9	12.9	18.2	5.3
A67	11.2	26.3	30.2	13.5	13.3	5.5

**Table 2.12B** Gaseous products from reaction of DECS-12 coal.

Exp. No	CO	CH <sub>4</sub>	CO <sub>2</sub>	C <sub>2</sub> H <sub>6</sub>	C <sub>3</sub> H <sub>8</sub>	C <sub>4</sub> H <sub>10</sub>
B1	0.1	29.1	36.6	17.0	11.2	5.8
B2	3.1	22.2	29.5	15.0	12.2	18.3
B3	0.2	40.2	18.5	22.7	13.7	4.9
B4	0.0	46.1	3.3	26.7	17.0	6.9
B5	1.7	30.8	13.8	20.8	19.7	13.3
B6	2.3	37.4	13.2	27.9	3.2	16.0
B7	0.8	37.0	14.1	23.5	21.0	3.6
B8	0.1	30.6	58.0	5.4	4.1	1.8
B9	2.7	27.4	38.7	18.7	9.1	3.3
B10	1.8	31.2	36.4	22.3	0.0	8.2
B11	5.7	35.3	11.5	24.2	17.7	5.5
B12	6.4	34.9	12.2	24.7	19.2	2.5



B13	1.8	31.2	36.4	22.3	0.0	8.2
B14	2.2	33.2	36.4	21.8	0.8	5.5
B15	5.2	31.3	10.6	23.6	22.0	7.2
B16	0.8	26.3	36.5	19.3	11.5	5.6
B17	7.8	27.4	35.0	19.7	3.8	6.1
B18	10.4	14.2	55.0	10.0	7.6	2.6
B19	0.4	32.8	23.3	23.0	6.5	4.6
B20	6.0	25.5	31.3	18.6	12.8	5.2
B21	4.6	30.4	22.6	24.1	11.4	6.7
B22	1.2	36.5	14.5	25.2	17.7	4.8
B25	2.8	16.5	47.8	18.4	9.8	4.7
B26	0.0	79.1	0.0	12.3	5.2	3.4
B27	4.6	19.8	47.2	14.9	7.9	5.6
B28	6.1	17.8	47.9	12.3	8.5	3.4
B29	5.4	15.4	53.9	13.2	7.6	4.5
B30	4.9	19.8	46.3	14.5	8.7	5.8
B31	4.7	22.3	43.9	14.7	7.8	6.6
B32	1.8	15.5	34.5	28.7	11.8	7.7
B33	1.3	22.6	5.8	30.0	30.4	9.8
B35	0.7	18.8	37.3	29.6	2.7	10.8
B36	0.1	37.6	11.0	26.3	19.2	9.9
B37	6.7	30.6	27.5	20.2	11.2	3.8
B38	10.3	21.6	36.5	14.8	12.1	3.5
B39	5.7	32.3	9.9	27.6	18.9	5.5
B40	4.8	33.1	11.8	24.5	19.8	6.0
B41	3.7	32.6	10.3	25.5	28.1	5.7
B42	9.8	33.6	6.5	25.3	17.9	6.7
B43	0.0	31.1	15.0	23.6	17.5	12.8
B44	0.0	29.4	2.4	24.8	22.8	20.5
B45	0.0	23.6	30.0	19.5	18.4	8.3
B46	0.0	30.0	22.6	25.4	23.0	0.0
B47	7.4	33.6	9.3	24.7	17.1	7.8
B48	0.0	39.3	0.0	31.7	20.4	8.6
B49	0.3	37.8	10.9	27.4	17.2	6.2
B50	0.7	33.6	13.6	25.4	19.2	7.2
B51	11.3	31.0	11.1	17.3	14.6	4.6
B52	15.0	23.8	15.0	20.5	18.7	5.8
B53	21.3	28.2	5.6	24.9	20.0	0.0
B54	17.6	19.9	7.7	23.4	23.5	7.8
B55	37.4	3.7	11.8	8.9	25.5	12.7
B56	20.7	3.3	34.0	8.3	22.1	11.5
B57	7.0	30.5	12.2	22.8	19.5	8.0
B58	3.7	38.2	9.0	25.7	18.4	5.0
B59	8.1	35.7	8.8	23.3	18.3	5.6
B60	6.3	33.7	9.3	18.9	17.9	13.9
B61	7.9	29.6	10.9	21.3	13.9	16.4
B62	9.3	30.2	15.9	17.6	19.3	7.7
B63	4.9	35.6	18.3	12.2	17.7	11.3
B64	7.6	21.2	31.3	18.2	13.2	8.5
B65	11.1	28.2	9.3	22.7	18.7	10.5
B66	7.2	30.5	10.7	19.9	21.3	10.4
B67	9.6	27.7	12.1	17.6	19.2	13.7

### 3.0 THERMAL STABILITY TESTING OF COPROCESSED LIQUIDS

*Four candidates for high thermal performance jet fuels, one coal derived (JP8C) and three petroleum derived (JP8P, DA/HT LCO, and HT LCO), were studied at 480°C with stressing periods of up to 2 hours. A light cycle oil, extensively hydrogenated to remove all aromatics and obtain a high content of cycloalkanes (DA/HT LCO), suppressed the solid deposition to a greater extent than did the more paraffinic JP8P by nearly 3 wt% after 2 hours at 480°C (900°F). Furthermore, the DA/HT LCO showed a performance comparable to that of the coal-derived fuel JP8C concerning the solid formation. The hydro-aromatic light cycle oil, HT LCO, gave the highest rate of solid deposition but the lowest gas yield. A solution-state  $^{13}\text{C}$  NMR investigation of the overall structure indicated that the solid deposition is a function of the rise in the aromatic content and also the amount and rate of development of the non-protonated aromatic carbons. Both the solution-state  $^{13}\text{C}$  NMR and GC/MS analysis of the stressed fractions confirmed that the paraffinic content is the component to be transformed first during the thermal stressing. As the gas yield for the DA/HT LCO was considerable higher than that of the coal-derived JP8C, a simple titration of DA/HT LCO removed paraffins above C15. However, only small improvements in the gas and solid yields were observed, which may be linked to the observation that the highly alkylated cycloalkanes present in the DA/HT LCO also contributed to the gas production.*

#### 3.1 Introduction

The ultimate goal of the ongoing jet-fuel project at PennState is to develop coal-based advanced jet fuels that meet the JP-900 thermal-stability requirement set up by the US Air Force [3]. Since the fuel functions as the main coolant for the different electronic and mechanical parts of the aircraft, thermal stability and especially depression of solid deposition are key elements in this research [4]. In current commercial planes, the fuel rarely is exposed to temperatures above 300 °C. However, as the flight speed will be increased, the fuel is expected to experience temperatures as high as 900 °F. Even though the residence time at such elevated temperatures is expected to be fairly short (a matter of minutes), the fuel will be recycled through the cooling process and consequently will have been exposed to coking temperatures for a considerably long time. Previous research at PennState has established that a solution to this problem can be

achieved using cycloalkane-rich fuels. [5,6] Coal-derived aviation jet fuels have been found to contain considerable amounts of cycloalkanes and indeed have shown superior thermal stability compared with petroleum-derived fuels which are rich in linear and branched alkanes. [7,8] Model compounds, such as linear alkanes and alkyl substituted ones, have been extensively studied at temperatures around 400-475 °C, where the superior stability of cycloalkanes, when compared with linear alkanes, has been confirmed. Cycloalkane-rich liquids can be readily derived through hydrogenation of inexpensive liquids with high contents of benzenes and naphthalenes. Coal liquids are a clear favorite in this aspect, but due to the higher availability of petroleum products, the latter have been considered in this study. The hydrogenation of a highly aromatic petroleum middle distillate has been a successful route in avoiding a high-alkaline content and producing a fuel rich in cycloalkanes at a lower cost. British Petroleum (BP) was contracted to produce such a fuel from an aromatic petroleum fraction. [9] The approach taken was dearomatization by hydrogenation of a light cycle oil (LCO). The differences in the chemical composition and thermal stability between this fuel and a conventional petroleum-derived jet fuel (JP8P) were, as expected, based on their differences in alkane content, where the hydro-treated LCO had a paraffin content of about 19 wt% compared with a content of about 56 wt% for the JP8P. This was reflected in a highly reduced solid deposition at 480 °C with a residence time of 2 hours, in which the JP8P had a solid deposition of about 8 wt% compared with about 4 wt% for the hydrogenated LCO. Further studies on a coal-derived jet fuel (JP8C) showed that the LCO-derived fuel performed similarly on the basis of solid deposition, but the coal-derived fuel was still superior when the gas production was considered.

### 3.2 Experimental

The hydro-treated light cycle oil (DA/HT LCO) was produced by BP through three stages: (i) severe hydrotreatment of the LCO at 350 °C, (ii) dearomatizing (335 °C), and (iii) further hydrotreatment at 320 °C. [9] The commercial petroleum-derived jet fuel analyzed was JP8P. The former was stressed at both 450 and 480 °C, while JP8P only at 480 °C. A volume of 5 ml was used, which was charged into a microautoclave with a total volume of 25 ml. [5] To remove entrapped air, the system was degassed 6 times with 1000 psi of ultra-high-purity N<sub>2</sub> (99.999%). Under an initial pressure of 100 psi N<sub>2</sub>, the mixtures were stressed with a continuous vertical movement of 40 strokes per minute in a fluidized sandbath. After reaction, the microautoclaves

were rinsed of sand and quenched with water for about 5 seconds for instant cooling. When the microautoclaves were cooled to ambient temperature, the gas phase and liquid fraction were removed for analysis. The tube and the stem of the microautoclave were washed in pentane until clear colored and dried. The weight gain from the amount of solid deposition was determined.

The GC-MS analysis was performed on a Hewlett-Packard 5890 Series II GC coupled with an HP 5971A MS detector. The column used was a slightly polar J&W DB-5 coated with 5% phenyl-95% methyl polysiloxane; it was heated from 40 to 290 °C at a heating rate of 3 to 6 °C min<sup>-1</sup>. Approximately 90-95 % of the area was investigated, accounting for approximately 200-300 peaks in each case.

The solution-state <sup>13</sup>C NMR was performed on a Bruker AMX360 with an 8.4-T field equivalent to a 90-MHz resonance frequency for <sup>13</sup>C. Approximately 0.2 ml was diluted in 1-ml CDCl<sub>3</sub> and charged into a 5-mm tube. The gated decoupling pulse sequence with a 7-second pulse delay was found to give a quantitative spectrum.

### 3.3 Results and Discussion

#### Characterization of the Fuels

Figure 3.1 shows the main compound groups present at the different stages during the production of DA/HT LCO. Based on the GC-MS analysis at PennState, the LCO itself contained about 91-mole% aromatics. The distribution of mono, di, and tri+ aromatics is about 34, 34, and 10 mole%, respectively, and a considerable amount of bi-phenyls and smaller amounts of indenenes and fluorenes make up the remainder, accounting for 13 mole%. The concentration of alkanes was low, close to 8 mole% and alkenes 2 mole%. After hydro-treatment, the DA/HT LCO fuel displayed around 66-mole% mono aromatics and small amounts of the other aromatic groups. Of the mono-aromatics only 1/3 was alkyl-substituted benzenes, while the majority was hydro-aromatics, mainly in the form of tetralins (30 mole%) and a minor amount of 2,3 dihydro-1H-indenenes (10 mole%). The alkane fraction was still low with an abundance of only 13 mole%. Through further dearomatization by hydrogenation, the goal of a highly cycloalkane-rich product with a low aromatic content was obtained (Figure 3.1). The DA/HT LCO fuel contains 79-mole% cycloalkanes, where cyclohexanes (32 mole%) and decalins (32 mole%) dominated. Other cycloalkanes (10 mole%) consisted mostly of cyclopentanes, octahydro-indenenes, and dicyclohexyl-type cycloalkanes. Also decahydro-

phenanthrenes and larger cycloalkane systems were found (5 mole%). Less than 1-mole% mono-aromatics, about 2-mole% alkenes, and a relatively small amount of linear (15 mole%) and branched (4 mole%) alkanes were observed. To summarize the process, the mono- and di-aromatics in the original LCO (both around 34 mole%), have been successfully transformed into their hydrogenated counterparts (cyclohexanes and decalins, both around 32 mole%).

The compositions of the petroleum-derived jet fuel, JP8P, and the coal-derived JP8C are compared in Figure 3.2. The JP8P shows a considerably high amount of paraffins, about 56 volume%, and a lower amount of cycloalkanes, about 16 volume%. The coal-derived jet fuel, JP8C, has a very low linear-alkane content of 10 volume% and a considerably higher cycloalkane content of 51 volume%. The JP8C has a further advantage of containing about 22-volume% hydroaromatics, where alkylated tetralins dominate, compared with JP8P, which is virtually free of these compounds. Both jet fuels contain 17-18 volume% of alkylated aromatics, but only JP8P contains larger aromatic-ring systems, such as naphthalenes (6 volume%). The differences between the two petroleum-derived jet fuels, JP8P and DA/HT LCO, are shown in Figure 3.3, where their GC/MS traces are compared. The alkane distribution is clearly different for the two fuels. For the JP8P, the dominant alkanes are C10-C14 at retention times between 5 and 20 minutes, while for the DA/HT LCO fuel, the alkanes are in general larger with major peaks appearing at retention times as long as 40 minutes. The differences shown through Figures 3.1-3.3 clearly indicate that solid deposition and gas production for the different fuels should differ significantly as shown below.

#### Thermal Performance of the Fuels.

Figure 3.4 shows the gas yield and amount of solid deposition for the DA/HT LCO fuel stressed at 450 °C for up to 16 hours. Solid formation starts at about 4 hours and increases to 6 wt% at 16 hours stressing. This is similar to results found for the coal-derived jet fuel JP8C at these temperatures and times. [5] However, gas formation is slightly higher than that observed from JP8C but still lower than that from the petroleum-derived jet fuel JP8P. [9] This indicates that the high content of cycloalkanes most likely prevents the formation of solids, whereas the relatively large concentration of linear/branched alkanes, such as in petroleum-derived JP8P, leads to a more dominant gas production when compared with the coal-derived jet fuel JP8C. [8]

A further thermal comparison has been performed on the three different petroleum-derived jet fuels, DA/HT LCO, HT LCO, and JP8P, and the coal-derived JP8C, at 482 °C (900°F) with stressing times of up to 2 hours. Figure 3.5 shows their gas yields at that temperature at different stressing times. As expected, JP8P has the highest gas production due to its high linear-alkane content (Figure 3.2). However, gas production from the severely hydrogenated light cycle oil DA/HT LCO is also generally high, reaching about 30 wt% after 2 hours. The lowest gas yield is obtained for HT LCO, where only 20 wt% of gas is produced after a 120-minute residence time at 480 °C. This is well below the gas yield for JP8C of 25 wt% at the same conditions. The low gas yield of HT LCO compared with DA/HT LCO can only be explained on the basis of the high content of hydroaromatics present in HT LCO (Figure 3.2). However, the formation of solid deposits, shown in Figure 3.6, indicates a different performance of the fuels studied. The HT LCO developed a surprisingly high amount of solids, 13 wt%, after 2 hours at 480 °C. This can be related to its high sulfur content (150 ppm wt%), but more likely to the high amount of 2- and 3-ring aromatics still present in this fuel (Figure 3.2). The transformation of tetralins to naphthalenes as the hydrogen is consumed by the thermal reactions during stressing is also likely to increase the aromatic content. DA/HT LCO shows a great reduction in the solid deposition with only 5-wt% residue, when compared with HT LCO. This is also an enhancement when compared with JP8P (about 8 wt% after 2 hours) and is similar to the one obtained for the coal-derived JP8C (4 wt%). However, JP8C is still the superior fuel when compared with the petroleum liquids.

#### Overall Chemical Changes during Stressing

The solution-state  $^{13}\text{C}$  NMR spectrum of the coal-derived jet fuel JP8C is shown in Figure 3.7, and indicates the general peak assignment used to interpret the different spectra. The solvent used,  $\text{CDCl}_3$ , appears at 77 ppm and is well removed from the two main areas of interest. The aliphatic carbons are grouped into methyls ( $\text{CH}_3$ , 24-0 ppm), methylenes, and methines ( $\text{CH}_2$  and  $\text{CH}$ , respectively, 50-24 ppm) and aliphatic carbon bound to heteroatoms (e.g. esters and methoxy, 100-50 ppm). The aromatic carbons appear at lower fields. The most shielded are the aromatic carbons bound to heteroatoms (mostly phenols, 220-148 ppm). There are two main differences between the different aromatic carbons, the ones bound to protons and the ones not bound to protons, referred to as protonated and non-protonated, respectively. The protonated

aromatic carbons are less shielded, and extensive research has established that the chemical shifts between 129.5 and 100 ppm are predominantly due to protonated aromatic carbon. Non-protonated aromatic carbons have been found to appear between 148 and 129.5 ppm. The change in the aliphatic and aromatic carbons as a function of heating is shown for the DA/HT LCO in Figure 3.8. DA/HT LCO shows no concentration of aromatic carbon as received, but after only 30 minutes of stressing, a clear indication of aromatic-carbon production is evident. As the stressing time is increased to 2 hours, there is a significant rise in the aromatic content. Figure 3.9 compares the rise in the aromatic content for the four jet fuels, DA/HT LCO, HT LCO, JP8P, and JP8C, at residence times up to 2 hours at 480 °C. As expected, HT LCO shows the highest aromaticity at all stressing times, which corresponds well with the high solid deposition observed. Both JP8C and DA/HT LCO show very low aromatic levels at all residence times. However, the rise in the production of aromatic carbon is much higher for DA/HT LCO than for the coal-derived jet fuel. This indicates that JP8C has a greater ability to slow down the aromatization process and subsequently prevent solid deposition to a greater extent than does DA/HT LCO. JP8P fuel has an initial aromatic ratio of 0.1, similar to that of the coal-derived fuel. However, as in DA/HT LCO, the increase in the aromatic-carbon content is higher, again corresponding to a higher rate of solid deposition.

From Figure 3.8 it is apparent that the increase in the aromatic content for DA/HT LCO appears primarily at 126 ppm, which is in the region for protonated aromatic carbons. Hence, the ratio of the non-protonated aromatic-carbon content can indicate the extent of condensation appearing as the residence time is increased. Figure 3.10 compares this ratio for the four jet fuels, DA/HT LCO, HT LCO, JP8P, and JP8C, at residence times of up to 2 hours at 480 °C. Again, HT LCO has by far the highest values, confirming that aromatization of the liquid is the factor most responsible for solid deposition. Even though JP8P and the coal-derived JP8C start out at the same level, the petroleum-derived fuel has a much-more rapid increase, resulting in higher solid deposition, as seen in Figure 3.6. Concerning aromaticity, DA/HT LCO again has the lowest starting point, but its increase in non-protonated aromatic carbon is much greater than that for the coal-derived fuel, resulting in comparable but slightly higher solid yields.

As a consequence of the increase in aromaticity with longer stressing times (Figure 3.8), the aliphatic content decreases. The ratio of the concentration of methylene and methine carbons (referred to as  $\text{CH}_2$ ) to the concentration of methyl carbons ( $\text{CH}_3$ ) can be viewed as the extent of

paraffinic cracking occurring during stressing. This fraction will be large for unreacted liquids, but as the chains are shortened and the hydrogen-transfer process from C-rich to H-rich becomes more extensive, this fraction will decrease. Figure 3.11 compares the  $\text{CH}_2/\text{CH}_3$  ratio for the four jet fuels, DA/HT LCO, HT LCO, JP8P, and JP8C, at residence times of up to 2 hours at 480 °C. The large cycloalkane content in JP8C and DA/HT LCO gives initial ratios between 2.5 and 3, while the lower values for JP8P and HT LCO indicate that these are branched or substituted aromatics. As the degree of thermal stressing increases, the  $\text{CH}_2/\text{CH}_3$  ratio falls for all the fuels. The fuel experiencing the most dramatic decrease is HT LCO, as expected from its high solid yield (Figure 3.6). JP8P also shows little ability to retain a highly aliphatic character, as the  $\text{CH}_2/\text{CH}_3$  ratio decreases by about 40%, from 1.8 as received, to about 1.1 after 2 hours of stressing at 480 °C. In comparison, JP8C and DA/HT LCO lose only 30% of their  $\text{CH}_2/\text{CH}_3$  ratio, indicating a greater ability to conserve their cycloalkanes.

The chemistry involved comprises a wide variety of organic reactions, and possibly catalytic interactions with the metal wall of the microautoclave and remaining heteroatoms in the fuel, such as sulfur and transition metals. Therefore, a crude separation into the main functional groups was made; Table 3.1 lists these for the original DA/HT LCO and JP8P and their liquid product at 45 minutes (480 °C) on the basis of initial liquid used. Clearly, the alkanes have been consumed in both fuels, falling from 54 to 13 mole% for JP8P and from 19 to 7 mole% for DA/HT LCO. The cycloalkanes show a minor decrease for JP8P, confirming their thermal stability as discussed previously. However, the cycloalkanes from DA/HT LCO experience a significant decrease of 27 mole%. The highest rise occurs, as expected, for the benzenes and naphthalenes, where the alkylbenzenes increased about 10-14 mole% and the naphthalenes 7-8 mole%.

### Upgrading of DA/HT LCO by Distillation

From Table 3.1 it is clear that the high gas yield from JP8P is due to linear alkanes being cracked during stressing. DA/HT LCO also shows a significant decrease in paraffinic yield (12 mole%) as demonstrated by significant gas production (Figure 3.5). This has been associated with the high content of alkanes (tetradecane and above, Figure 3.3), which are readily cracked at elevated temperatures. During the hydrogenation of the light cycle oil, the aromatic compounds



were targeted due to their transformation into thermally stable cycloalkanes, while the linear alkanes remained unconverted. A literature search produced the distillation plot for linear alkanes shown in Figure 3.12, where the boiling-point ranges for the cycloalkanes of interest are included. Therefore, a simple distillation of a mixture with a cut-point between 240 and 250 °C should result in a separation of the linear alkanes from the cycloalkanes, yielding a potentially superior, thermally stable jet fuel. The GC traces shown in Figure 3.13 indicate that a successful separation of the linear alkanes from the cycloalkanes was obtained. The original DA/HT LCO (bottom) shows a significant concentration of long-chain alkanes at longer retention times. The fraction boiling off below 250 °C (middle) is virtually free from the long-chain alkane compounds, which were retained in the fraction with boiling points above 250 °C (top).

The GC traces in Figure 3.13 indicate that a successful separation of the linear alkanes (above 250 °C) from the cycloalkanes (below 250 °C, B250) had been achieved. GC/MS analysis has been performed to analyze further the product distribution in these fractions and is shown in Figure 3.14. The fraction distilled off below 250 °C (B250) has an improved cycloalkane content of about 92 mole% compared with 79 mole% for DA/HT LCO. This has been achieved largely by a reduction in the long-chain alkanes (pentadecane and higher), where the remaining 7 mole% of alkanes are in the decane-to-tetradecane range. The reduction in alkanes is gained mostly by an increase in mono-cycloalkanes (mainly substituted cyclohexane and some cyclopentane). These mono-cycloalkanes are also enhanced due to a reduction in the tri<sup>+</sup>-cycloalkanes (14H-phenanthrene and higher). However, the di-cycloalkane (mostly substituted decalins) concentration has remained fairly stable around 31 mole%. The composition of this distilled fraction is very promising. Its thermal performance is shown in Figure 3.15, where the gaseous product is compared with the solid residue formed during the stressing of B250 at 480 °C for up to 2 hours. The solid formation appears after 60 minutes of stressing and reaches a level of about 4.8 wt% after 2 hours. Compared with the situation for DA/HT LCO at 480 °C (Figure 3.6), where the solid deposition also appears after 1 hour, the rate at which the solids accumulate is similar; however, B250 has 0.2 to 0.5 wt% less solid deposition overall. However, the solid deposition is generally 0.3 to 0.6 wt% higher for B250 than for the coal-derived JP8C. The gas formation for B250 is also similar but slightly less than that for DA/HT LCO (1-5 wt%) reaching 32 wt% after 2 hours of stressing. Again, coal-derived JP8C shows better performance than does B250 in that JP8C has a 3-9 wt% lower gas production

overall. The reduced gas formation for JP8C is probably due to its high content of hydro-aromatics (mainly tetralin and related compounds) and a higher proportion of branched cycloalkanes in B250.

### 3.4 Conclusion

The thermal performance of four jet fuels, one coal derived (JP8C) and three petroleum derived (JP8P, DA/HT LCO, and HT LCO), has been studied at 480 °C with stressing periods of up to 2 hours. The extensively hydrogenated light cycle oil (DA/HT LCO) suppressed the solid deposition to a greater extent (by nearly 3 wt%) than did the more paraffinic JP8P and showed performance comparable with that of JP8C. The hydro-aromatic HT LCO had the highest rate of solid deposition but the lowest gas yield. A solution-state  $^{13}\text{C}$  NMR investigation of the overall structure indicates that solid deposition is a function of the rise in aromatic content and the amount and rate of formation of non-protonated aromatic carbons. Both solution-state  $^{13}\text{C}$  NMR and GC/MS analysis of the stressed fractions confirmed that the paraffinic content is the component to be transformed first during thermal stressing. As the gas yield for DA/HT LCO was considerably higher than that for the coal-derived JP8C, a simple titration of DA/HT LCO removed paraffins above C15. However, only a small improvement in the gas and solid yields was observed, which may be linked to the high content of alkylated cycloalkanes present in DA/HT LCO and its lack of hydroaromatics.

**Table 3.1** Distribution of the chemical composition for DA/HT LCO and JP8P on the basis of initial amount, both original and stressed at 480 °C for 45 min under 100 psi  $\text{N}_2$ .

	DA/HT LCO mole%	DA/HT LCO 45 min / mole%	JP8P mole%	JP8P 45 min mole%
Alkanes	18.8	6.7	54.1	13.0
Cyclo-alkanes	78.8	52.0	16.6	11.1
Alkenes	2.0	0.4	3.5	1.0
Hydroaromatics	<0.1	7.5	0.3	5.5
Alkyl-Benzenes	0.4	9.7	19.0	33.6
Bi-phenyls	< 0.1	5.8	0.4	2.4
Naphthalenes	< 0.1	6.7	6.2	14.7
Phenanthrenes	< 0.1	0.4	< 0.1	0.3
Pyrenes+	< 0.1	< 0.1	< 0.1	0.4

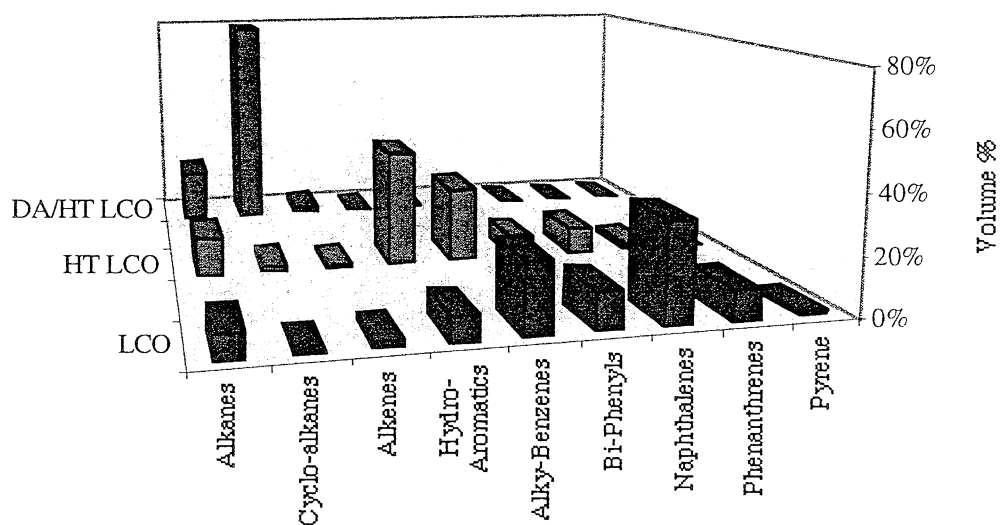


**Figure 3.1** Changes in chemical composition during hydrotreatment and dearomatization for the light cycle oil.

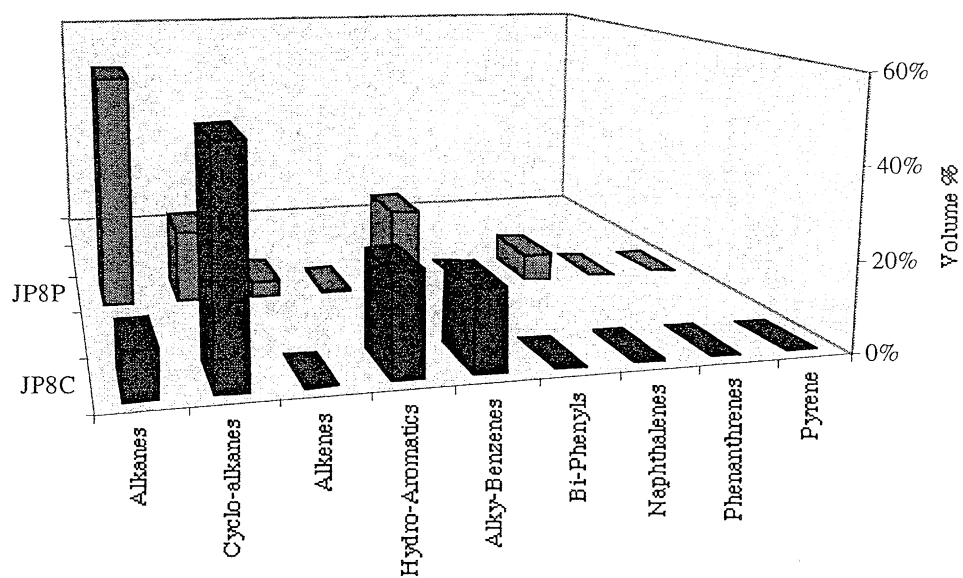


**Figure 3.2** Differences in the chemical composition of the petroleum-derived jet fuel JP8P and the coal-derived JP8C.

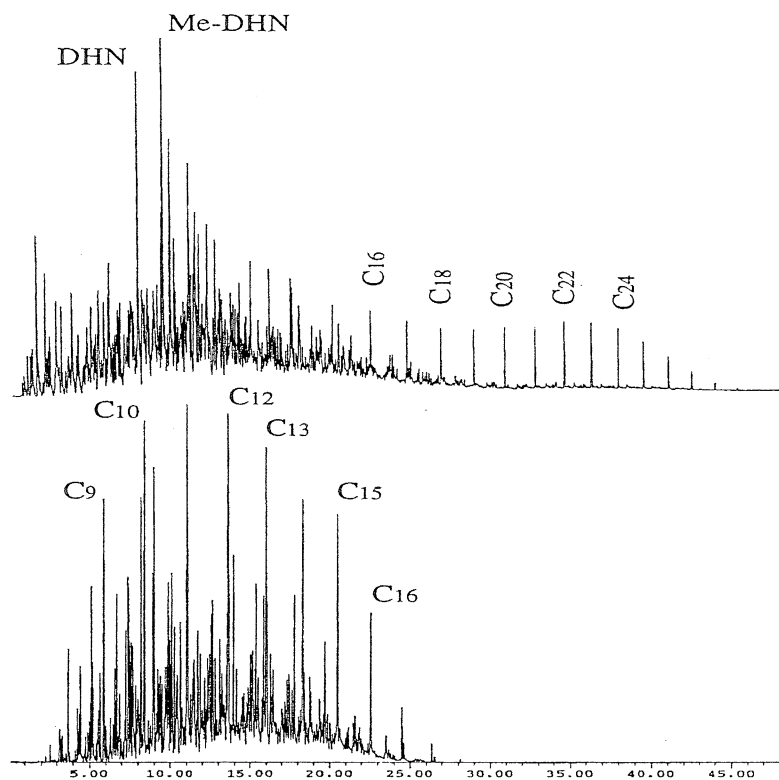


**Figure 3.3** GC-MS traces of the DA/HT LCO (top) and JP8P (bottom).

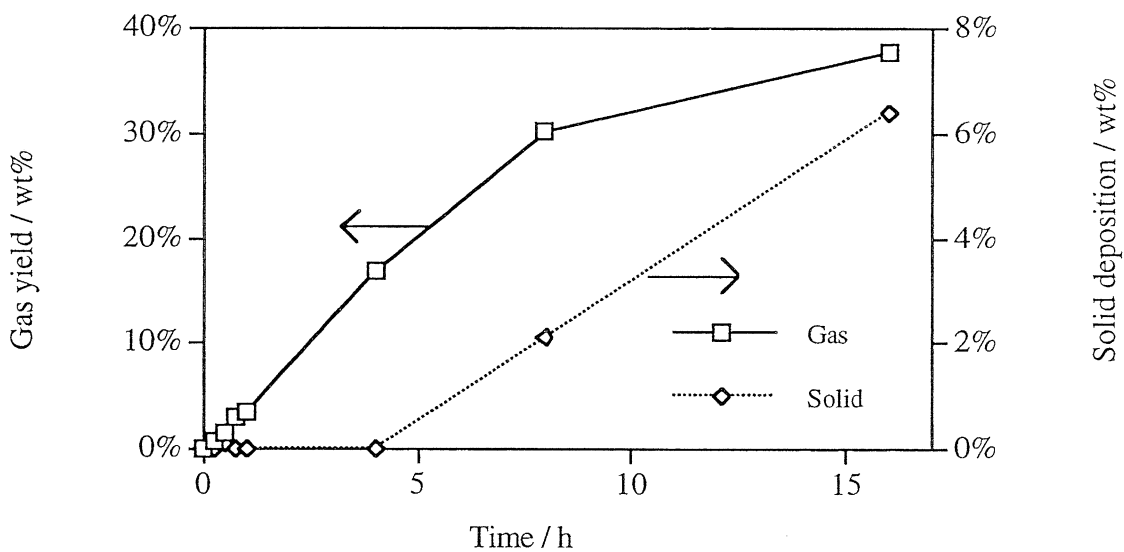


**Figure 3.4** Changes in gas and solid yields during stressing of DA/HT LCO at 450 °C under 100 psi N<sub>2</sub>.

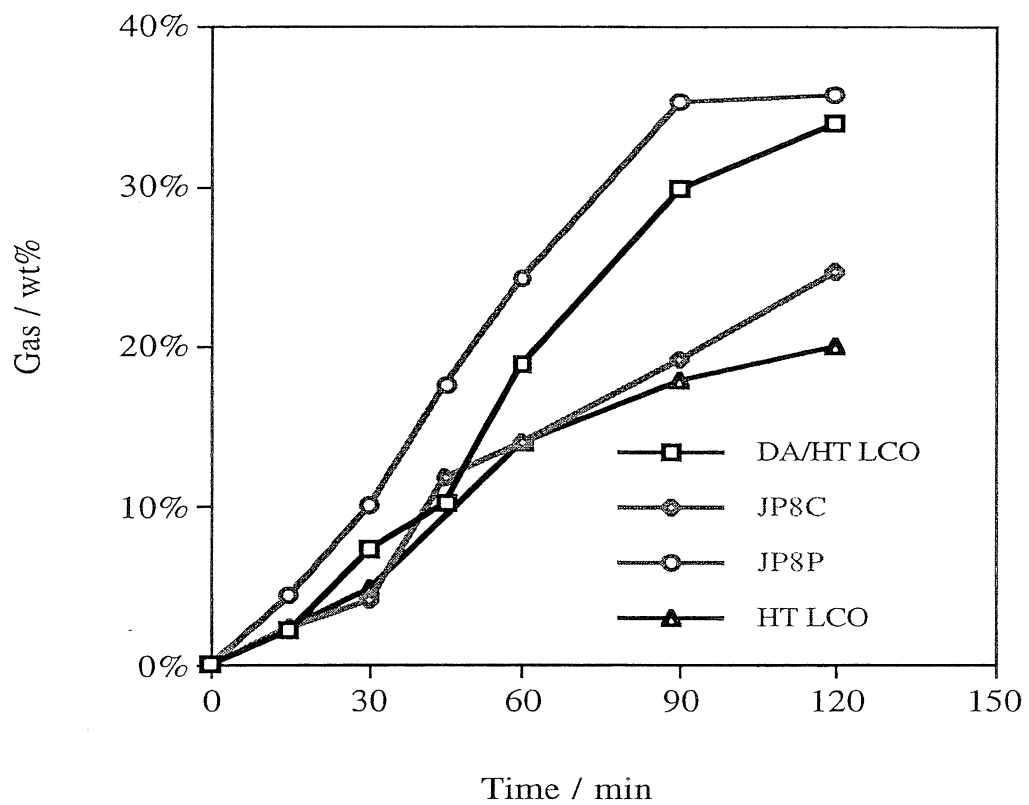


**Figure 3.5** Variation in gas yield for DA/HT LCO, HT LCO, JP8P, and JP8C at 480°C (900F).

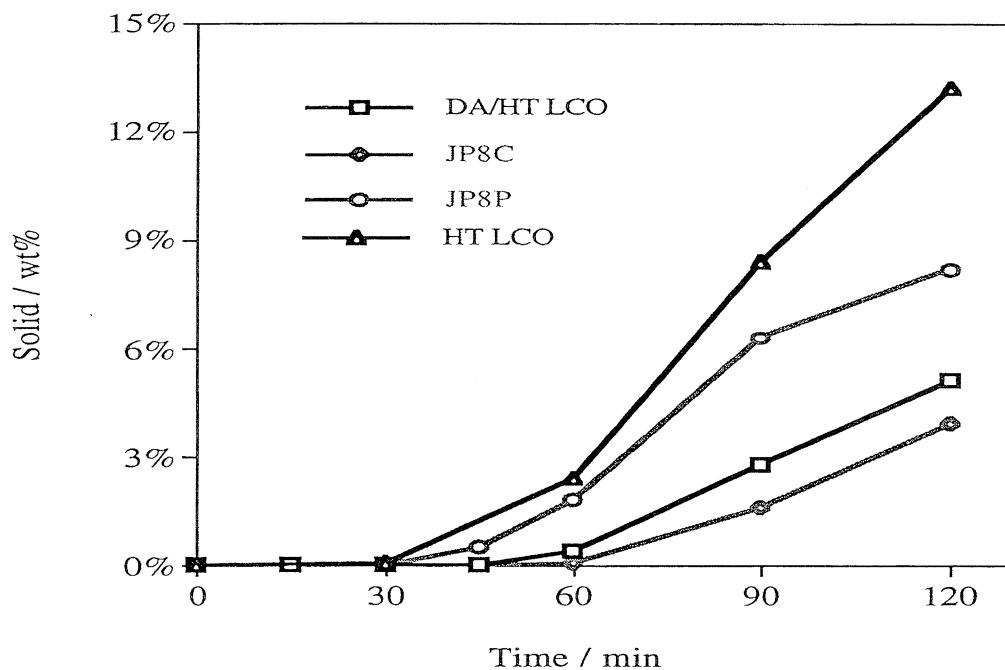


**Figure 3.6** Differences in the solid deposition formation for DA/HT LCO, HT LCO, JP8P, and JP8C at 480 °C.

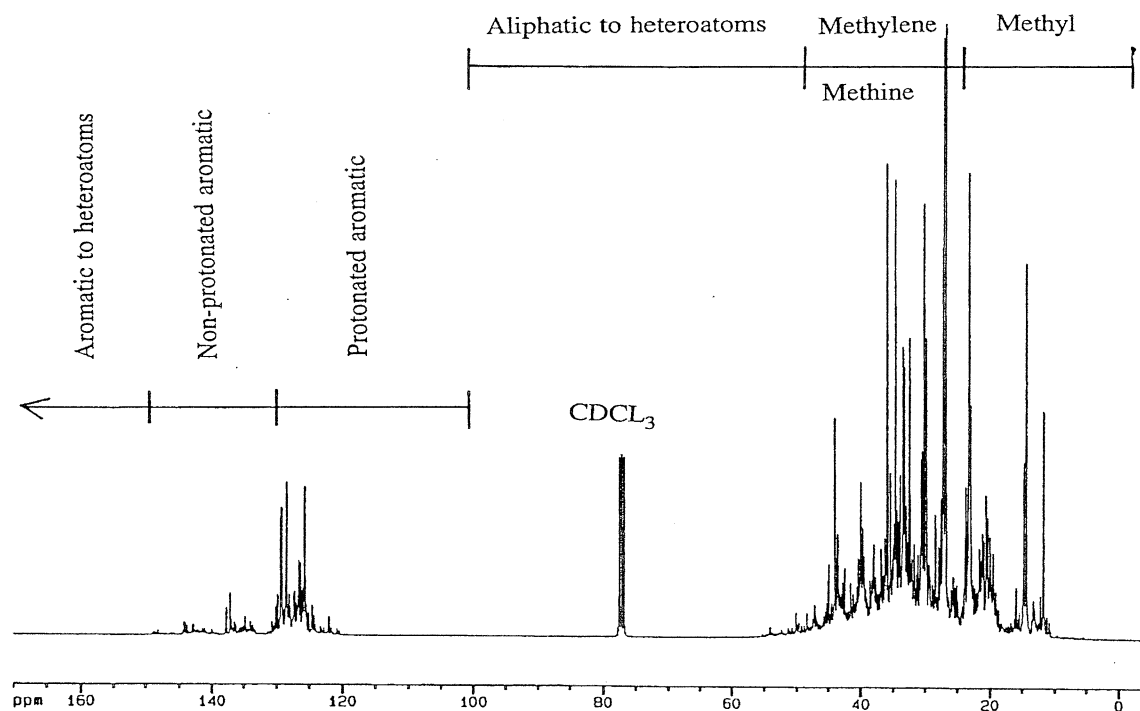


**Figure 3.7** The solution-state  $^{13}\text{C}$  NMR spectrum of the coal-derived jet fuel, JP8C, showing the general peak assignment.

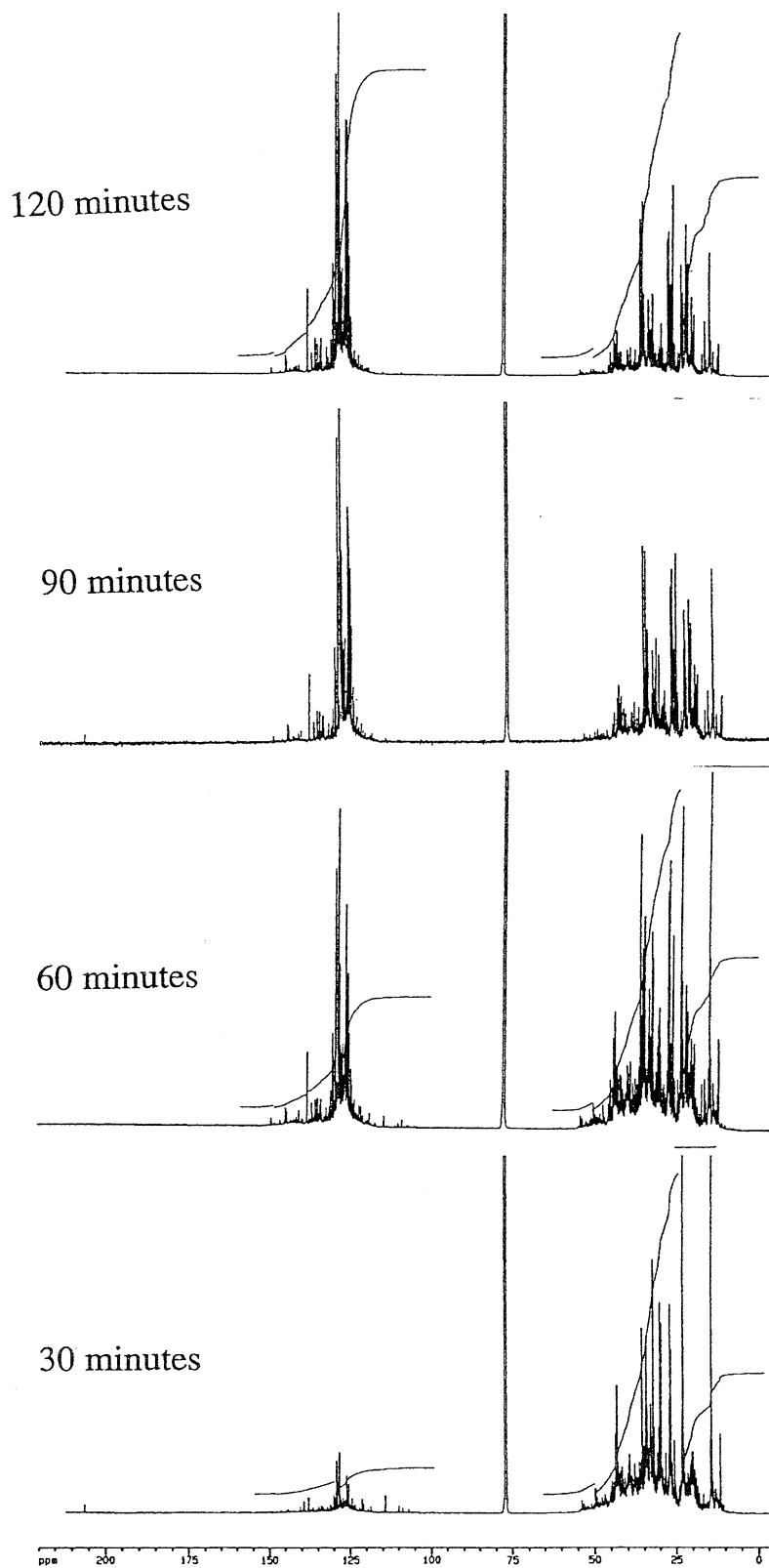


**Figure 3.8** Changes in the main functional groups for DA/HT LCO as the residence time at 480 °C is increased from 30 minutes to 2 hours.

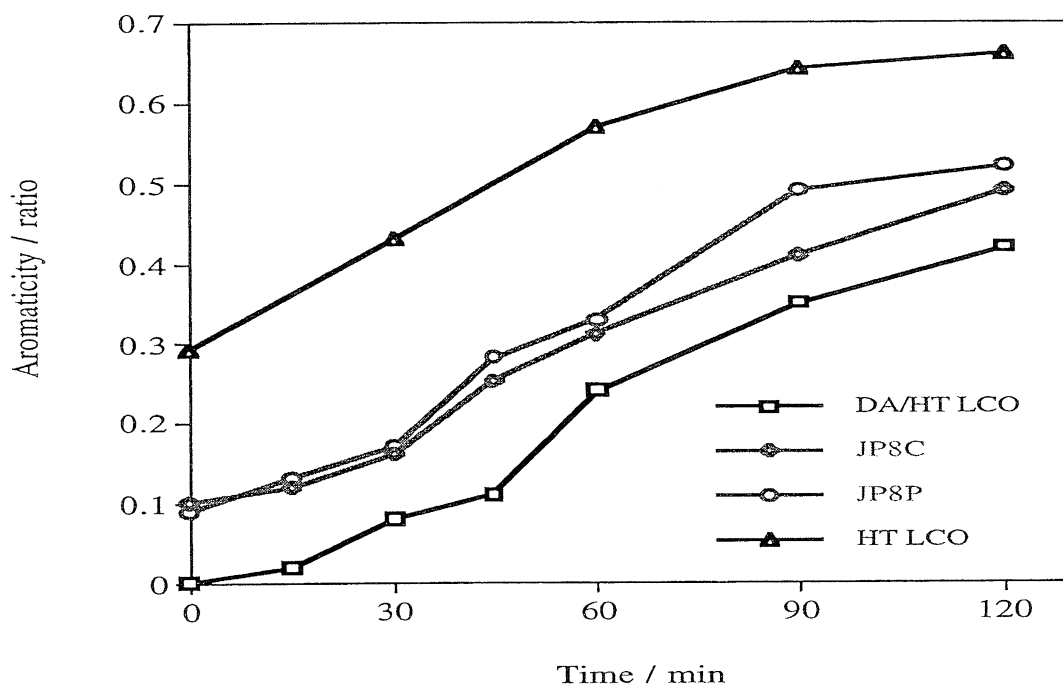


**Figure 3.9** Changes in the aromatic content for the four jet fuels, DA/HT LCO, HT LCO, JP8P, and JP8C, stressed at 480 °C with residence times of up to 2 hours.

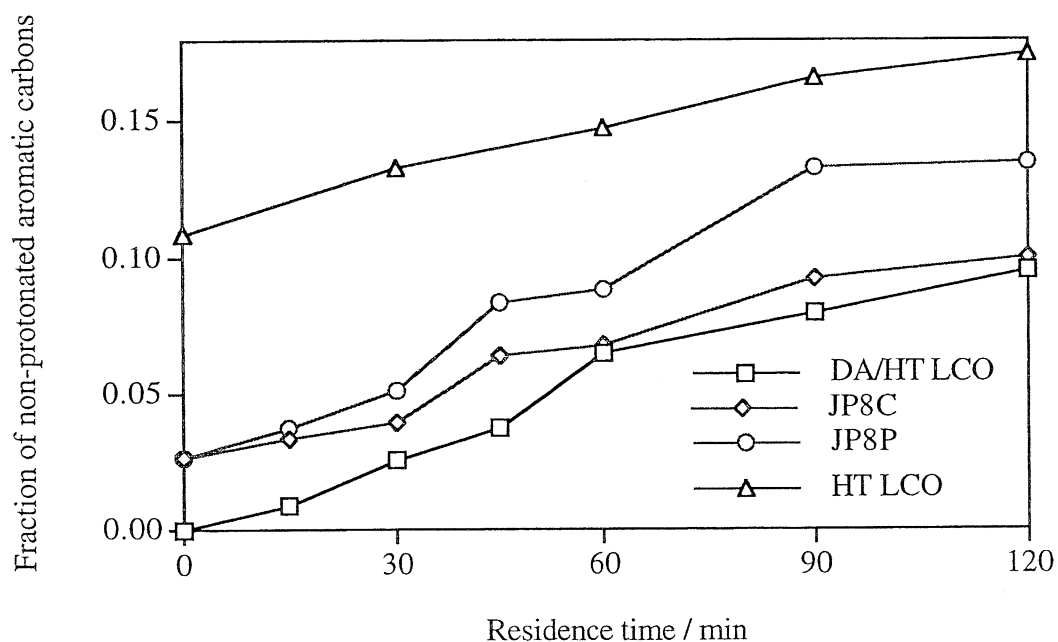


**Figure 3.10** Comparison of the ratio of the non-protonated aromatic-carbon content for the four jet fuels, DA/HT LCO, HT LCO, JP8P, and JP8C, with residence times up to 2 hours at 480°C.



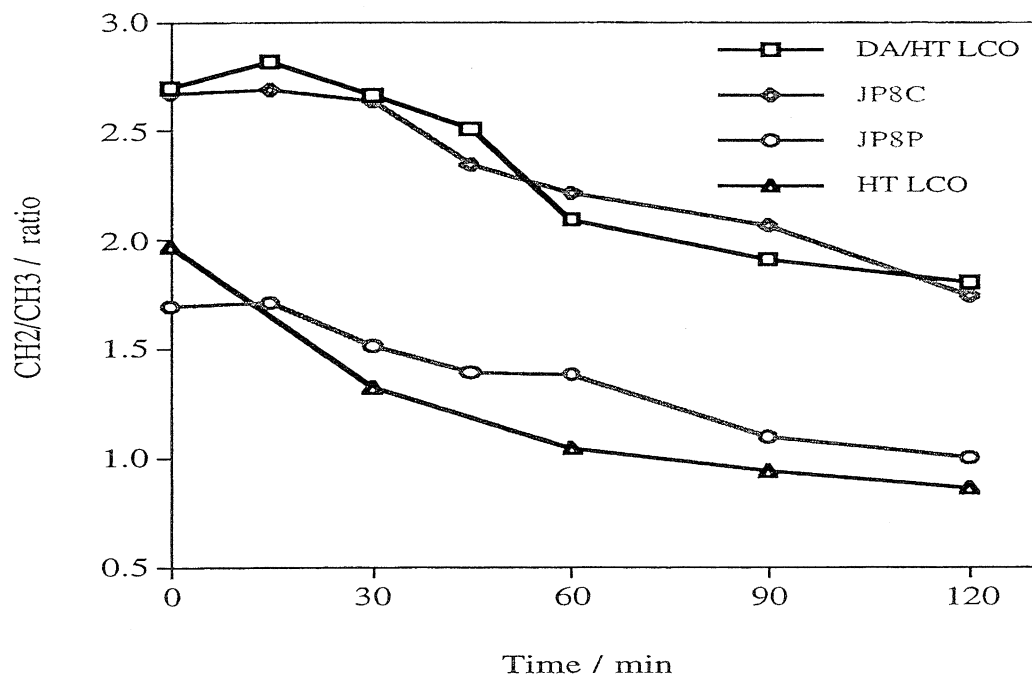


**Figure 3.11** Comparison of the  $\text{CH}_2/\text{CH}_3$  ratio for the four jet fuels, DA/HT LCO, HT LCO, JP8P, and JP8C, at 480 °C with residence times of up to 2 hours.

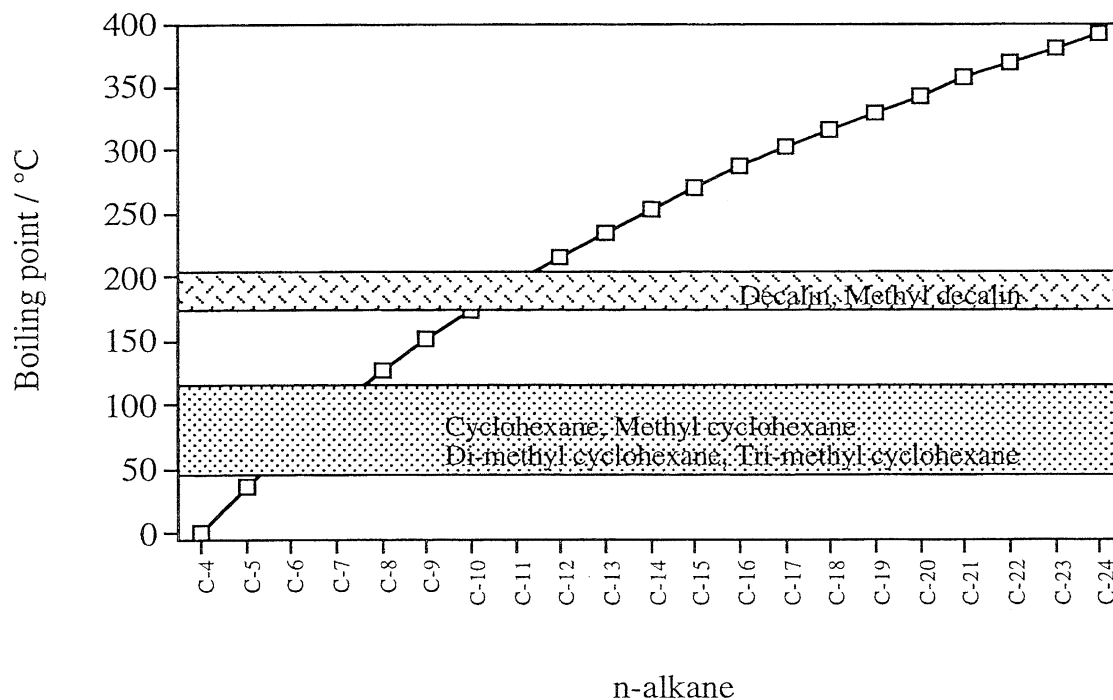


**Figure 3.12** Distillation plot for linear alkanes and boiling ranges for cycloalkanes generally found in DA/HT LCO fuel.

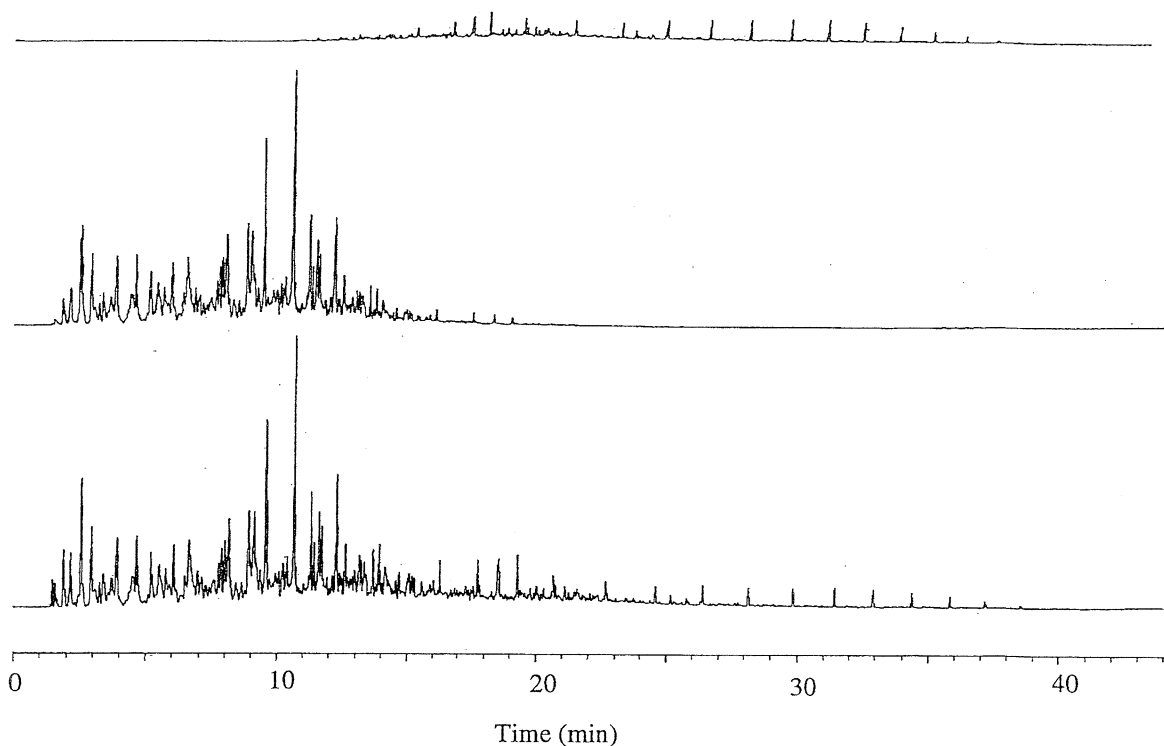


**Figure 3.13** GC traces of original severely hydro-treated light cycle oil (DA/HT LCO, bottom), the cut-point below 250°C (middle), and the cut-point above 250°C (top).

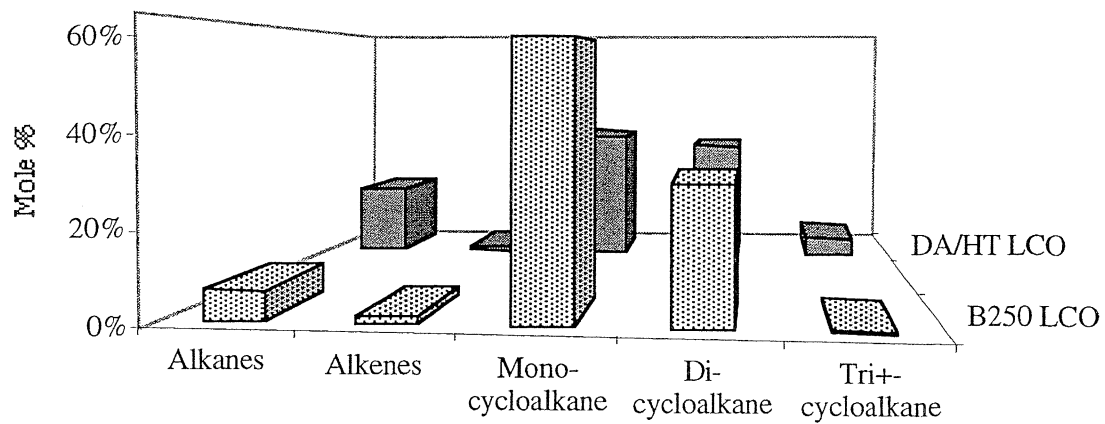


**Figure 3.14** Differences in the chemical composition of the original severely hydro-treated light cycle oil (DA/HT LCO, back) and the cut-point below 250 °C (B250, front).

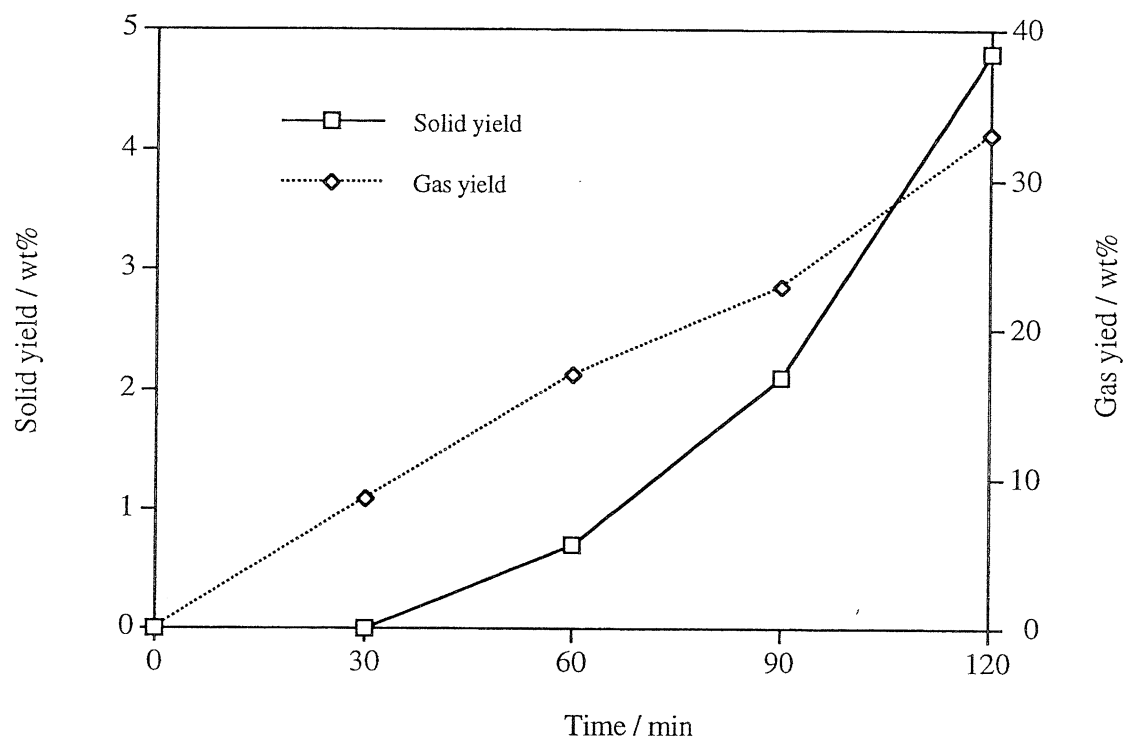


**Figure 3.15** Comparison of the gas product and the solid residue formed during stressing of the B250 fraction of DA/HT LCO at 480 °C with time.

## 4.0 CO-COKING OF PETROLEUM RESIDUE AND COAL

### 4.1 Aims

The aim of the subtask is to investigate the utilization of existing processing techniques that could incorporate the coprocessing of coal, and through such reactions produce a feedstock for thermally stable jet-fuel production. This can be achieved by assessing the viability of co-coking coal and petroleum resid under simulated delayed-coking conditions.

### 4.2 Introduction

Delayed coking is a process used in many petroleum refineries throughout the world for the conversion of heavy petroleum streams, *e.g.* vacuum resid and decant oil, into light distillate fractions and coke. This is achieved by the pyrolysis and thermal degradation of the feedstock in a semi-continuous process, at temperatures between 450 and 500° C, in an inert atmosphere, and at pressures of approximately 10 psig. The volatiles produced during the thermal degradation of the feedstock are vented during the operation and transferred to a distillation tower, where they are fractionated into the appropriate distillates. The coke product builds up in the reaction vessel over a period of 18 hours, at which point the feed is switched to pump into a parallel reaction vessel. The coke is then removed from the full vessel. The coke produced has varying qualities that depend on feedstock and reaction conditions.

With the introduction of coal into the process stream, it is assumed that volatile constituents of coal may be produced along with the volatiles from the petroleum feed and subsequently fractionated. The structural integrity of the coal should be maintained. That is, aromatic-ring systems are being produced. These aromatics could then be utilized with the petroleum-derived compounds as a feedstock for thermally stable jet fuel.

The following is an account of work performed during a nine-month study. It includes small-scale co-coking studies measuring the effect of temperature conditions and different coals on product fractions. In addition, the effect of combining coal and petroleum feedstocks on the fluidity of the mixture and the effect of co-coking on the morphology and quality of the coke product were studied.

### 4.3 Feedstocks Used

The vacuum resid used was obtained from British Petroleum (BP), and is a typical feedstock for delayed-coking operations.

A search of the Penn State Data Base and survey of some of the coal companies supplying metallurgical-grade coals to the coke-making industry revealed that most of the naturally high-thermoplastic coals are located in western Pennsylvania, southeastern Kentucky, and southwestern Virginia. From this survey, a 9-kg car-top composite sample of 2.4-mm coal was obtained from A.T. Massey for both the Powellton- and Eagle-seam coals from Virginia. As shown in Table 4.1, these coals were selected because of their comparative rank with the Upper Banner and Pittsburgh-seam coals already employed in a previous study [10-11], as well as their high fluidity, relatively low ash yield, and high content of reactive macerals. Furthermore, the fluid properties of Massey's coals are reported to be well out of the range of measurement by the ASTM method.

**Table 4.1** Analysis of project coals.

	<b>Illinois #6</b>	<b>Pittsburgh</b>	<b>Upper Banner</b>	<b>Powellton</b>	<b>Eagle</b>
<b>Rank</b>	<b>h<sub>v</sub>C<sub>b</sub></b>	<b>h<sub>v</sub>A<sub>b</sub></b>	<b>h<sub>v</sub>A<sub>B</sub></b>	<b>h<sub>v</sub>A<sub>b</sub></b>	<b>h<sub>v</sub>A<sub>b</sub></b>
<b>Vitrinite Reflectance, %</b>	0.49	0.87	1.00	1.03	1.01
<b>% Reactive Macerals</b>	94.3	89.1	80.9	80.9	78.8
<b>Moisture</b>	13.2	2.4	2.44	6.75	6.75
<b>% Ash Yield</b>	11.62	10.0	6.2	5.0	5.5
<b>% Volatile Matter</b>	47.1	43.5	36.6	33.5	34.5
<b>%C</b>	76.3	83.3	86.6	87.6	87.3
<b>%H</b>	5.3	5.7	5.5	5.8	5.6
<b>%N</b>	1.3	1.4	1.6	1.6	1.6
<b>%S</b>	6.4	1.3	0.6	0.9	-
<b>%O</b>	10.7	8.4	5.7	3.9	-
<b>Max. Fluid. Ddpm</b>	49	20,002	8,942	>30,000	>30,000
<b>Max. Fluid. T°C</b>	410	438	447	448	437
<b>Softening T°C</b>	365	390	396	387	401
<b>Resolidification T°C</b>	446	476	486	490	493

#### 4.4 Co-coking Studies

Co-coking experiments were performed using 25-ml stainless-steel-tubing bomb-type reactors. For the purpose of this study certain reaction conditions were kept constant. Feedstock ratios were kept at 2:1, resid to coal, with approximately 6 g of resid and 3 g of coal used in each experiment. The length of each run was also kept constant at 2 hours. Temperatures of 450, 465, 475, and 500 °C were used during these experiments. Heating was achieved via the immersion of the loaded reactor in a preheated fluidized sandbath. Prior to heating, the coal had been heated to 110 °C for 1 hour to remove any excess water. Once the reactor was loaded, it was purged with nitrogen to obtain an inert atmosphere, which was kept at ambient pressure. Typically the pressure inside the reactor, during the run, rose to between 1500 and 2200 psig, depending on the temperature of reaction.

After the run, the reactor was allowed to cool to room temperature. The reactor was weighed; the gas was vented; and the reactor re-weighed, to obtain the mass of gas evolved during the reaction. At this point, the other products of the reaction were removed from the reactor and subjected to exhaustive solvent extraction, using a Soxhlet extractor. They were separated using hexane, toluene, and THF into the oils, asphaltenes, pre-asphaltenes, and coke fractions and weighed.

The oil fraction was subjected to analysis using a Perkin Elmer 8500 gas chromatograph (GC) and a Hewlett Packard 5890 gas chromatograph coupled to a 5971 mass-selective detector (GC-MS), to obtain qualitative data on the type of compounds present in the fraction. Elemental analysis and optical microscopy were performed on the THF-insoluble fraction (coke).

Table 4.2 shows the percentage yields of different fractions from various co-coking runs using Eagle, Powellton, and Pittsburgh coal. Although the results seem inconsistent through coal type, temperature trends in the data are noticeable. First, with increasing reaction temperature there is an overall increase in the percentage of gas formed. This is due to the increased cracking of the products to  $C_1$ - $C_4$  compounds, mainly from the alkane compounds present in the BP coker feed. Second, with the increase in temperature there is an increase in the amount of oils produced. This is due to the asphaltenes and preasphaltenes being thermally cracked. Finally, the higher the temperature the greater the coke yield, due to the increase in the number of condensation reactions.

Table 4.2 Percent yields of different fractions.

TEMPERATURE	COAL	PERCENT YIELDS				
		GAS	OILS	ASPHALTENES	PREASPHALTENES	COKE
450 °C	EAGLE	16.77	27.54	2.54	3.25	49.89
	POWELLTON	11.73	31.42	16.79	3.87	36.19
	PITTSBURGH	14.97	24.01	5.35	4.66	54.48
465 °C	EAGLE	23.91	14.20	2.83	5.02	54.05
	POWELLTON	26.17	13.85	0.75	1.73	57.50
	PITTSBURGH	20.69	19.46	2.09	1.21	56.55
475 °C	EAGLE	21.50	10.68	8.93	2.71	56.18
	POWELLTON	26.31	13.24	1.42	4.75	54.27
	PITTSBURGH	22.44	7.15	0.33	5.82	64.26
500 °C	EAGLE	32.14	7.57	0.34	2.48	57.46
	POWELLTON	32.08	7.12	0.52	3.05	57.23
	PITTSBURGH	28.30	9.23	0.28	10.63	51.57

Conditions/Yields

Delayed Coker

Co-coking\*

Temperature	450-500 °C	465 °C
Time (hours)	18	2
Gas (%)	10	24
Liquids (%)	70	22
Coke (%)	20	54

\*Eagle coal.

These results differ from those of a conventional delayed-coking operation. Below is a set of comparable conditions and yields from a typical delayed-coking operation and our co-coking experiments using the same vacuum-resid feed.

Previous studies [12] have shown that pyrolysis reactions in a sealed reaction vessel at elevated pressures tend to yield a higher carbon content, and the higher the pressure the higher the carbon yield. In our co-coking reactions we have experienced pressures ranging from 1500 to 2200 psi, depending on the maximum temperature. Also, being sealed in, the liquid products experience higher temperatures for a long time, creating an increased opportunity for further cracking reactions that lead to coke formation and gas evolution, which in turn lead to higher pressures in the reactor. In a delayed-coking operation, although the reaction is under a slight overpressure (about 10 psig), the reaction vessel is vented, so that any volatile liquids or gases formed are not exposed to high temperatures in the reaction vessel and therefore are less likely to undergo further cracking reactions.

The hexane-soluble fractions (oils) from the co-coking runs were characterized by gas chromatography. Using the data from the runs with Powellton coal as an example, at 450°C the dominant compounds are aliphatic, ranging from  $C_8$  to beyond  $C_{30}$ . Aromatic compounds with 1- to 3-ring structures are present at lower concentrations. This result indicates that the majority of the compounds, i.e., aliphatics, has been produced by the thermal cracking of higher-molecular-weight compounds in the coker feed, and, to a lesser extent, there is inclusion of coal-derived, low-molecular weight aromatics from easily cleaved coal constituents. However, analysis of the oil fractions from runs at 465 and 475°C shows that increasing the temperature of reaction has changed the molecular makeup of the fraction. The majority of the compounds are now aromatic in nature, i.e., coal-derived. Coal-derived aromatics with three to five rings are observed, which were not present in the runs at 450°C.



It can be seen that the chromatograms at 465 °C using Eagle and Powellton coals have a very similar composition to those at 475 °C, yet the yields for the hexane-soluble fraction at 465 °C are slightly higher, especially for the Eagle. Therefore, in terms of yields of desired aromatic compounds derived from coal dissolution, 465 °C may be a more suitable reaction temperature. When we compare the Pittsburgh results with those of the Eagle and Powellton coals, the yield for the hexane-soluble fraction has almost tripled by reducing the temperature from 475 °C to 465 °C.

The hexane-soluble fractions were analyzed using high-temperature-simulation distillation gas chromatography. The jet-fuel boiling range for these co-coking experiments is designated to be 200-260 °C. We found that as the temperature of these reactions increases, the total percent of oils obtained from the co-coking experiments with Powellton coal and coker feed (in a 1:2 ratio) decreases. Figure 4.1 displays the results for Powellton coal and coker feed at 450, 465, 475, and 500 °C. An increase in the jet-fuel-range yield going from 475 to 500 °C is accompanied by a significant decrease in the 260-450 °C boiling-range yield. This most likely can be explained by decomposition occurring with the 260-450 °C range oils. The 260-450 °C boiling range for the four different temperatures contained the highest quantity of sample in the oil fractions. If the oil fraction were subjected to severe hydrotreatment processes, a higher yield of the jet-fuel boiling-point fraction would be produced, due to the decomposition of the 260-450 °C range fraction. Overall a significant quantity of oils is produced in these co-coking experiments.

Figure 4.2 shows the boiling range for the three different coals with coker feed, as well as for the coker feed and heat-treated coals only. The coals with the coker feed show yields similar to that of Powellton coal (Figure 4.1). From Figure 4.2, however, we can see that combining both the coker feed and the coal lowers the yield of the jet-fuels fraction by about half. It seems that the coal is acting as a catalyst for decomposition. When coal is present, there is an increase in both gas and coke yields. In view of the decrease in liquids yields, we can assume the extra coke and gas come from decomposition of the coker feed. One reason for this decomposition may be the presence of relatively high quantities of phenols produced from the coal under the reaction conditions. Phenols are known to be good sources of radicals, which in turn can initiate retrogressive polymerization reactions, resulting in an increased yield of coke. Table 4.3 shows that significant quantities of phenols are produced during the coking of coal alone. However,

these phenols have been reduced to undetectable levels in co-coking reactions, and hence, must have been removed from the liquid fractions through chemical reactions.

Semi-quantitative analysis was performed using GC-MS. This method allowed us to identify all the major components in the chromatograms and express them as a percentage of the total area for the whole chromatogram. Table 4.3 shows the percentage of compounds identified that fell into various compound classes.

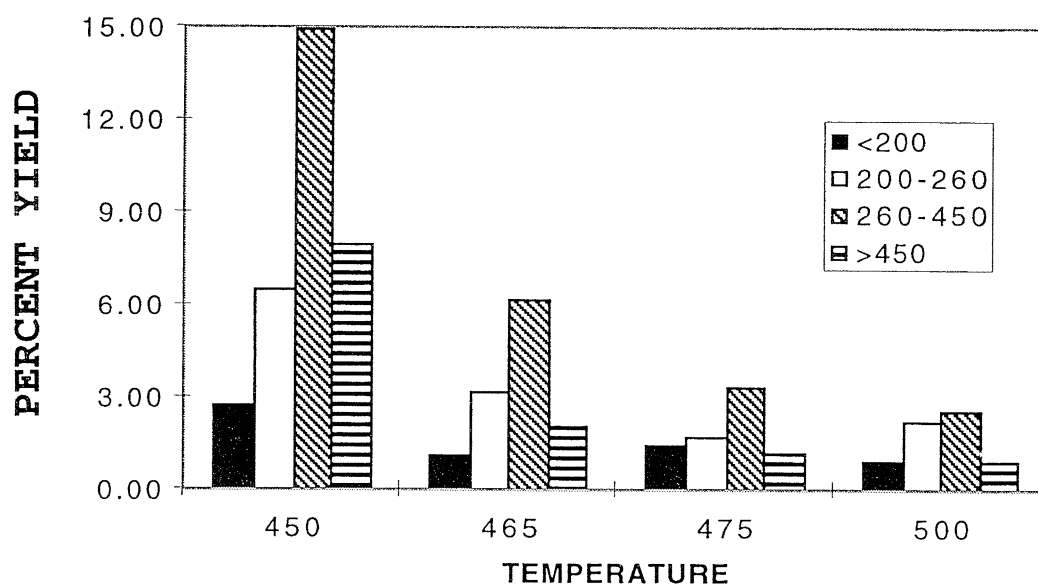


**Figure 4.1** Effect of temperature on the yields in the different boiling ranges.

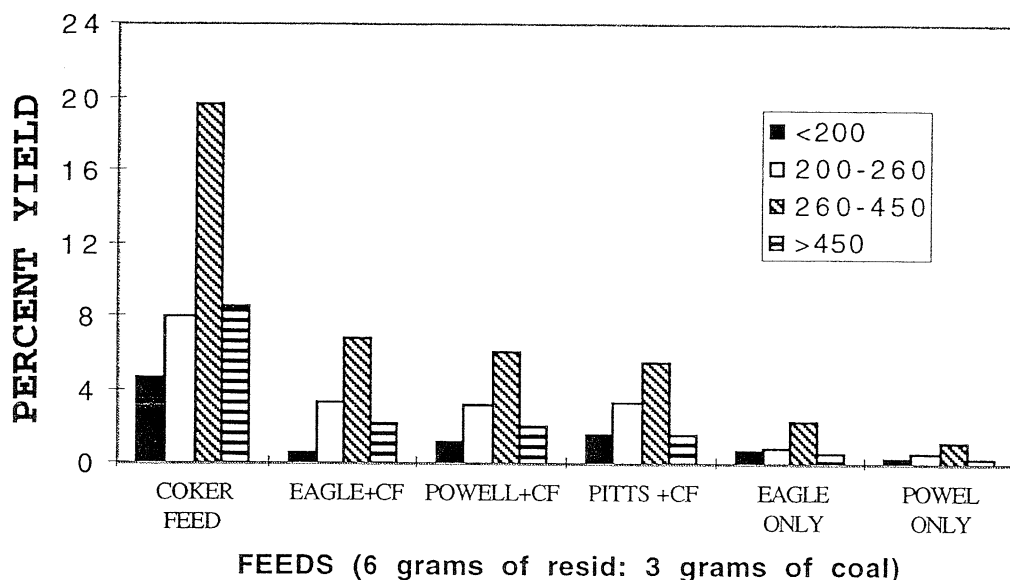


**Figure 4.2** Effect of feed on boiling ranges of the products of co-coking at 465 °C.

From Table 4.3 we can see that as the temperature of the reaction is increased, the presence of aromatic compounds increases. This indicates that the coal conversion and the inclusion of coal-derived material in the products increases. The coker feed, on the other hand, consists of mainly saturated alkanes, which contributes to the high alkane content for the co-coking reactions at lower temperatures. It is also worth noting that different coals produced coal-derived compounds at similar reaction temperatures. For example, co-coking experiments performed at 465 °C with Eagle coal produced high quantities of naphthenes; Pittsburgh coal produced high quantities of pyrenes; and Powellton coal had compounds that averaged out across the range of those identified

**Table 4.3** Compound distribution of co-coking products.

REACTION	Benzenes	Phenols	Alkanes	Naphthenes	Fluorenes	Anthracenes/ Phenanthrenes	Pyrenes	Total **
Powellton 450	8.68	5.52	11.92	0.81	4.88	-	-	31.81
Eagle 450	-	6.79	6.92	12.10	-	3.90	-	29.71
Coker 465	-	-	38.32	2.04	-	-	-	40.36
Co-Eagle 465	1.44	1.19	9.85	22.61	1.45	5.68	0.58	42.81
Co-Pitts 465	-	-	12.20	11.19	-	2.07	27.41	52.87
Co-Pow 450	-	-	35.25	-	-	-	-	35.25
Co-Pow 465	0.89	-	3.32	18.57	0.75	6.89	1.26	31.67
Co-Pow 475	4.09	-	-	23.76	1.36	9.93	1.66	40.80
Co-Pow 500	-	-	-	22.93	1.70	13.70	4.31	42.63

\*\* This column indicates the total percent of identified major peaks; the remaining percent are unidentified minor peaks. The values above are absolute values and not those from just the identified peaks. "Co" indicates a co-coking experiment.

Table 4.4 shows the compound-distribution yield (in percent based on the total oil yield) for the hexane-soluble fractions from the co-coking reactions.

**Table 4.4** Compound-distribution yield in the hexane-soluble fraction.

FEED	Oil Yield	Benzenes	Phenols	Alkanes	Napthenes	Fluorenes	Anthracenes/ Phenanthrenes	Pyrenes
Eagle 450	4.4	-	0.30	0.31	0.53	-	0.17	-
Pow 450	2.3	0.20	0.13	0.27	0.02	0.11	-	-
Coker 465	47.7	-	-	18.28	0.97	-	-	-
CoEagle 465	13.2	0.19	0.16	1.30	2.99	0.19	0.75	0.08
CoPitts 465	16.9	-	-	2.06	1.89	-	0.35	4.63
CoPow 450	32.2	-	-	11.34	-	-	-	-
CoPow 465	14.1	0.13	-	0.47	2.62	0.11	0.97	0.18
CoPow 475	7.7	0.32	-	-	1.84	0.11	0.77	0.13
CoPow 500	6.7	-	-	-	1.52	0.11	0.91	0.29

The values above give some indication of the quantities of the individual compounds in the oil samples. These values are ratios of those in Table 4.1 but corrected for the oil yield produced during the reactions.

Tables 4.5a and 4.5b show the percentage yields of methyl-substituted compounds that were identified in the oil fraction from co-coking experiments. C1, C2, C3, etc., correspond to the mono-, di-, and tri-substituted compound, respectively. It is clear that heat-treated coker feed does not contribute significant quantities of substituted aromatic compounds to the oil fraction. Therefore, all the aromatics identified come from the coal-derived material.

It is apparent that different coals produce compounds with differing levels of substitution, thus reflecting the differences in the molecular composition of the coals, even though they are of the same rank classification. The effect of temperature is exemplified in the series of tests performed on Powellton coal between 450 and 500 °C. The general trend shown is that with an increase in temperature there is a decrease in the amount of substitution. This is due to the increased cleavage of the methyl groups from the ring at elevated temperatures. This in turn leads to the formation of gaseous products.

**Table 4.5a** Substituted-compound distribution and yield for the hexane-soluble fraction.

REACTION	OIL YIELD	Benzene			Phenols			Naphthenes		
		C1	C3	C4	C1	C2	C3	C1	C2	C3
Pow 450	2.30	-	-	-	0.07	0.09	0.04	0.08	0.14	0.06
Eagle 450	4.41	-	-	-	-	0.21	0.09	0.21	0.25	-
Coker 465	47.71	-	-	-	-	-	-	0.97	-	-
CoEagle 465	13.22	-	-	0.15	0.05	0.11	-	0.76	1.21	0.88
CoPitts 465	16.90	-	-	-	-	-	-	0.56	0.98	0.35
CoPow 450	32.18	-	-	-	-	-	-	-	-	-
CoPow 465	14.11	0.11	-	-	-	-	-	0.78	1.17	0.48
CoPow 475	7.74	-	0.04	0.27	-	-	-	0.61	0.74	0.29
CoPow 500	6.65	-	-	-	-	-	-	0.59	0.60	0.15

**Table 4.5b** Substituted-compound distribution and yield for the hexane-soluble fraction.

REACTION	OIL YIELD	Fluorene	Anthracene/ Phenanthrene		Pyrene
		C1	C1	C2	C1
Pow 450	2.30	0.02	0.09	-	-
Eagle 450	4.41	-	0.11	-	-
Coker 465	47.71	-	-	-	-
CoEagle 465	13.22	0.19	0.53	0.09	0.04
CoPitts 465	16.90	-	0.20	-	-
CoPow 450	32.18	-	-	-	-
CoPow 465	14.11	0.11	0.49	0.30	-
CoPow 475	7.74	0.11	0.45	0.15	0.05
CoPow 500	6.65	0.05	0.50	0.12	0.08

## 4.5 Fluidity Studies

### Experimental

A Gieseler constant-torque plastometer was used to evaluate the thermoplastic properties of coal/coker-feed blends. Five grams of -40 mesh (0.42 mm) sample is placed around a rabble-

arm stirrer in the instrument crucible and pounded into place with a 10-kg weight according to the ASTM method [13]. The crucible apparatus is assembled, fitted onto the instrument, and immersed into a solder pot held at 300°C. A constant torque of  $\approx 101.6$  g-cm is applied to the rabble arm during the course of the test. After reaching equilibrium, the temperature is increased at 3°C/min to a maximum temperature of  $\approx 500^\circ\text{C}$ , and both temperature and displacement of the rabble arm (in dial divisions per minute) are recorded at 3-minute intervals to give a fluidity profile. Without resistance, the applied torque results in a maximum of 30,000 (or 4.48 log scale) dial divisions per minute (ddpm).

Because of the sticky and thixotropic nature of the VR1 petroleum resid, the sample-handling procedure was altered. In order to make the resid brittle, it was cooled in liquid nitrogen so it could be milled into fine particles and added to a pre-weighed amount of coal. The blends were homogenized by using the weigh paper like a roll cloth, quickly adding the material to the crucible, and pounding into position. Increasing concentrations of resid, from 5 to 20 wt.%, were used with four different 40-mesh coals, including Illinois #6, Pittsburgh, Upper Banner, and Powellton-seam coals (Table 4.1).

## Results

Figure 4.3 compares the fluidity profiles, log ddpm vs temperature, for Powellton- and Upper Banner-seam coals and coal/resid blends. As shown in Figure 4.3a, the coal fluidity for the Powellton-seam coal slowly begins around 380°C, reaches its maximum fluidity around 443°C, and remains at the maximum for about 10 °C before rapidly diminishing, as the material resolidifies, at 490 °C. With incremental additions of petroleum resid, the fluidity profile broadens or, in other words, the fluid-temperature range increases with increasing resid concentration, as does the temperature range over which the blends exhibit their maximum fluidity. For the Upper Banner-seam coal, Figure 4.3b shows that maximum fluidity of the coal can be enhanced with even small additions of resid ( $\approx 5\%$ ). With some variation, similar results were obtained with the hvAb Pittsburgh-seam coal (Figure 4.4a), although the duration of maximum fluidity was not influenced as greatly as with the other hvAb coals tested. As shown in Figure 4.4b, fluid-property readings for the hvCb Illinois #6 blends never achieved the maximum dial divisions obtainable with the instrument. The fluid temperature range of Illinois #6 begins and ends at a significantly lower temperature and is not as broad as that for the hvAb

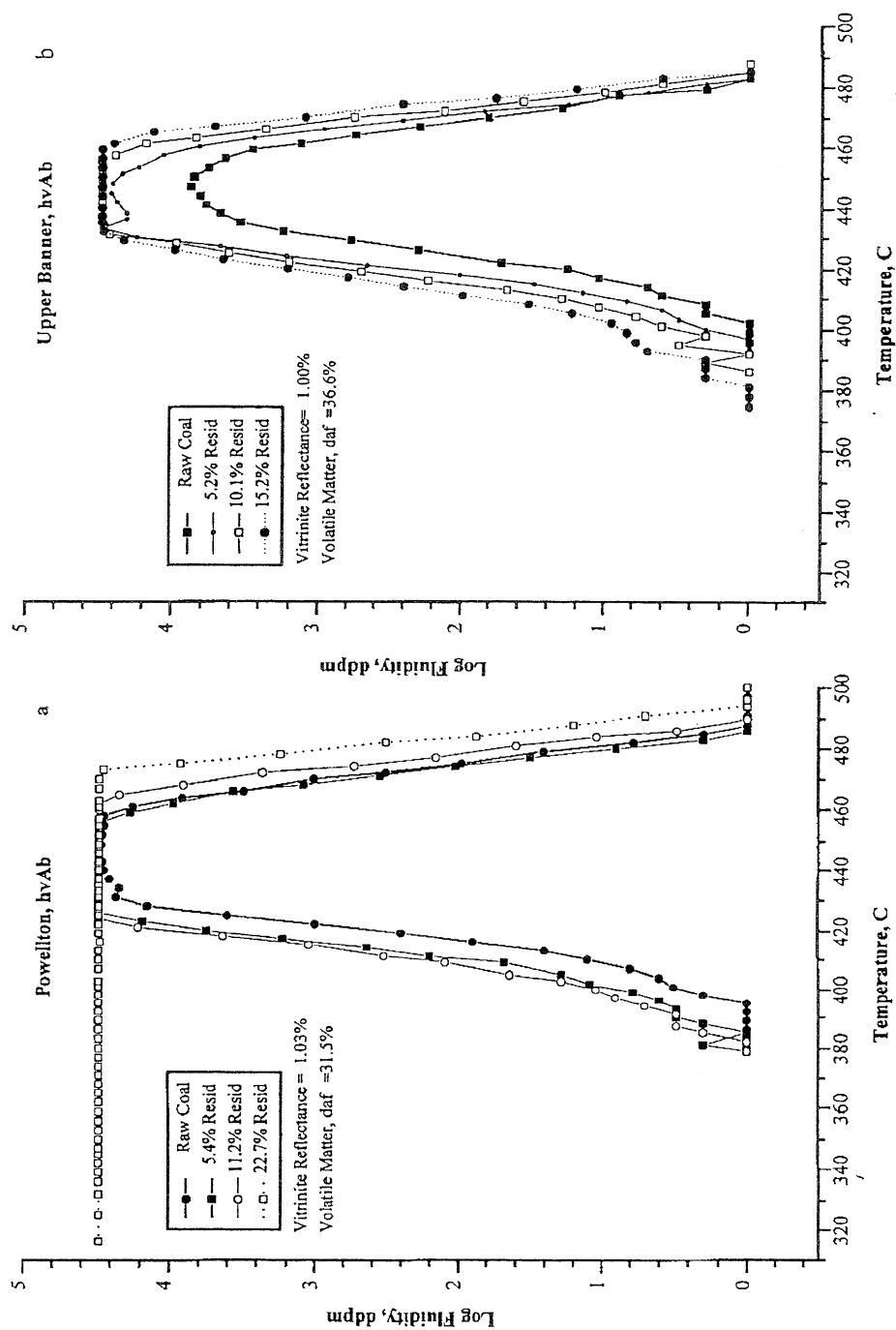


**Figure 4.3** Comparison of the thermoplastic profiles of coal/resid blends for the Powellton and Upper Banner seam coals

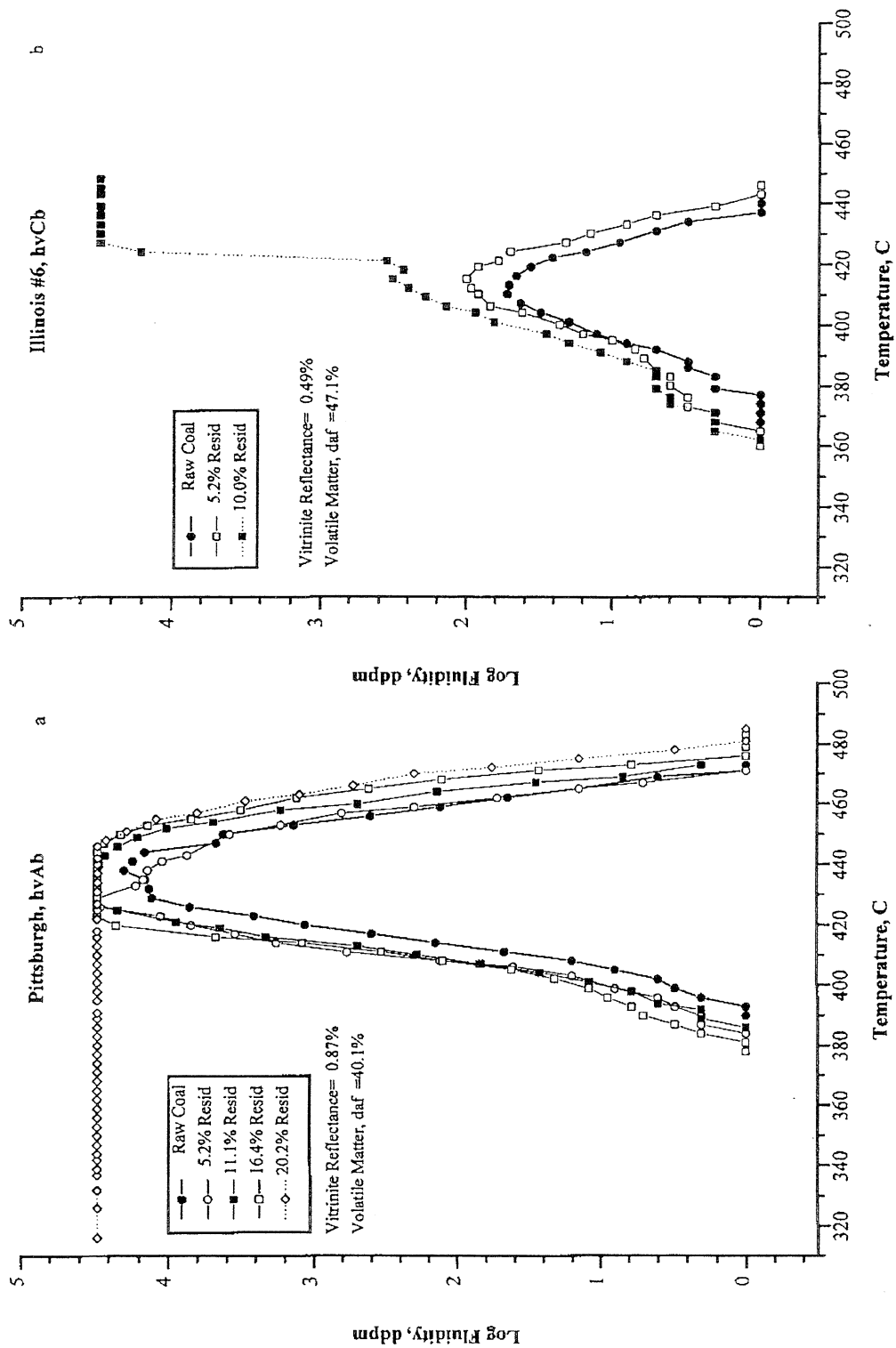


**Figure 4.4** Comparison of the thermoplastic profiles of coal/resid blends of Pittsburgh and Illinois #6 seam coals



coals studied. This may explain why the fluidity profile does not appear to exhibit complete resolidification of the material at higher resid concentrations (>10%).

Under the heating conditions employed, these observations indicate that hvAb coals and resid are mutually fluid and devolatilize over the same temperature range. This would be an essential condition for the homogenization of the reactive components of coal with the carbon product remaining from the resid. A microscopic inspection of the microautoclave residues from earlier experiments with the Pittsburgh- and an hvAb Lower Sunnyside-seam coals showed only a minor amount of interaction between the coal and resid components [11]. Angular coal particles with weakly developed anisotropic properties were observed in a carbon matrix clearly derived from the resid. It will be interesting to view residues from the newly acquired Powellton and Eagle coals to see if their exceptionally high fluid properties influence the nature and quality of the semicoke.

## **4.6 Study of Coke Quality and Morphology**

### Optical Microscopy

Using optical microscopy, coke residues derived from coker feed alone at carbonization runs at 450, 465, 475, and 500 °C and from carbonization runs at 465 °C with Eagle Powellton and Pittsburgh coals were characterized. The carbon materials produced from the coker feed have a distinctive texture compared with those derived from coal. Therefore, textural elements were identified by their isotropic/anisotropic nature and by the size of their isochromatic units, and a point-count procedure was employed to establish the volume percent of recognizable components of the residues. In addition, the relative anisotropy of the different carbon textures was determined by measuring the mean maximum and apparent minimum reflectance. These studies will provide a basis of comparison for residues generated from co-coking coker feed and coal.

Coker-feed residues were embedded in a cold-setting epoxy resin and, after hardening, were polished for reflected-light microscopy. The carbon material was evaluated in white light using air and oil-immersion objectives at a total magnification of 500 X in polarized or cross-polarized light. Point-count analysis was determined at 625 X magnification in oil-immersion by traversing the sample using a 0.4 x 0.4 mm grid and identifying the textural elements under a crosshair held in the microscope eyepiece. Total counts accumulated ranged from 430 to 910

and correlated with the mass of coke material recovered following carbonization and sample workup.

Measurement of reflectance and anisotropy was performed on a Leitz MPV-2 research microscope photometer system. Areas of different textural elements were rotated 360° to determine the maximum and minimum amount of light reflecting from the surface in polarized light. These measured values are indicative of the principal axes of a uniaxial negative crystal and reveal relative changes in crystallite alignment and aromaticity in low-temperature carbons. The photoelectric system is standardized with respect to glass standards in the range of measured reflectance; the sample is then traversed in a grid-like fashion. One hundred readings were taken on different textural elements, and the mean values were determined and reported as the mean maximum and apparent minimum reflectance.

Six different textural elements were identified in the four residues and are described as follows:

**Isotropic** – a relatively low-reflecting, dark-gray carbon material displaying no or very little optical activity under polarized light.

**Mosaic** – a higher-reflecting carbon material that displays optical anisotropy and is characterized by isochromatic units of less than 10 µm.

**Small Domain** – an anisotropic carbon exhibiting optical anisotropy with larger isochromatic units of between 10 and 60 µm.

**Domain** – an anisotropic carbon having much larger isochromatic units of greater than 60 µm.

**Flow Domain** – an anisotropic texture exhibiting elongated isochromatic areas greater than 60-µm in length and less than 10 µm in width.

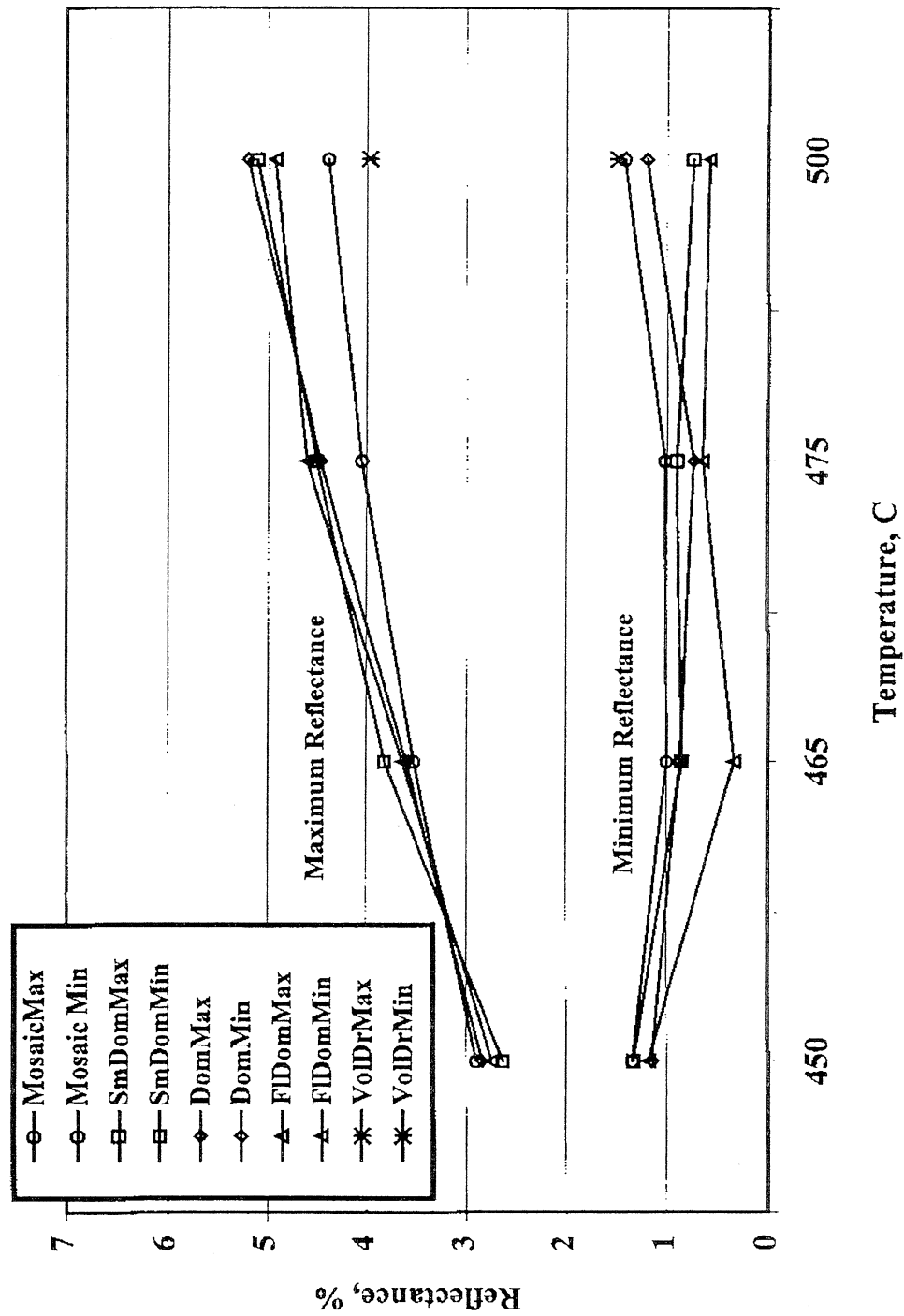
**Volatile-Derived Mosaic** – a textural component identified as wall-deposit material in the 500 °C residue and composed of a variety of different textures. The carbon material closest to the reactor wall has the appearance of vapor-deposited carbon which grades into a relatively low-reflecting, fine, anisotropic mosaic carbon of less than 10 µm.

Figure 4.5 shows the results of reflectance analyses for all of the different anisotropic carbon textures described above. The maximum reflectance increases with increasing reaction temperature and is slightly higher for the larger-size optical textures (flow domain, domain, and small domain) compared with the mosaic textures (mosaic and volatile-derived). In addition, the

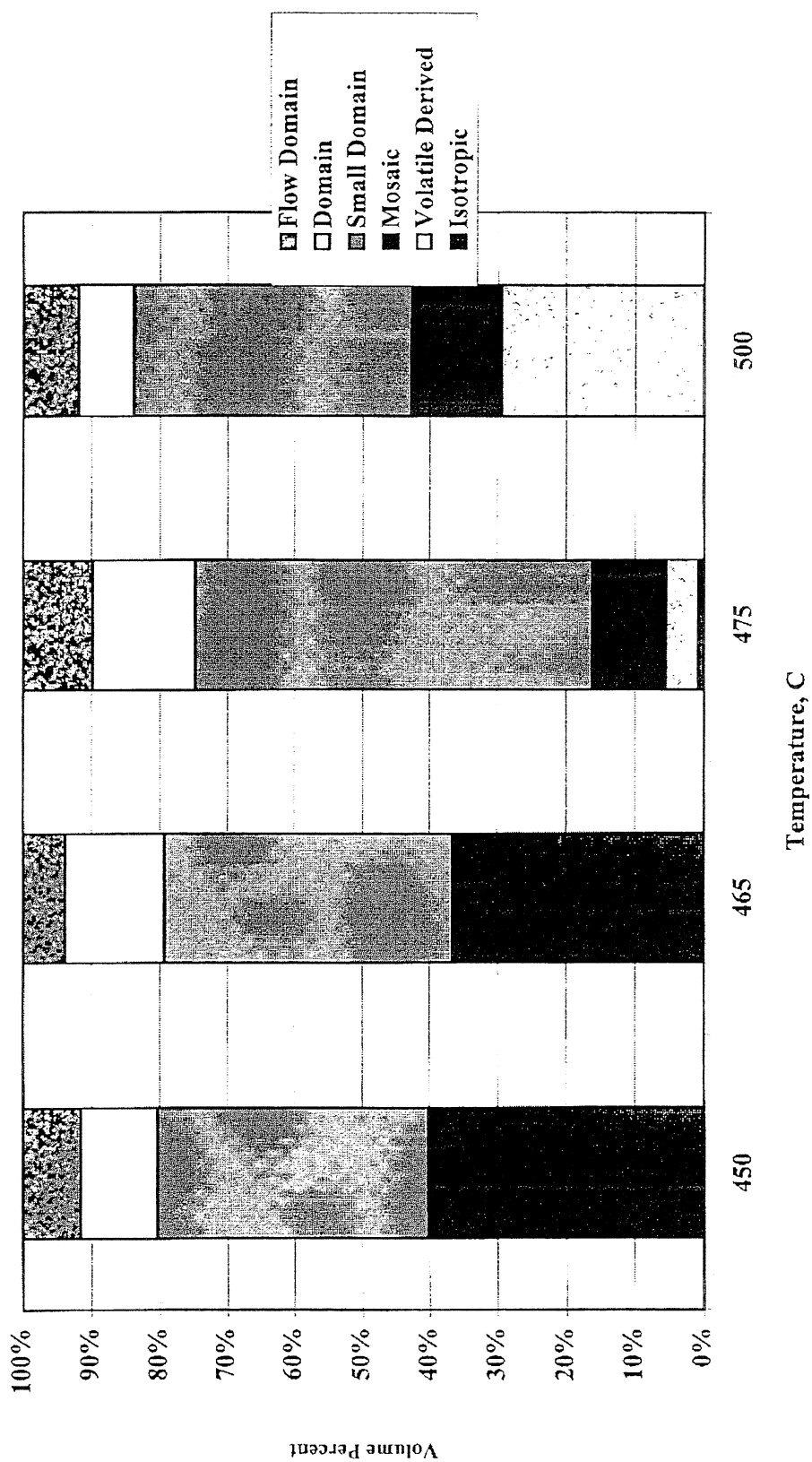
difference between the maximum and apparent minimum reflectance values, which is a measure of the anisotropy, increases with increasing temperature. The significantly lower reflectance and anisotropy of the carbon material produced at 450 °C is partly a result of the very soft nature of the carbon and the poor quality of the polish obtained as a result. However, the trend is maintained by the reflectance values obtained from the 465 °C residue.

Figure 4.6 shows the variation of the distribution of carbon textures as the carbonization temperature increases. What is apparent from this data is that after 2 hours of reaction, there is a considerable amount of isotropic carbon remaining in the two lower-temperature residues (450 and 465 °C). Isotropic carbon represents the once-fluid coker-feed precursor from which mesophase and solid anisotropic carbons are generated. Given a longer residence time or higher temperature, the isotropic material may be completely converted to anisotropic carbon. Less than 1% isotropic carbon was observed in the residue at 475 °C and none at 500 °C. With some variation, the concentrations of mosaic, domain, and flow-domain textures are fairly consistent with increasing reaction temperature, whereas an increase in the concentration of small-domain textures was observed at the higher temperatures (475 and 500 °C).

Figure 4.5 Change in Reflectance and Anisotropy of Coker Feed with Temperature



**Figure 4.6** Distribution of Carbon Textures with Carbonization Temperature of Coker Feed



The carbon texture identified as wall deposit in the 500 °C residue (volatile-derived mosaic) was also found in low concentration at 475 °C. The fact that it was observed as wall scale at the highest temperature and exhibits a characteristic form in the layers closest to where it attached to the reactor wall suggests that this material results from secondary reactions of the vapor-phase volatile matter being released from the coker feed. The mosaic carbon that deposits in additional successive layers may be a combination of vapor and primary liquid phases. The importance of this observation is that during the course of operating a delayed coker in which the volatile components escape freely, this carbon texture probably would not be observed.

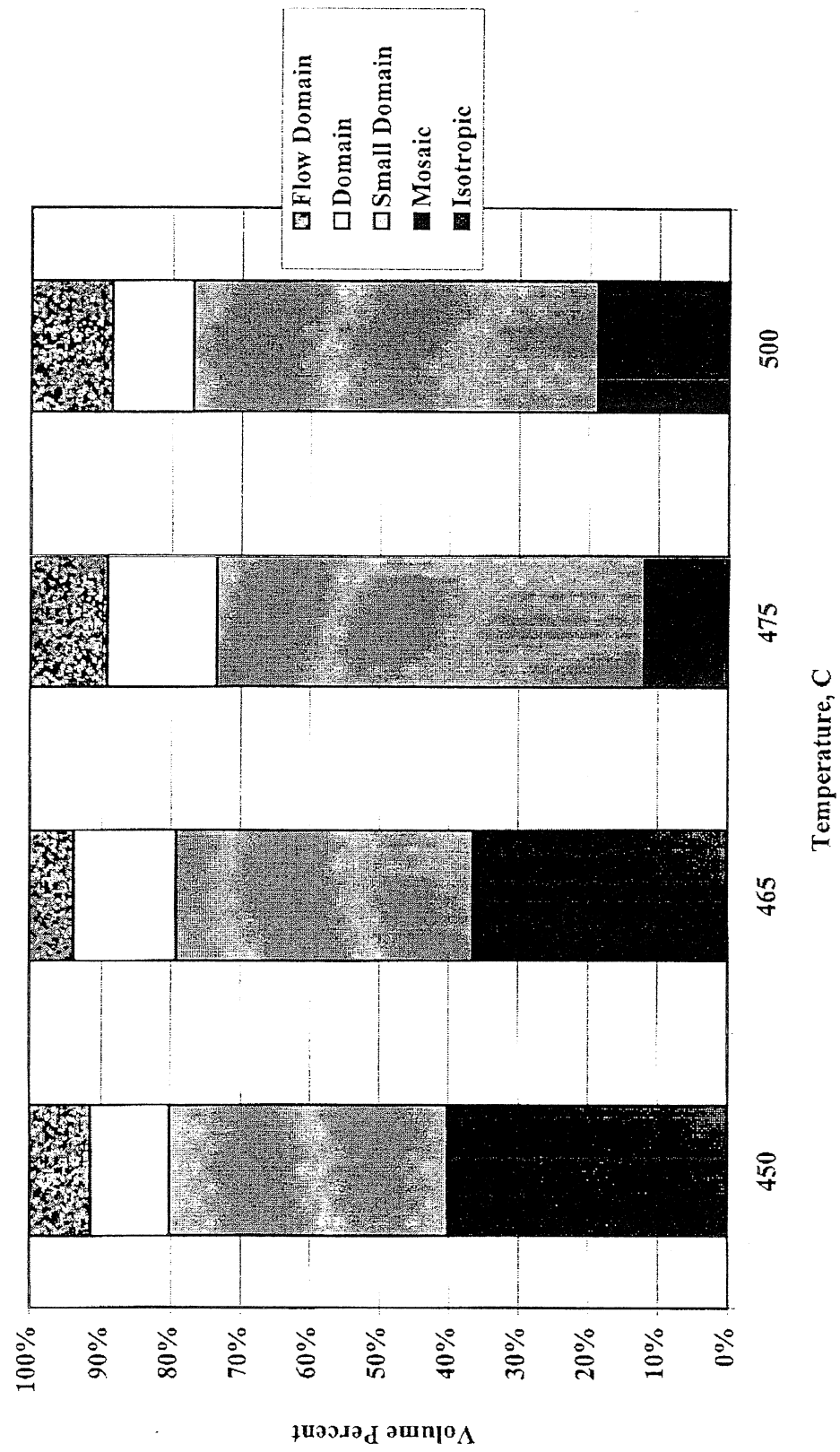
Figure 4.7 shows the distribution of carbon textures free of the volatile-derived mosaic component and better illustrates the apparent increase in the concentration of the small-domain carbon at higher temperatures. Presumably, the small-domain texture increases in concentration at the expense of the isotropic carbon.

Figure 4.8 illustrates the relative distribution of carbon textures derived from coals with the sum of all textures derived from the coker feed and shows that more than 60 vol.% of the coke residue was derived from coal. These results demonstrate that coal contributes more to the coke residue than does the coker feed at 465 °C. Evaluation of the interaction of different carbon entities using optical microscopy suggests that there was fairly uniform mixing of the coal particles within the coker feed. The fact that coker-feed material was found trapped in gas vacuoles generated in coal particles and that deformed coal-particle remnants conform to the textural alignments observed in the coker feed may be regarded as evidence that both materials were simultaneously fluid. Unfortunately, only minor evidence was found of homogeneous chemical interaction of the two blend components. Enlargement of the anisotropic mosaic was observed at the edges of some small coal particles (<20- $\mu$ m diameter), particularly for the Eagle-seam coal, but generally boundaries between remnant coal particles and coker-feed-derived carbon forms were fairly distinct in residues from all coals.

Figure 4.9 shows the distribution of carbon textures derived only from the coker-feed fraction of the co-carbonization residues. These are compared with the distributions obtained when coker feed was carbonized alone at 465 and 475 °C. A number of observations can be made, including the fact that very little isotropic carbon was found in the co-carbonized residues, whereas this carbon had a significant concentration in the 465 °C coker-feed residue. Also, much less of the larger carbon textures (domain and flow domain) was found when coal was present.

Furthermore, the concentration of mosaic textures increased and that of small-domain carbon decreased during co-carbonization with Eagle >Pittsburgh > Powellton. In terms of the general reflectance and distribution of carbon textures, the experiments using the Eagle-seam coal have a greater similarity to the coker-feed product carbonized at 475 °C. However, it is apparent that the presence of coal has a profound influence on carbon forms derived from the coker feed.

**Figure 4.7** Distribution of Carbon Textures with Carbonization Temperature, Volatile-Derived Free Basis





**Figure 4.8** Distribution of coal-and Coker Feed-Derived Carbon Textures at 465 C

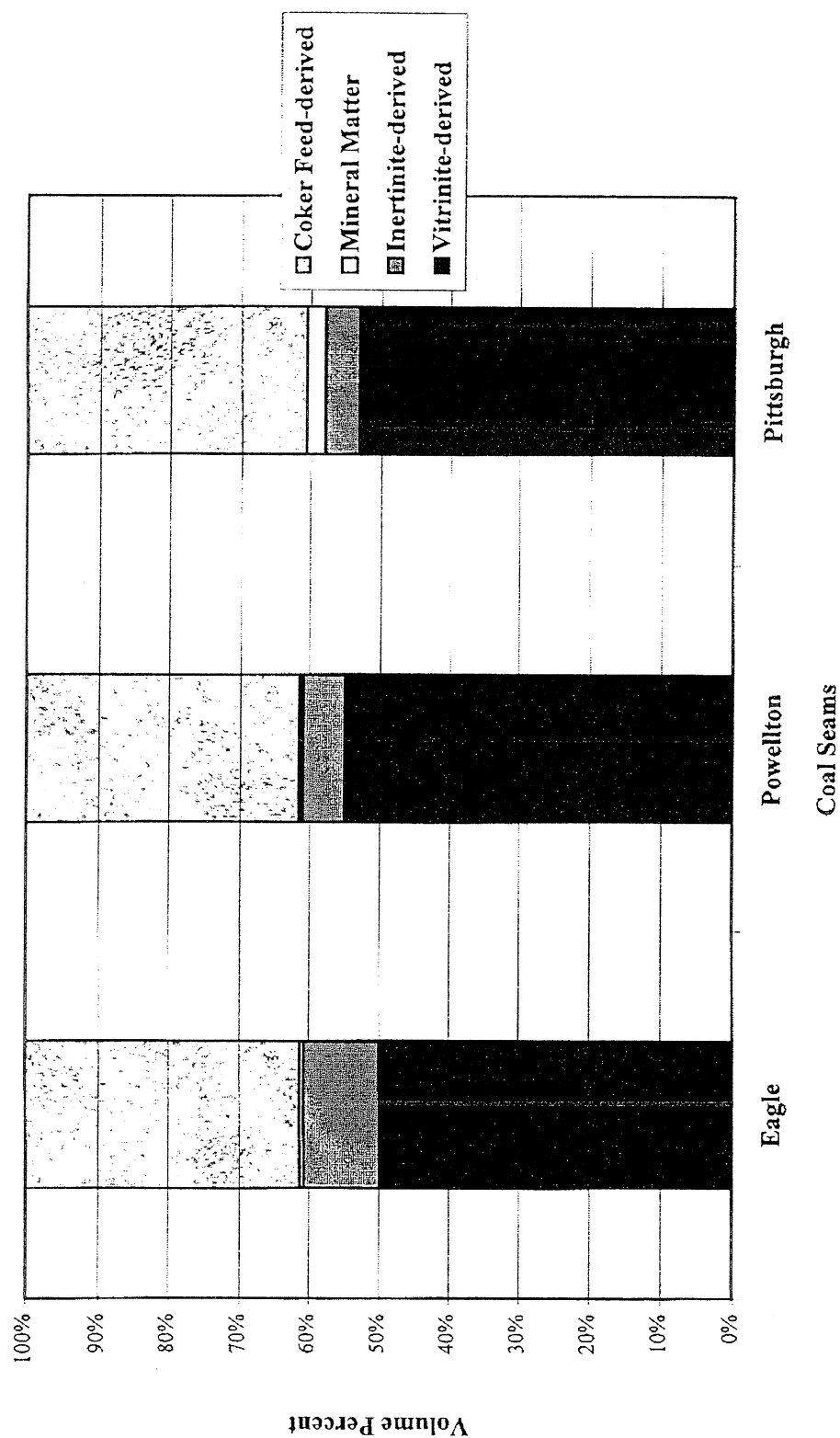
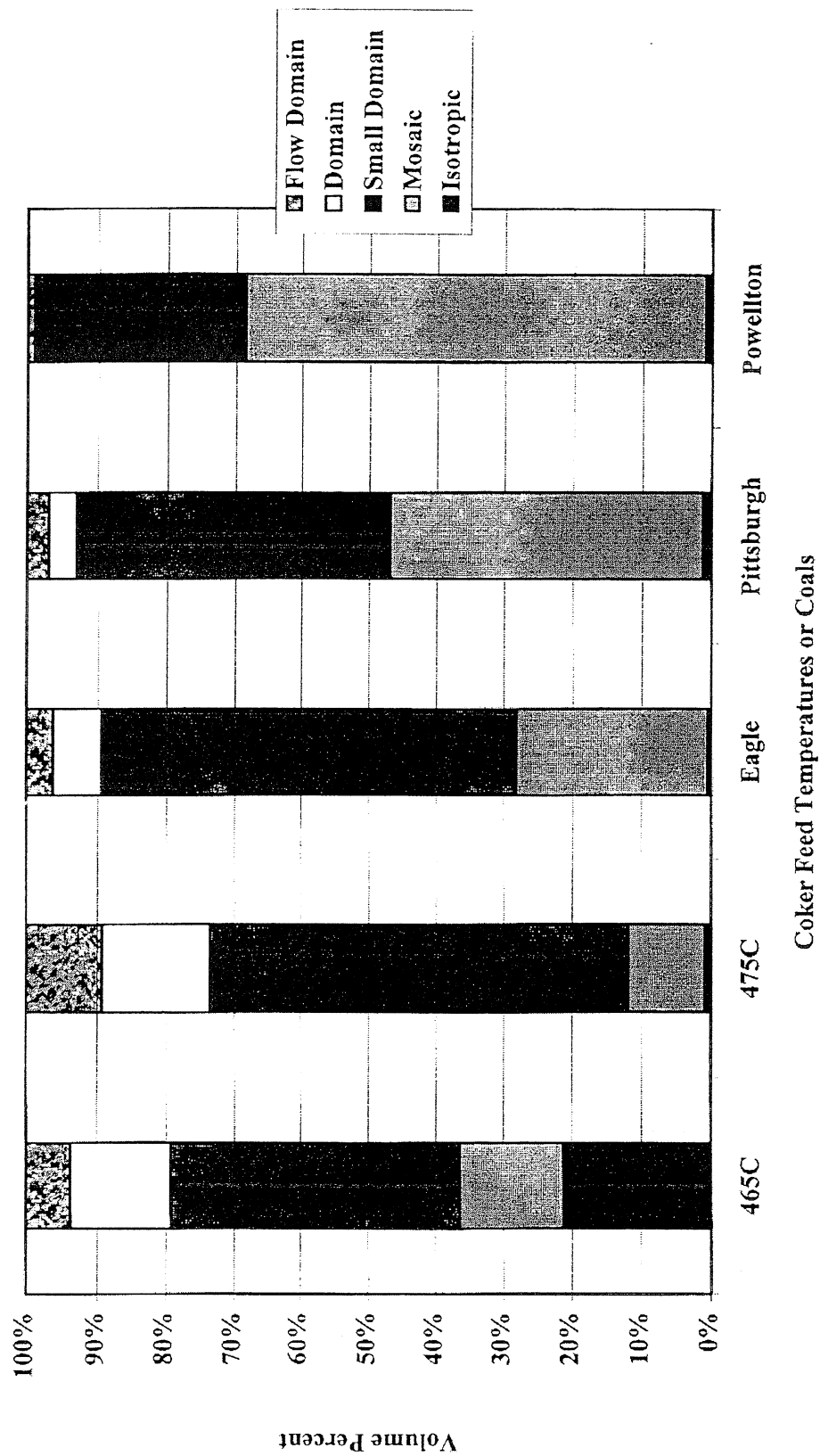


**Figure 4.9** Distribution of Coker Feed Carbon Textures in Coker Feed/Coal Blends



### Elemental Analysis

The data reported (Tables 4.6-4.10) are related to the elemental analysis of the solid products produced from co-coking runs. The solid products are classed as the THF-insoluble fraction remaining after sequential solvent extraction of the reaction products from co-coking experiments. The reaction conditions for each sample of coal, Pittsburgh, Eagle, and Powellton, included temperatures ranging from 450 to 500 °C, a run time of 2 hours, and a ratio of coal to resid of 1:2.

Table 4.6 shows the C, H, N, and ash contents (d.a.f. basis) of the coal and resid feeds used in these experiments.

**Table 4.6** Elemental analysis of co-coking feedstocks (C, H, N reported on d.a.f. basis).

FEED	% C	% H	% N	% ASH	H/C
EAGLE	87.3	5.6	1.6	5.70	0.77
POWELLTON	88.1	5.6	1.5	4.94	0.76
PITTSBURGH	84.8	5.7	1.4	10.50	0.81
COKER RESID	88.9	11.7	0.4	-	1.58

Tables 4.7-4.10 show the elemental analyses of the THF-insoluble products from co-coking runs and the heat-treated resid coker feed at various temperatures.

**Table 4.7** Elemental analysis of THF-insoluble products from co-coking runs and heat-treated resid coker feed at 450 °C.

	% C	% H	% N	% ASH	H/C
EAGLE	89.9	3.7	1.5	4.23	0.50
POWELLTON	93.1	3.6	1.6	9.90	0.46
PITTSBURGH	90.6	4.4	1.5	8.69	0.58
COKER FEED	92.6	4.3	1.3	0.0	0.55

**Table 4.8** Elemental analysis of THF-insoluble products from co-coking runs and heat-treated resid coker feed at 465 °C.

	% C	% H	% N	% ASH	H/C
EAGLE	92.2	4.0	1.5	4.24	0.52
POWELLTON	91.5	3.7	1.4	3.24	0.49
PITTSBURGH	90.7	3.9	1.6	8.43	0.52
COKER FEED	92.2	4.2	1.3	0.00	0.54

**Table 4.9** Elemental analysis of THF-insoluble products from co-coking runs and heat-treated resid coker feed at 475 °C.

	% C	% H	% N	% ASH	H/C
EAGLE	95.8	3.4	1.6	9.81	0.42
POWELLTON	92.5	3.6	1.5	3.49	0.46
PITTSBURGH	92.7	3.7	1.7	7.74	0.48
COKER FEED	93.2	4.1	1.2	0.00	0.52

**Table 4.10** Elemental analysis of THF-insoluble products from co-coking runs and heat-treated resid coker feed at 500 °C.

	% C	% H	% N	% ASH	H/C
EAGLE	100.9	3.4	1.6	11.95	0.40
POWELLTON	93.3	3.2	1.3	3.31	0.41
PITTSBURGH	93.5	3.3	1.6	7.74	0.42
COKER FEED	92.8	3.9	1.2	0.00	0.50

From these results we can deduce that, as expected, with an increase in temperature there is a decrease in the H/C ratio of the THF-insoluble products. The decrease relates to the formation of a more carbon-rich product through the devolatilization of the coal and resid feeds.

It is worth noting that in most cases the H/C values are lower when coals are included in the coking feed than when the resid coker feed is heat treated alone. This may indicate that synergism toward the formation of a more-carbon-rich product is achieved by combining the two feeds. Taking the average H/C ratios for the heat-treated coals and coker feed alone, the values calculated are higher than the actual values recorded. The reason for this is not yet fully understood, but could be related to an enhanced dealkylation effect brought on by liquid/solid surface interactions. From the studies on the fluidity properties of the coals used, we can see for the Powellton and Pittsburgh coals that at the reaction temperatures used (except 500 °C), the coals are still undergoing devolatilization, and hence may not yet have achieved a low H/C ratio.

#### 4.7 Conclusions and Recommendations for Future Work

The work that has been performed in this subtask has met the aims it set out to achieve. We can say that coal-derived compounds useful in the production of thermally stable jet fuel can be produced with the simultaneous upgrading of coal and petroleum resid under delayed-coking

conditions. It is possible to tailor the conditions to produce specific feedstocks for hydrogenation processing, to produce thermally stable jet fuel. This was shown when reaction temperatures at 465 and 475 °C produced oils high in 3- to 5-ring aromatics. If the hydrogenation process were to be severe, then the 3- to 5-ring aromatics would be converted into 1- and 2-ring cycloalkanes and hydroaromatics, which are essential constituents of a thermally stable jet fuel. On the other hand, if the hydrogenation process were to be of low severity, then the products from co-coking at 500 °C would be used. These products are high in 1- to 3-ring aromatics. The yield of sample boiling in the jet-fuel range is lower for co-coking experiments than for the coking of petroleum coker feed alone. This is mainly due to phenolic compounds derived from the coal, which have a tendency to initiate retrogressive reactions and produce more coke and gas.

The solid products formed during co-coking experiments have some interesting properties that merit further investigation. For example, the products from co-coking have lower H/C values than those for the coals and coker feed heat-treated individually. This suggests that coker feed may somehow abstract hydrogen from the coal structure, thus producing a more carbon-rich product. The mechanism for this is not yet fully understood. By turning to a cleaned-coal fraction which has less ash and a smaller particle size than the samples used to date, one might produce a product that is more uniform in composition, and hence of better quality.

Further work must be done to increase the yields of the oil fraction. This may be achieved in several ways. First, a vented system must be used. Our current sealed system prolongs the exposure of the volatile products to high temperatures, which leads to thermal degradation and hence lower yields. Second, the use of decant oil as a feedstock could increase oil yield. This may occur because decant oil can dissolve more coal-derived species, as it is aromatic in nature. Being aromatic it may be more thermally stable than the predominantly aliphatic vacuum resid, even though it contains a high proportion of alkyl side chains. Decant oil is also used to produce high-quality carbon in delayed cokers, which is used as a precursor to needle coke. Finally, by manipulating the reaction conditions such as reaction length and oil-to-coal ratio, we may enhance the oil yield.

To improve the quality of the coke product, the mineral-matter content must be reduced. This can be achieved using coal which has been washed to remove some of the mineral matter. Samples of washed coal have been produced and will be used in the continuation studies in

future work. In addition, the use of smaller particles may improve the evolution of volatiles from the coal and improve the possible dissolution effects when using decant oil. It has already been observed that smaller coal particles produce larger flow domains in the coke product, and hence, a potentially more homogeneous and higher-quality coke.

## **5.0 BLENDING OF COAL-TAR-PITCH DISTILLATES WITH SUITABLE REFINERY STREAMS**

### **5.1 Aims**

The aim of this subtask is to assess the coprocessing capability of coal-tar-pitch distillates with suitable petroleum-based refinery streams, and to see how they could be utilized as precursors to coal-based, thermally stable jet fuel.

### **5.2 Introduction**

As part of the development of processes for the production of coal-based, thermally stable jet fuels, coal-tar pitch could become a potential source. This is due to its adequate supply and cyclic-structure content, which indicates an ability to be upgraded into cycloalkanes and hydroaromatic compounds that may contribute toward high fuel stability at elevated temperatures.

Coal-tar pitch is a by-product from the metallurgical coke industry. It is made up of the volatile compounds evolved during coal carbonization. The predominant usage of coal-tar pitch currently includes the manufacture of electrodes for arc furnaces and the production of fine chemicals through refining. Coal-tar pitch is distilled into various streams. The streams along with their applications include high-quinoline insolubles (QI), low-QI fractions used in electrodes, carbon-black oil for carbon-black production, creosote oil for wood preservation, naphthalene solvent residue (NSR), refined chemical oil (RCO), and light distillates for fine chemical production. Some of these fractions have been selected for this study.

In addition, suitable petroleum-refinery streams have been selected for the coprocessing experiments. These middle distillates have been chosen for their differences in characteristics and availability. First, a kerosene-fraction sample mainly aliphatic in nature was chosen to see how it would blend with the mainly aromatic coal-tar-pitch distillates, as it is also a major feedstock for current jet-fuel production. Second, a light cycle oil (LCO) made up of predominantly aromatic, hydroaromatic, and cycloalkene compounds was chosen, as it contains compounds that may be suitable for thermally stable jet fuel.

### 5.3 Experimental

#### Analysis Performed

Ultimate analysis of carbon, hydrogen, and nitrogen composition and sulfur analysis were performed using a CHN-600 analyzer and a SC-132 sulfur-determination analyzer (LECO). The feedstocks and products were analyzed by high-temperature simulated distillation (HT-SimDis) GC analysis using a Hewlett-Packard 5890 series II plus (fitted with a FID detector) and a Restek MXT-500 column. The samples were diluted with CS<sub>2</sub> and injected into a cool, on-column injector under the following GC conditions: initial oven temperature, 40 °C; total run time, 55 min; and detector temperature, 435 °C. The boiling-point distribution and the cut point of the 200-260 °C fraction, known as the jet-fuel range, were determined. Qualitative analysis and chemical speciation was performed on the feeds and samples using a Hewlett Packard 5890 GC fitted with a 5971 mass-selective detector (MSD) fitted with a J+W DB17 capillary column.

#### Catalyst Preparation

Two different catalysts have been employed in this work. For the desulfurization, a Ni/Mo HDS 1443 CY catalyst was used; for hydrogenation, a Co/Mo 344 TL catalyst was used. Both catalysts were produced by Criterion Catalysts. Prior to their use, the catalysts were sulfided according to the following method:

The catalyst was crushed and passed through a sieve with a 60-mesh (0.25-mm) opening. Into a 25-ml tubing bomb reactor was placed 6 g of dodecane, 1.2 g of carbon disulfide, and 1.6 g of catalyst. The reactor was sealed, purged with hydrogen gas, and pressurized to 250 psig.

The reactor was placed in a sand bath, maintained at 200 °C, for 2.5 hours and agitated at 50 strokes per minute. The temperature was then raised to 350 °C over the course of 1 hour and held at this temperature for 1.5 hours.

When the reaction was complete, the reactor was taken out of the sand bath and allowed to cool down. The gases were released from the reactor in a fume hood, and the reactor's contents were removed and filtered. The catalyst was washed with hexane first and then with acetone. The catalyst was then placed into a sealed vial and dried in a vacuum oven at 110 °C for 2 hours to remove any remaining solvents.



### Samples Used.

Kerosene and LCO were supplied by British Petroleum (BP). The LCO was processed into two additional products. LCO underwent hydrogenation to produce hydroaromatic compounds, which subsequently were subjected to deep hydrogenation to yield a product rich in cycloalkanes. Koppers Industries supplied the coal-tar pitch and coal-tar-distillate samples. Table 5.1 shows the ultimate analysis of the feedstocks used in these experiments.

### Methods for Hydrodesulfurization and Hydrogenation

For a typical hydrodesulfurization run, 2 g of reactants and 0.2 g of CoMo catalyst were loaded into the reactor. The sealed reactor was flushed with H<sub>2</sub>, pressurized to 1000 psig, and then plunged into the sand bath, which had been preheated to a given temperature (usually 400 °C). After the reaction, the reactor was quenched in a cold-water bath and then allowed to cool to room temperature. After collecting a small part of the reaction products from the reactor, the remainder was recovered with THF followed by filtration. The solid yield was estimated from the difference between the weight of the THF-insoluble solid residue and the catalyst. The products from desulfurization were hydrogenated at temperatures between 300 and 400 °C for 1-2 hrs using the NiMo catalyst.

**Table 5.1** Feedstock chemical analysis.

Feed	Ultimate Analysis				H/C Ratio	Jet Range Fraction
	%C	%H	%N	%S		
Kerosene	80.1	14.2	0.1	<0.05	2.14	49.5
LCO <sup>a</sup>	90.0	10.8	0.1	<0.05	1.44	-
LCO <sup>b</sup>	88.8	11.3	0.1	<0.05	1.53	-
LCO <sup>c</sup>	83.8	14.0	0.4	<0.05	2.00	32.5
Coal Tar	-	-	-	0.7	-	13.1
CBO	90.1	5.4	0.6	0.5	0.72	11.4
RCO	92.0	6.1	0.8	0.34	0.79	14.9

LCO<sup>a</sup> light cycle oil feed. LCO<sup>b</sup> hydrogenated light cycle oil. LCO<sup>c</sup> deeply hydrogenated light cycle oil. The value of <0.05% for the sulfur analysis comes from the fact that the sulfur determinator used in this subtask can only accurately measure sulfur levels down to 0.05%. Greater accuracy at lower values can be achieved using alternative techniques, but in the experimentation performed here, not enough sample was produced to employ them.

Variations in the ratio of feedstocks were used to assess their effect on product composition, extent of desulfurization, change in ultimate analysis, and jet-fuel fraction.

## 5.4 Results and Discussion

Initial desulfurization experiments were done using low-QI coal-tar pitch with various concentrations of kerosene. Table 5.2 shows the sulfur levels present after desulfurization and the amount of sulfur removed during the tests.

**Table 5.2** Level of desulfurization in mixtures of coal-tar pitch and kerosene.

Sample Coal tar: Kerosene	% Sulfur	% Removed sulfur
100:0	0.37	47.0
67:33	0.40	18.4
50:50	0.31	16.3
33:67	*	*
0:100	*	*

\* indicates that the sulfur level was below that measurable by our instrument.

With the addition of kerosene, the level of sulfur in the mixtures would have been diluted. However, the percentage of sulfur for the 67:33 mix went up after the reaction, and the overall amount of sulfur removed dropped for both the 67:33 and 50:50 mixes. We believe this is due to a decrease in catalyst performance brought on by the deposition of precipitate. The precipitate was formed when polar constituents of the coal-tar pitch separated from the solution with the addition of non-polar kerosene. The precipitate clogged the pores, which reduced the number of active catalyst sites and led to reduced desulfurization .

Using mixtures of CBO and kerosene, we included a filtered sample to see if the amount of desulfurization increased. We found that about 1.2 wt% of the CBO could be precipitated from the solution using kerosene. This value is somewhat lower than that for the coal-tar pitch precipitate, which was near 10 wt%.

Tables 5.3-5.6 show the results of the desulfurization and hydrogenation of the pure feeds and 50:50 mixes, with and without filtration.

**Table 5.3** Properties and analyses of kerosene, 100%.

Reaction	Mass fraction of products			% Liquid recovery	Ultimate analysis			% S	H/C ratio	200-260 °C fraction (%)
	Solid	Liquid	Gas		% C	% H	% N			
No reaction					80.1	14.2	0.1	*	2.14	N/A
Desulfurization	0	0.7315	0.2685	88.55	82.0	14.8	0.1	*	2.15	55.3
Hydrogenation	0.002	0.507	0.4915	99.03	82.5	14.0	0.1	*	2.04	55.4

\* not measurable.

**Table 5.4** Properties and analyses of carbon-black oil, 100%.

Reaction	Mass fraction of products			% Liquid recovery	Ultimate analysis			% S	H/C ratio	200-260 °C fraction (%)
	Solid	Liquid	Gas		% C	% H	% N			
No reaction					90.1	5.4	0.6	0.50	0.72	11.4
Desulfurization	0	0.7299	0.2701	98.64	85.0	6.7	0.4	0.18	0.94	13.8
Hydrogenation	0	0.5868	0.4132	99.4	82.4	6.7	0.3	0.24	0.98	12.3

**Table 5.5** Properties and analyses of 50% kerosene and 50% carbon-black oil (no filtration).

Reaction	Mass fraction of products			% Liquid recovery	Ultimate analysis			% S	H/C ratio	200-260 °C fraction (%)
	Solid	Liquid	Gas		% C	% H	% N			
Desulfurization	0	0.6328	0.3672	90.46	85.0	10.1	0.2	0.20	1.42	N/A
Hydrogenation	0	0.5928	0.4072	91.71	82.3	9.6	0.2	0.16	1.41	31.8

**Table 5.6** Properties and analyses of 50% kerosene and 50% carbon-black oil (with filtration).

Reaction	Mass fraction of products			% Liquid recovery	Ultimate analysis			%S	H/C ratio	200-260 °C fraction (%)
	Solid	Liquid	Gas		% C	% H	% N			
Desulfurization	0.001	0.7788	0.2201	99.06	82.4	9.6	0.2	0.15	1.40	N/A
Hydrogenation	0	0.8033	0.1967	89.85	86.2	9.8	0.2	0.18	1.37	32.7

Desulfurization of the CBO was as much as 64 wt%. CBO showed signs of undergoing substantial hydrogenation, with an increase in the H/C ratio of over 25%. Filtration did not seem to affect the overall levels of desulfurization and increase in H/C ratio. This is probably because the amount of precipitate produced from mixing CBO and kerosene is low. Mixing of CBO and kerosene had a negative effect on the H/C ratio and jet-fuel range fraction. Using values for the 100% feeds after hydrogenation and estimating values for the 50:50 mixes, yielded values of 1.5 for the H/C ratio and 34 % for the jet-fuel fraction. The actual values from the

experiments were around 1.4 and 32 %. The reason for this result is unclear, but the same result was observed when LCO<sup>c</sup> and CBO were used (Tables 5.7 and 5.8).

**Table 5.7** Properties and analyses of deeply hydrogenated light cycle oil (LCO<sup>c</sup>).

Reaction	Ultimate analysis			% S	H/C ratio	200-260 °C Fraction (%)
	% C	% H	% N			
No reaction	83.8	13.9	0.4	*	1.99	32.5
Desulfurization	85.8	13.8	0.4	*	1.93	42.1
Hydrogenation	77.9	13.6	0.4	*	2.09	40.3

\* not measurable

**Table 5.8** Properties and analyses of 50% LCO<sup>c</sup> and 50% CBO (no filtration).

Reaction	Ultimate analysis			% S	H/C ratio	200-260 °C Fraction (%)
	% C	% H	% N			
No reaction	87.0	9.4	0.8	0.29	1.30	N/A
Desulfurization	84.5	10.3	0.5	0.08	1.46	26.8
Hydrogenation	80.3	9.6	0.6	0.02	1.43	26.4

Once again the H/C ratio for the hydrogenated products of the 50:50 mix is 0.1 lower than the value calculated from the pure-feed results. This implies that CBO is not undergoing hydrogenation in mixtures to the same extent as when in the pure form. It is less successful than kerosene or LCO<sup>c</sup> in competing for hydrogen. In mixtures of LCO<sup>c</sup> and CBO there was no decrease in the measured jet-fuel-range fraction when compared with the estimated value. Sulfur removal in mixtures of LCO<sup>3</sup> and CBO was as high as 93 wt%. The effect of filtering the sample after mixing was noticeable with the LCO<sup>c</sup> and CBO mixtures. The sulfur levels decreased from 0.29% to 0.14% after filtering. However, Figures 5.2 and 5.4 show that filtration lowers the overall H/C ratio and conversion to the jet-fuel range. As the level of sulfur approaches 0.02 wt% after hydrogenation, even without filtration, it may not be necessary in this case.

Refined chemical oil (RCO) is a distillate fraction derived from coal-tar pitch. About 60 wt% of the RCO is naphthalene and methylnaphthalene. Table 5.9 shows the results of desulfurization tests on RCO and mixtures of RCO with LCO<sup>c</sup>.

**Table 5.9** Properties and analyses of refined chemical oil (RCO) and its 50% mixture with light cycle oil (LCO<sup>c</sup>).

Reaction	Ultimate analysis			% S	H/C atomic ratio	200-260 °C Fraction (%)
	% C	% H	% N			
RCO	92.0	6.1	0.8	0.34	0.79	14.9
RCO (HDS)	86.2	6.6	0.6	0.08	0.92	16.8
RCO:LCO <sup>c</sup> (HDS)	87.4	9.4	0.3	0.02	1.32	32.1

It can be seen that as with mixtures of LCO<sup>c</sup> and CBO, the LCO<sup>c</sup>:RCO mix achieved a sulfur reduction of about 94 %. Again there is a lowering by about 0.1 in the H/C ratio for the mixture, but the jet-fuel-range fraction has experienced some synergism and is 2.6% higher than the predicted value taken from processing the feeds alone.

At this stage in the experimental work, it was decided that future studies would focus on an RCO feed. Mixtures of RCO and LCO<sup>a-c</sup> would be assessed and the reaction parameters optimized.

The effects of changing the reaction time and temperature in the desulfurization experiments on RCO and 50:50 mixtures of RCO and LCO<sup>c</sup> to 350 °C for 1 and 2 hours are shown in Tables 5.10 and 5.11.

**Table 5.10** Properties and analyses of refined chemical oil (RCO) using a CoMo catalyst and reaction temperature of 350 °C.

Reaction	Ultimate analysis			% S	H/C atomic ratio	200-260 °C Fraction (%)
	% C	% H	% N			
RCO	92.0	6.1	0.8	0.34	0.79	14.9
RCO (CoMo, 1 hr)	84.3	6.8	0.3	0.06	0.97	38.8
RCO (CoMo, 2 hr)	88.9	7.4	0.3	0.03	1.00	37.2

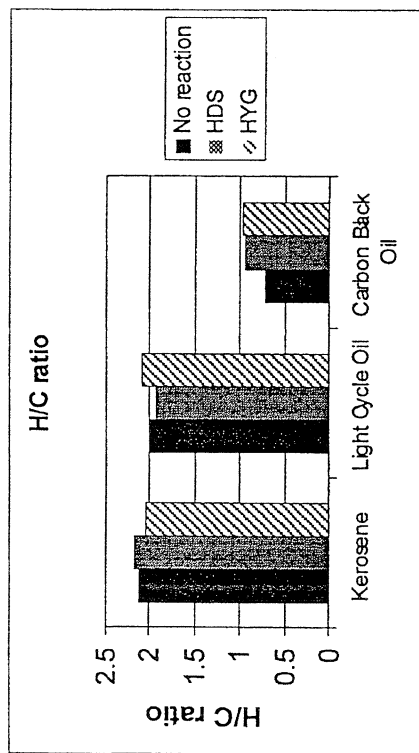


Figure 5.1: The comparison of hydrogen-to-carbon ratio between different feedstocks and reactions.

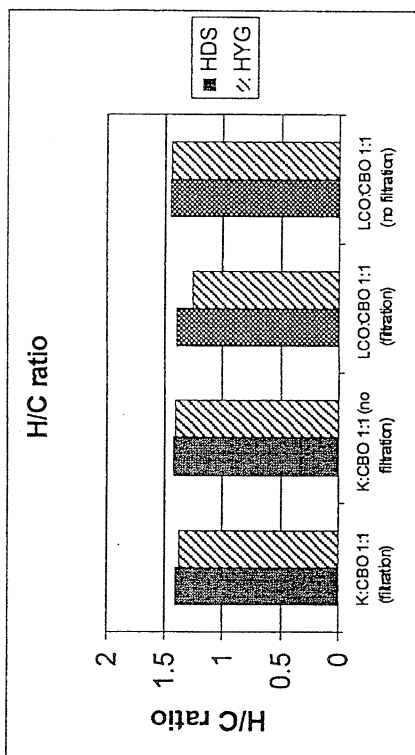


Figure 5.2: The comparison of hydrogen-to-carbon ratio between different mixtures and reactions.

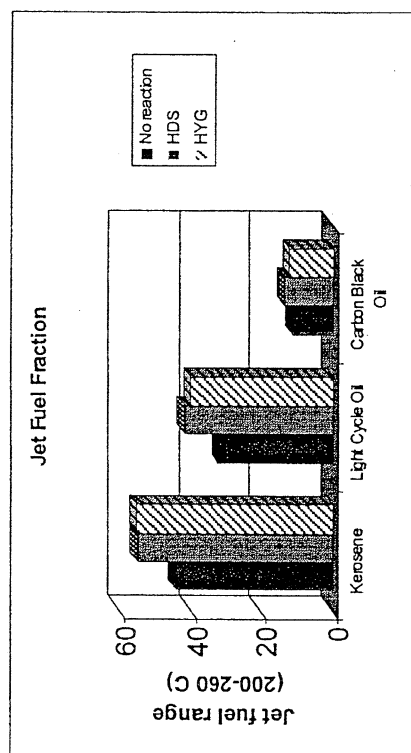


Figure 5.3: The comparison of jet fuel fraction between different feedstocks and reactions.

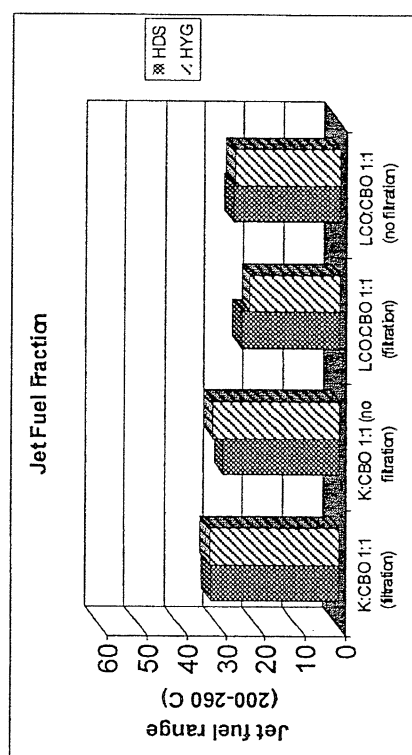


Figure 5.4: The comparison of jet fuel fraction between different mixtures and reactions.

**Table 5.11** Properties and analyses of a refined chemical oil (RCO) and light cycle oil (LCO<sup>c</sup>) mixture reacted at 350 °C using a CoMo catalyst.

Reaction	Ultimate analysis			%S	H/C atomic ratio	200-260 °C Fraction (%)
	% C	% H	% N			
RCO:LCO <sup>c</sup>	88.4	10.0	0.6	0.14	1.35	23.7
RCO:LCO <sup>c</sup> (CoMo, 1 hr)	87.5	10.8	0.1	0.02	1.47	47.1
RCO:LCO <sup>c</sup> (CoMo, 2 hr)	88.0	11.6	0.03	0.02	1.57	39.9

By lowering the temperature of desulfurization from 400 °C to 350 °C, the level of desulfurization in the RCO has remained comparable, but the H/C ratio increased and the fraction of sample in the jet-fuel range more than doubled (176%). By increasing the length of the run to 2 hours an even greater desulfurization was achieved, along with a higher H/C ratio. However, a small drop in jet-fuel range components was noticed. The main reason for these changes is that a reaction temperature of 400 °C leads to the decomposition of the samples into low-boiling liquids and gases. This is most evident in the changes in the jet-fuels fraction; the lower H/C ratios indicate the evolution of lighter-hydrocarbon gases (C<sub>1</sub>-C<sub>4</sub>). With the mixtures of LCO<sup>c</sup> and RCO, similar improvements in the quality of the products at 350 °C were noted.

The GC chromatograms for the RCO and LCO<sup>c</sup> mixtures before and after reacting using NiMo under conditions of 1000 psig, 350 °C, and a 1-hour reaction time are shown in Figures 5.5 and 5.6. The mixture before reaction has some decalin from LCO<sup>c</sup> plus naphthalene and methylnaphthalene from RCO. The chromatogram taken after the reaction has a higher amount of tetralin and some naphthalene. This is due to hydrogen-transfer reactions from the hydroaromatic compounds in the LCO<sup>c</sup> and catalytic hydrogenation reactions.

The effects of time, temperature, and H<sub>2</sub> pressure on the hydrogenation of RCO and RCO:LCO<sup>c</sup> mixtures using the NiMo catalyst were measured. The results are shown in Tables 5.12 and 5.13.

**Table 5.12** Analyses of hydrogenated products from refined chemical oil (RCO) under varying conditions.

Reaction	Ultimate analysis			H/C atomic Ratio	200-260 °C Fraction (%)
	% C	% H	% N		
Condition: 1000 psi, 350°C					
RCO (2 hr)	87.9	7.2	0.4	0.99	23.4
RCO (1 hr)	87.3	6.9	0.4	0.95	25.8
Condition: 1000 psi, 375°C					
RCO (2 hr)	81.8	8.3	0.2	1.21	56.0
RCO (1 hr)	79.4	7.4	0.2	1.12	57.1
Condition: 1300 psi, 350°C					
RCO (2 hr)	84.9	7.3	0.3	1.03	62.1
RCO (1 hr)	87.1	7.9	0.2	1.09	58.1



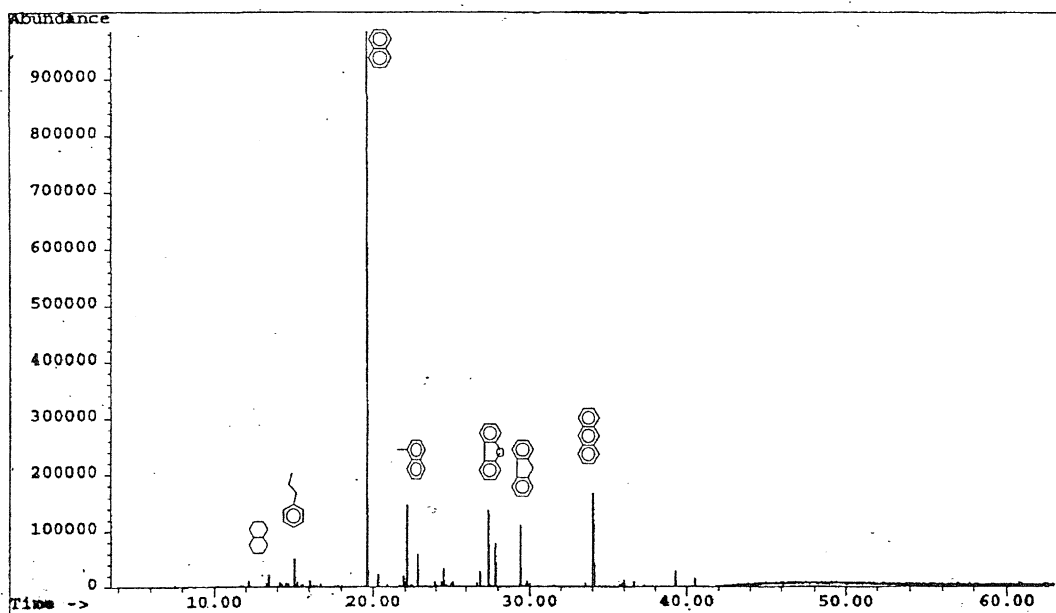


Figure 5: GC-MS of refined chemical oil and light cycle oil before reaction.

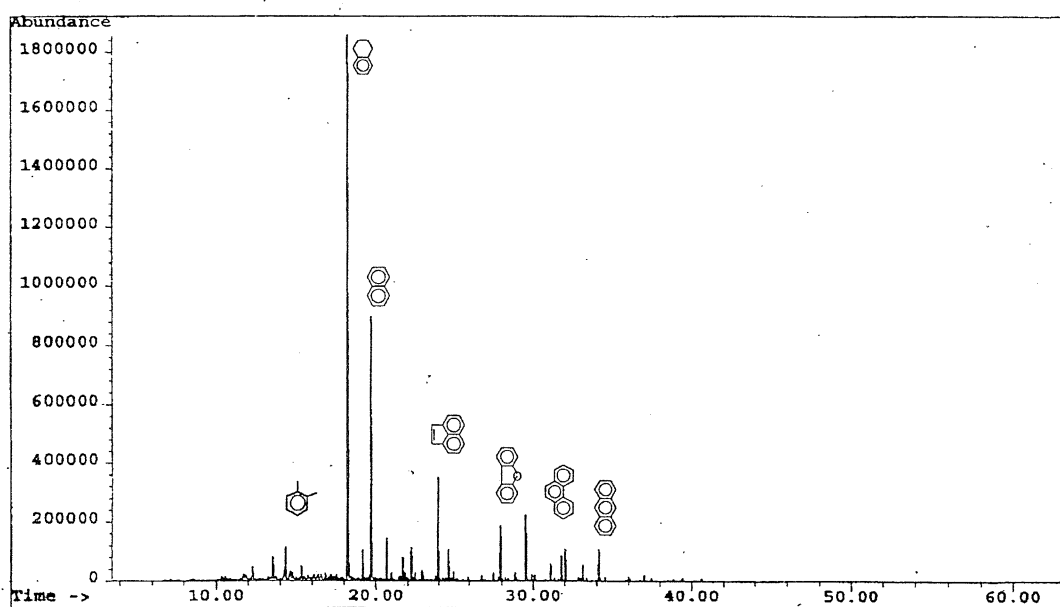


Figure 6: GC-MS of refined chemical oil and light cycle oil after reaction (NiMo, 350°C, 1 hr)

**Figures 5.5 and 5.6** GC-MS of refined chemical oil and light cycle oil before (top) and after (bottom) reaction.

**Table 5.13** Analyses of hydrogenated products from the blends of refined chemical oil (RCO) and deeply hydrotreated light cycle oil (LCO<sup>c</sup>) under varying conditions.

Reaction	Ultimate analysis			H/C atomic Ratio	200-260 °C Fraction (%)
	% C	% H	% N		
Condition: 1000 psi, 350°C					
LCO <sup>c</sup> : RCO (2 hr)	84.1	10.6	0.1	1.51	47.5
LCO <sup>c</sup> :RCO (1 hr)	86.9	11.0	0.1	1.52	52.4
Condition: 1000 psi, 375°C					
LCO <sup>c</sup> :RCO (2 hr)	85.5	11.1	0.1	1.56	55.2
LCO <sup>c</sup> :RCO (1 hr)	86.5	11.3	0.1	1.57	49.7
Condition: 1300 psi, 350°C					
LCO <sup>c</sup> :RCO (2 hr)	87.6	12.2	0.1	1.67	62.7
LCO <sup>c</sup> :RCO (1 hr)	87.7	11.5	0.1	1.58	52.3

It can be seen that there are improvements in the H/C ratio and fraction of the sample boiling in the jet-fuel range, with both increases in temperature and pressure.

Table 5.14 shows that with the use of different LCO feeds, the increase in hydrotreatment which then undergo results in a change in the H/C ratio and fraction boiling in the jet-fuel range. The increase in hydrotreatment increases the species that can participate in hydrogen-transfer and hydrogen-donation reactions, thus improving and upgrading the RCO.

**Table 5.14** Analyses of different LCO: RCO mixtures, 1000 psig H<sub>2</sub> pressure and 350°C.

Reaction	Ultimate analysis			H/C atomic ratio	200-260 °C Fraction (%)
	% C	% H	% N		
LCO <sup>a</sup> :RCO (2 hr)	89.1	10.1	0.2	1.35	N/A
LCO <sup>a</sup> :RCO (1 hr)	82.8	10.0	0.1	1.45	42.4
LCO <sup>b</sup> :RCO (2 hr)	88.2	10.2	0.1	1.39	N/A
LCO <sup>b</sup> :RCO (1 hr)	88.5	10.0	0.1	1.35	49.1
LCO <sup>c</sup> :RCO (2 hr)	84.1	10.6	0.1	1.51	47.5
LCO <sup>c</sup> :RCO (1 hr)	86.9	11.0	0.1	1.52	52.4

Figures 5.7-5.12 show GC chromatograms from different runs using RCO and RCO:LCO<sup>c</sup> mixtures under various hydrogenation-reaction conditions. As in Figures 5.5 and 5.6, it can be seen that the major products are tetralin and naphthalene. The effect of hydrogenation conditions on the composition of the final products is exemplified in the differences among Figures 5.10, 5.11, and 5.12. By raising the temperature or increasing the pressure, a complex mixture of compounds can be refined into a sample containing predominantly tetralin or naphthalene, respectively.

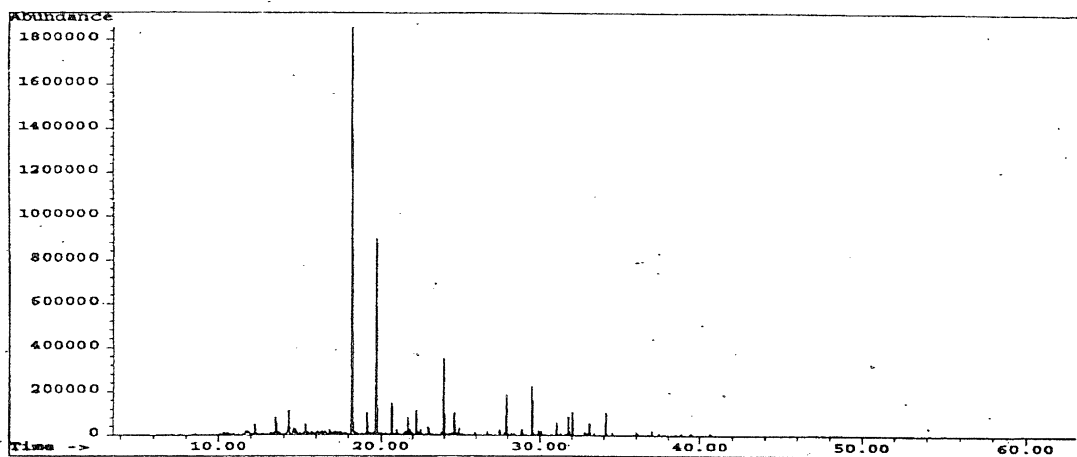


Figure 5.7 GC-MS of RCO and deeply hydrotreated LCO at 1000 psig  $H_2$  pressure and 350°C, 1 hour. (Tetralin peak: 18.1 minutes; naphthalene peak: 19.6 minutes)

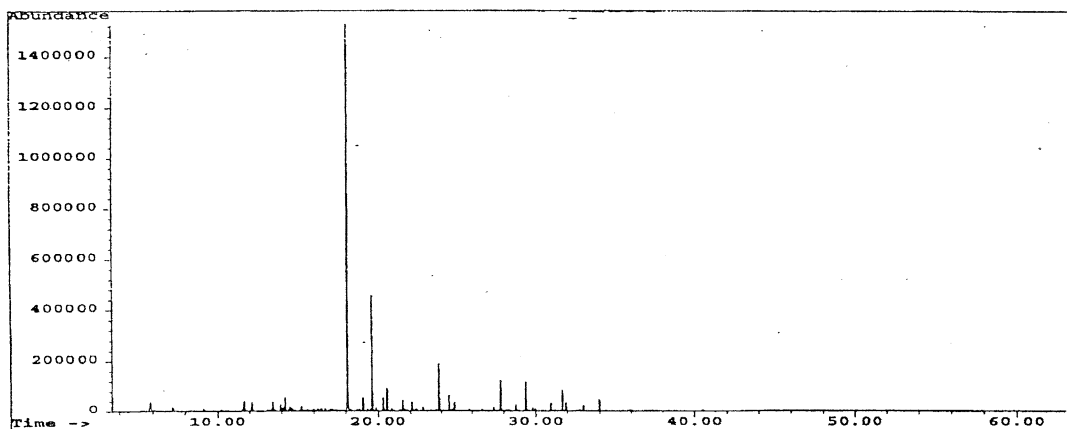


Figure 5.8 GC-MS of RCO and deeply hydrotreated LCO at 1000 psig  $H_2$  pressure and 375°C, 1 hour.

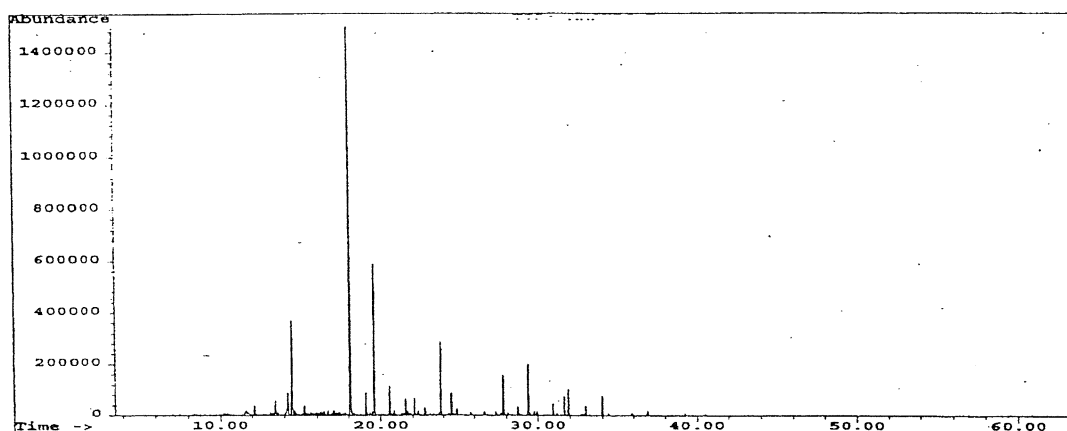


Figure 5.9 GC-MS of RCO and deeply hydrotreated LCO at 1300 psig  $H_2$  pressure and 350°C, 1 hour.

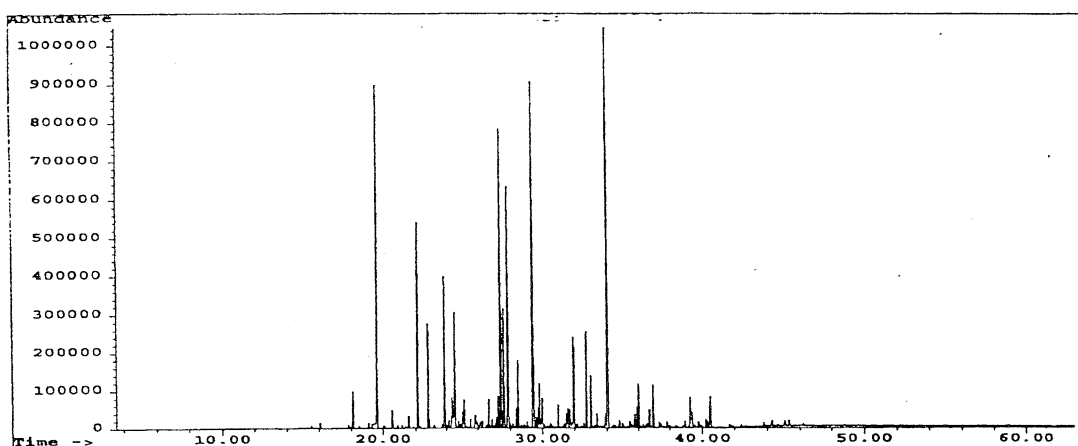


Figure 5.10 GC-MS of RCO at 1000 psig H<sub>2</sub> pressure and 350°C, 2 hours.

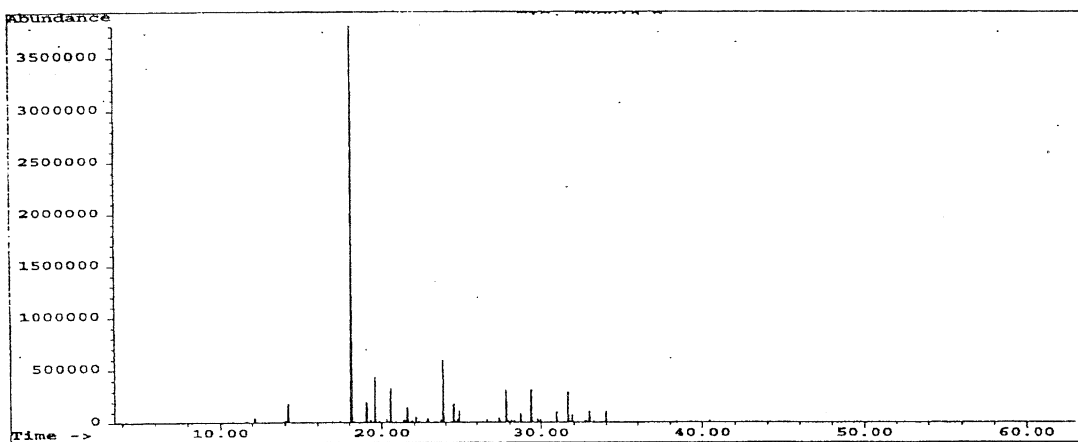


Figure 5.11 GC-MS of RCO at 1000 psig H<sub>2</sub> pressure and 375°C, 2 hours.

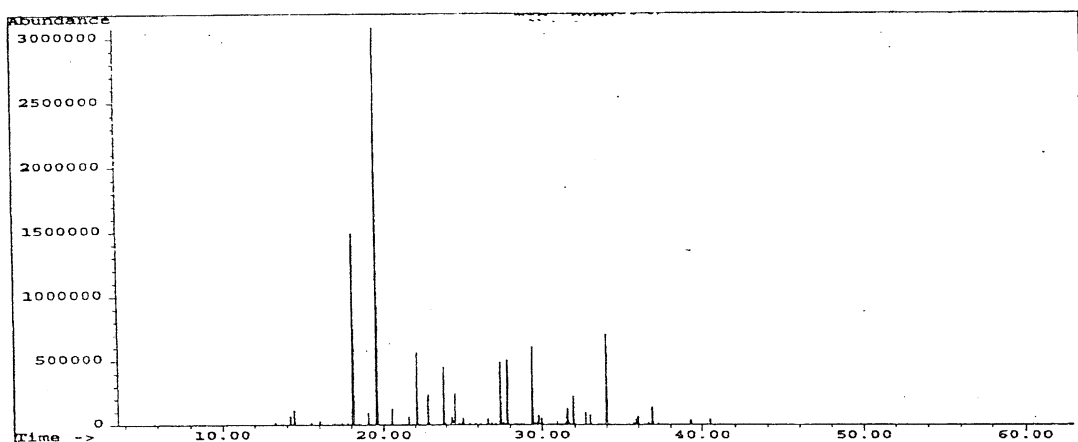


Figure 5.12 GC-MS of RCO at 1300 psig H<sub>2</sub> pressure and 350°C, 2 hours.

Figures 5.10, 5.11, and 5.12. GC-MS of RCO at various pressures and temperatures.

## 5.5 Conclusions and Future Recommendations

The aims of the subtask have been met. Suitable coal-tar-pitch distillates have been found, and when coprocessed with certain refinery streams, produce products that would make good candidates for upgrading to jet fuel. To date the best combinations used are mixtures of refined chemical oil from coal-tar pitch and deeply hydrogenated light cycle oil. Under certain reaction conditions, we have produced a sample having over 60% of its content boiling in the jet-fuel range (200-260 °C) and having had its sulfur and nitrogen levels reduced by over 95% and 0.1 wt%, respectively. In addition, a significant upgrading of the refined chemical oil to hydroaromatic species has been achieved.

To date the best coal-tar distillate found would be refined chemical oil. It is both high in suitable components for conversion into 2-ring cycloalkanes, and it also blends well with the refinery streams used. The light cycle oil used proved to be a better refinery stream than kerosene. The higher aromatic content results in a higher conversion to hydroaromatics and cycloalkanes, which may contribute toward producing thermally stable jet fuel. We have shown that by changing the temperature of the process by just a few degrees, we can change the overall product fractions and components simultaneously. In future work the parameters will be optimized further.

Suitable coal-liquid sources and refinery streams must still be investigated. To this end a coal liquid produced by SGI International has been obtained. The neutral oil fraction will be separated from the tar acid fraction before processing. This will be done as preliminary studies with the whole oil gave less than satisfactory results. It may also be possible to combine the desulfurization and hydrogenation stages using a single catalyst. Through consulting Criterion Catalysts, a possible candidate catalyst has been identified for such a purpose. However, the reaction conditions that can be achieved in a small tubing bomb reactor are less than ideal. By increasing the scale of the operation to a large stirred-tank reactor (STR) or a continuous-flow reactor (CFR) system, an even better conversion may be achieved. This may apply especially to the conversion of aromatic components to cycloalkanes, instead of the intermediate hydroaromatic compounds already produced. We have at our disposal a 300-ml STR and soon will have a 1000-ml CFR; plans to utilize this new apparatus are in place.

## 6.0 ENHANCING STABILITY OF THE PETROLEUM AND COAL-DERIVED COMPONENT

### 6.1 Thermal-Stability Testing of Naphthenic Liquids

The objective of this subtask is to examine the thermal stability of jet fuels derived from the hydrogenation of pyrolysis oils that are already available at Propulsion Directorate of the Air Force Research Laboratory and the thermal stability of jet fuels made by hydrogenating LCO (obtained from BP). The rationale is that the hydrogenated pyrolysis oils from Propulsion Directorate of the Air Force Research Laboratory and hydrogenated LCO from BP are cycloalkane-rich, and may be suitable candidate jet fuels with improved thermal stability. To accomplish this objective a flow-reactor experiment has been developed, refined, and used to study the thermal stability of various fuel samples.

The flow reactor was first tested in the summer of 1998 with four fuels: straight-run kerosene, JP-8P, hydrotreated light cycle oil (HT LCO), and dearomatized hydrotreated light cycle oil (DA/HT LCO). Each run was analyzed for carbon deposition. It was found that the results obtained were not reproducible. Figure 6.1 shows the carbon-deposition profiles and wetted-wall temperature profiles for the two kerosene runs.

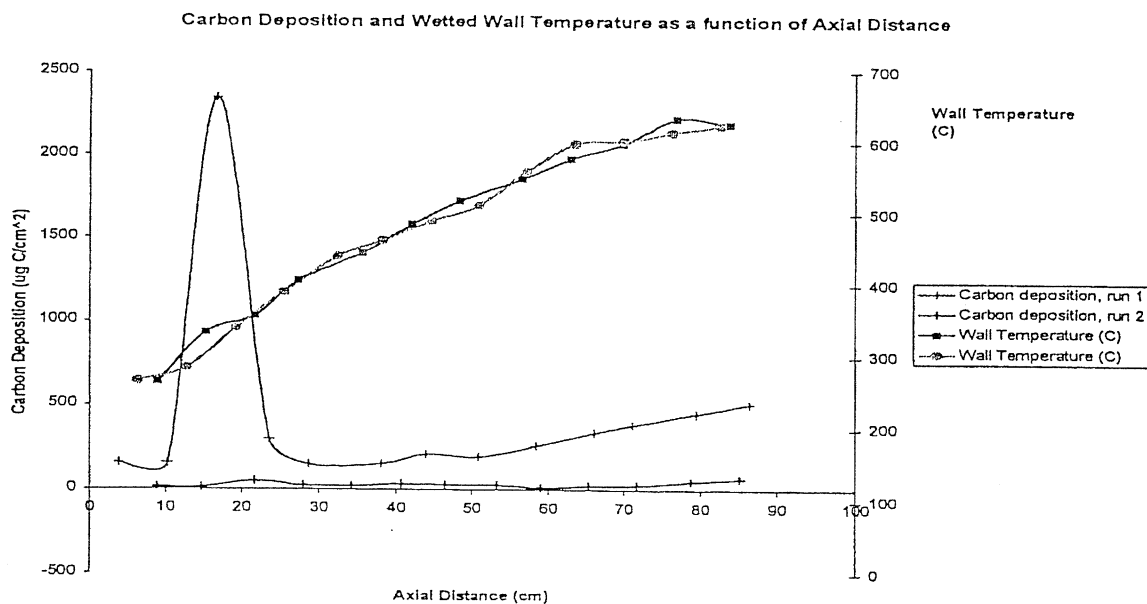


**Figure 6.1** Carbon-deposition and wetted-wall temperature versus axial distance for two kerosene runs. Furnace temperature, 700 °C; pressure, 700 psig; flow rate, 12 mL/min; duration, 7 hours.

As can be seen from the temperature profiles in Figure 6.1, the fuels were exposed to a very similar environment in terms of temperature. The bulk-fuel outlet temperatures, measured by a thermocouple inserted into the stream, were very similar in both runs. The first run had a bulk-fuel temperature of 468 °C, and the second was measured to be 475 °C. However, it is also apparent from Figure 6.1 that the deposition profiles vary greatly. There is a large amount of deposition in the autoxidative regime in the first run and a minimal amount in the second. The quantity of deposition in the pyrolytic regime differs between the two runs by an order of magnitude.

Similar variations were seen in the runs using JP-8. HT LCO was so unstable it was impossible to complete a run at the time. In contrast, there was very little variation in the runs using DA/HT LCO. The DA/HT LCO, which closely resembles coal-derived jet fuels, appeared to be very stable; very little deposition was produced. Another significant feature of the two runs using DA/HT LCO was that the pressure rarely fluctuated throughout the run, whereas significant fluctuations were observed in the other runs.

The pressure in the flow reactor is controlled using a backpressure valve, which was manually adjusted when the pressure rose or fell beyond a certain point. When pressure increases, the fuel may experience a longer residence time in the furnace. Because the residence time in a flow reactor is so short, any variation may have a significant effect. The DA/HT LCO, which had very small pressure fluctuations, showed much less variation in carbon deposition profiles than did any of the other fuels.

As a result of this observation, an automated pressure system has been designed and installed. A transducer measures the pressure and relays the results to the computer. This serves two purposes. The first is to create a pressure history, which can be referred to after the run. Pressure fluctuations can be quantified more accurately. The second purpose is to provide input for controlling the pressure. The control program assesses the input, and a stepper motor turns the backpressure valve if needed. It is hoped that this method of controlling the pressure of the reactor will be more accurate than manual control. At this point, the pressure transducer is in place, but the system is not yet automated.

Another noted source of variation was the amount of variation occurring in the autoxidative regime. Both the first run with kerosene and the first run with JP-8 showed large amounts of carbon deposition in the 150-300 °C range, whereas the second run for both fuels did not. It appears that the amount of oxygen within the fuel is inconsistent between runs. As a result, it was decided that sparging with an appropriate gas was necessary. For the studies currently being done, UHP N<sub>2</sub> is being used.

A few other problems were noted during the preliminary runs and were fixed. Bulk insolubles were previously not collected. A post-furnace filter was added to remedy this oversight. An attempt was made to use a 0.5-um filter, but it was found that the filter clogged too quickly when an unstable fuel was used. A 2-um filter was used instead. In addition, liquid was being entrained in the gas samples. Although the phase change from a supercritical fluid to a liquid and gas occurred in the heat exchanger as the product mixture is cooled, the phase separation occurred in the backpressure valve. The distance between the backpressure valve and the gas-collection port was inadequate for proper separation to occur. Adding a subsequent condenser has extended the distance and enhanced the separation.

In the past month, five runs using kerosene have been performed using the improved reactor. The carbon deposition from one run is shown in Figure 6.2.

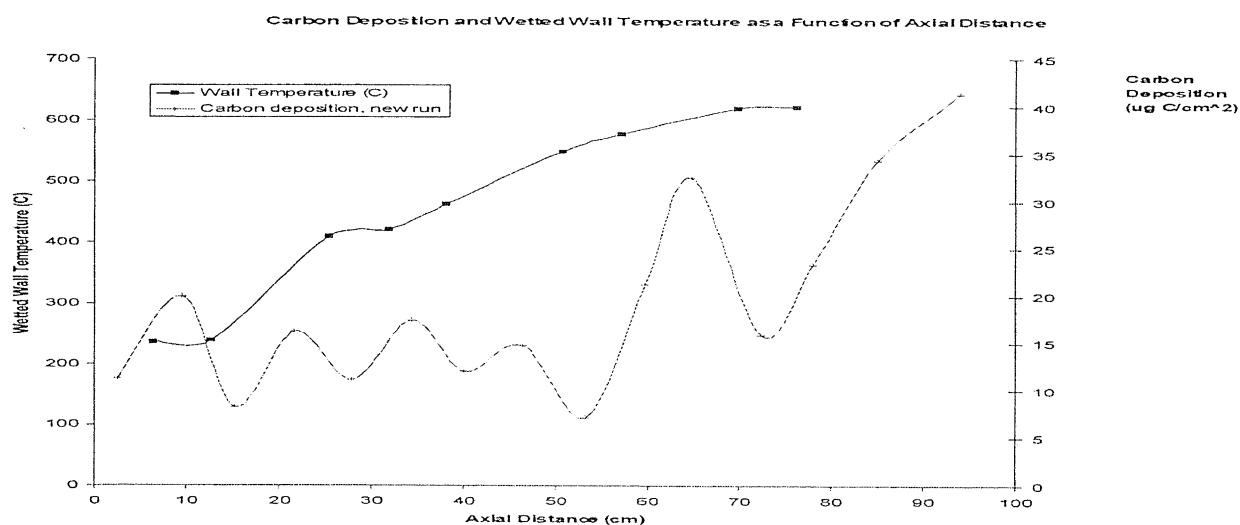


**Figure 6.2** Carbon deposition and wetted-wall temperature profiles for kerosene run on improved reactor. Furnace temperature, 700 °C; pressure, 700 psig; flow rate, 10 mL/min; duration, 7 hours.



The fuel was sparged for two hours with UHP N<sub>2</sub> to remove the oxygen. Pressure was monitored using the transducer. The kerosene was remarkably stable, and no automatic pressure control was required. The recorded pressure history has shown that the standard deviation of the values was around 10 psig.

The data from the other four runs has not been completely analyzed to date due to equipment availability and the length of time needed per analysis.

## 6.2 Summary

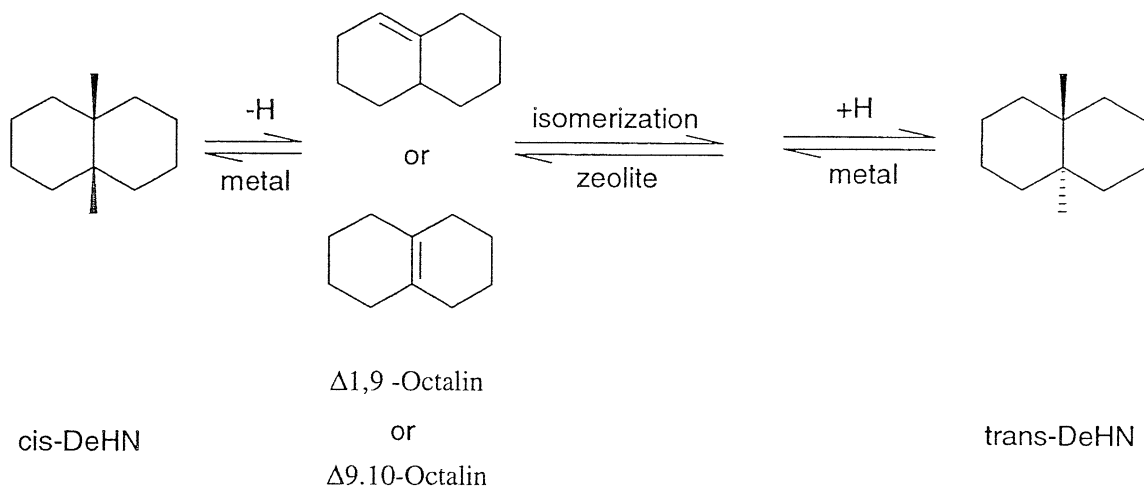
At present, an extensive matrix of fuel tests is underway in this flow reactor, and the experimental uncertainty in the current configuration is being assessed. Our preliminary results have shown that JP-8 is highly unstable under pyrolytic conditions, as is HT LCO. In contrast, both kerosene and the DA/HT LCO fuels have shown very high stability. Controlling the dissolved-oxygen concentration in the fuel prior to testing remains a concern that must be addressed in our present work. For the time being, sparging will allow us to remove O<sub>2</sub>, but we cannot include precise amounts of oxygen in the fuel.

## 7.0 CONFORMATIONAL ISOMERIZATION OF CYCLOALKANES

### 7.1 Introduction

In order to meet the requirements of future high-Mach aircraft, a new generation of advanced jet fuels needs to have good thermal stability at high temperatures, up to 900 °F. [14] It is well-established that coal-derived jet fuels are more thermally stable than petroleum-based fuels because the former are rich in alkylcycloalkanes, decalins, and tetralins. [14,15] Based on the stereo-structures of hydrocarbons such as cycloalkanes, cis-isomers are generally less stable (thermodynamically and chemically) than their corresponding trans-compounds. Earlier studies by Song and Lai have shown that trans-decahydronaphthalene (DeHN) is more thermally stable than cis-DeHN [16] and trans-1,2-dimethylcyclohexane (DMCH) is more stable than cis-1,2-DMCH [17]. Therefore, those more thermally stable isomers are highly desirable components in future jet fuels. To achieve this goal, conformational isomerization with dual-functional catalysts has proven to be an effective method to increase the content of those thermally stable isomers. For conformational isomerization of hydrocarbons, dual-functional catalysts, which consist of an acidic support and a metal, are commonly used to accelerate the isomerization reactions. In general, the metal loaded is platinum or palladium. Although the catalysts play a key role in the conversion from the cis- to trans-isomer, operating conditions such as reaction temperatures, initial hydrogen pressures, and residence times will have some impact on the isomerization process. A possible mechanism for conformational isomerization can be described as follows. First, cycloalkane molecules diffuse into the internal channel of a zeolite and are absorbed on the surface of the zeolite. The absorbed cycloalkanes are then dehydrogenated by active-metal centers to form the corresponding cycloalkenes. The intermediates (cycloalkenes) obtained then undergo conformational isomerization which is controlled not only by the acidic strength but also by the pore size and channel structure of the zeolites. Finally, the isomerized cycloalkene molecules are hydrogenated to produce the desired cycloalkane isomers by the active-metal sites. The isomer obtained will diffuse out into the bulk phase. For demonstration purposes, the conversion of cis-DeHN to trans-DeHN is described in detail in Scheme 1. Although the desired conformational isomerization reaction is the dominant process, accompanying side reactions such as hydrocracking and skeletal isomerization take place. These side reactions can be minimized by selecting acidic support materials and adjusting reaction conditions. In this report,

model compounds such as cis-DeHN, cis-1,2-DMCH, and cis-1,4-DMCH have been selected. The support used in our investigation is ultrastable Y (CBV740) or dealuminated mordenite (CBV30A), as shown in Table 7.1.



Scheme 1. Possible mechanism for conversion of cis-DeHN to trans-DeHN. [16]

This final report will present the results and a discussion of the conformational isomerization of the model compounds with zeolite-supported noble-metal catalysts under different reaction conditions.

## 7.2 Experimental

The catalysts examined were 0.5Pt/CBV740, 0.5Pt/CBV30, 0.5Pd/CBV740, and 0.5Pd/CBV30A, which were prepared by the incipient-wetness impregnation of an aqueous solution of  $[\text{Pt}(\text{NH}_3)_4]\text{Cl}_2 \cdot x\text{H}_2\text{O}$  (Aldrich, 99.99%) or  $[\text{Pd}(\text{NH}_3)_4]\text{Cl}_2 \cdot \text{H}_2\text{O}$  (Aldrich, +99.99%). The metal loading ratio of each catalyst was 0.5 wt %. After impregnation, the zeolites obtained were vacuum dried at 120 °C for 8 h and then calcined in air at 450 °C for 4 h. Cis-DeHN, cis-1,2-DMCH, and cis-1,4-DMCH (all from Aldrich, 99 %) were used in the study. The reduction of all catalyst precursors was carried out *in situ*. In a typical run, a model compound and a catalyst precursor were charged into a 25-ml horizontal tubing bomb reactor. The reactor was sealed, purged with 1000-psig UHP hydrogen, and pressurized (at selected pressure) with hydrogen. When a reaction was completed, the reactor was quenched immediately by immersion into a cold-water bath and then air dried. The liquid products were separated from the solid catalyst by

filtration. The products obtained were analyzed on a Perkin-Elmer 8500 GC equipped with a capillary column (DB-17) and an FID detector, and operated in the split-injection mode. The product identification was based on a GC/MS analysis and a comparison with the GC analytical results of standard compounds.

**Table 7.1** Typical properties of zeolites used.

Trade name (name used in this report)	Cation form	Na <sub>2</sub> O (wt-%)	SiO <sub>2</sub> /Al <sub>2</sub> O <sub>3</sub> (molar ratio)	Surface area (m <sup>2</sup> /g)	Provider
CBV740(USY40)	hydrogen	0.03	40	750	Zeolyst
CBV30A(HM30A)	ammonium	0.02	35	600	PQ

**Table 7.2** Feed conditions used for conformational isomerization of cycloalkanes.

Model compound	Catalyst precursor (g)	Reactant feed (g)
cis-DeHN	0.15	3.60
cis-1,2-DMCH	0.10	1.60
cis-1,4-DMCH	0.10	1.60
cis-1,3-DMCH	0.10	1.60

**Table 7.3** GC analysis programs used for liquid products.

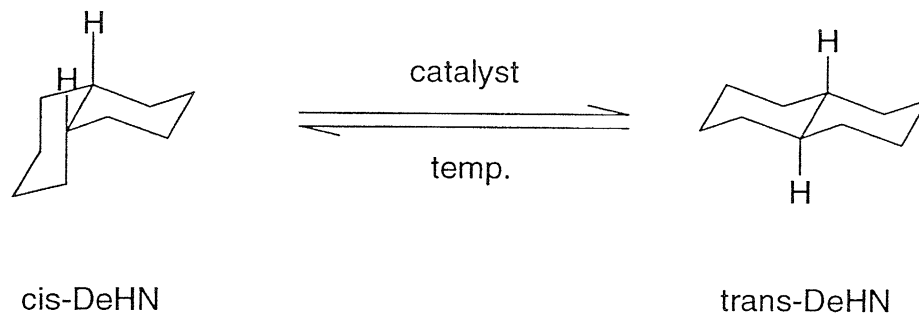
Model comp.	Initial temp. (°C)	Isothermal (min)	Ramp rate (°C/min)	End temp. (°C)	Isothermal (min)
cis-DeHN	40	5	6	240	5
cis-1,2-DMCH	40	5	4	160	5
cis-1,4-DMCH	40	5	4	160	5
cis-1,3-DMCH	40	5	4	160	5

### 7.3 Results and Discussion

This section is divided into two parts which discuss the conformational isomerization of cis-DeHN and cis-DMCHs separately.

### Conformational Isomerization of cis-DeHN

In order to have a better look at stereostructural differences and the effects of configurational structures during the conformational isomerization process, the general path from cis-DeHN to trans-DeHN is illustrated in detail in Scheme 2.



Scheme 2. Conversion from cis-DeHN to trans-DeHN.

### *The Effect of Temperature on Conformational Isomerization of cis-DeHN*

It is well known that the reaction temperature is related to the reaction rate constant and activation energy by the Arrhenius equation. Temperature is also thermodynamically linked to the equilibrium constant by the equation,  $\ln(K) = -\Delta G^0/RT$ . Thus, temperature is one of the most important factors influencing isomerization reactions. The effect of temperature was investigated using the four CBV30A- or CBV740-supported noble-metal catalysts. In this report, the conformational isomerization of cis-DeHN was carried out in a temperature range from 483 to 643 K with an initial hydrogen pressure 1000 psig. The results obtained are shown in Figs. 7.1 and 7.2. Figure 7.1 shows that the conversion of cis-DeHN increased with the reaction temperature with each of the four catalysts used. When the temperature was above 573 K, the Pd catalysts appeared to be more active than the Pt-loaded catalysts at lower temperatures. Pd on mordenite (0.5Pd/CBV30A) is the most active catalyst at temperatures from 483 to 503 K, with about 90 % conversion. A possible reason is that there were more available Pd sites on the surface of the catalysts due to its lower atomic number compared with Pt. When the temperature was above 543 K, similar conversions were observed for both Pd- and Pt-containing catalysts,

which could be attributed to the more active Pt hydrogenating/dehydrogenating sites. Furthermore, the catalyst supporters CBV740 and CBV30A exhibited little difference in the conversion to trans-DeHN in the temperature range of 543-643 K.

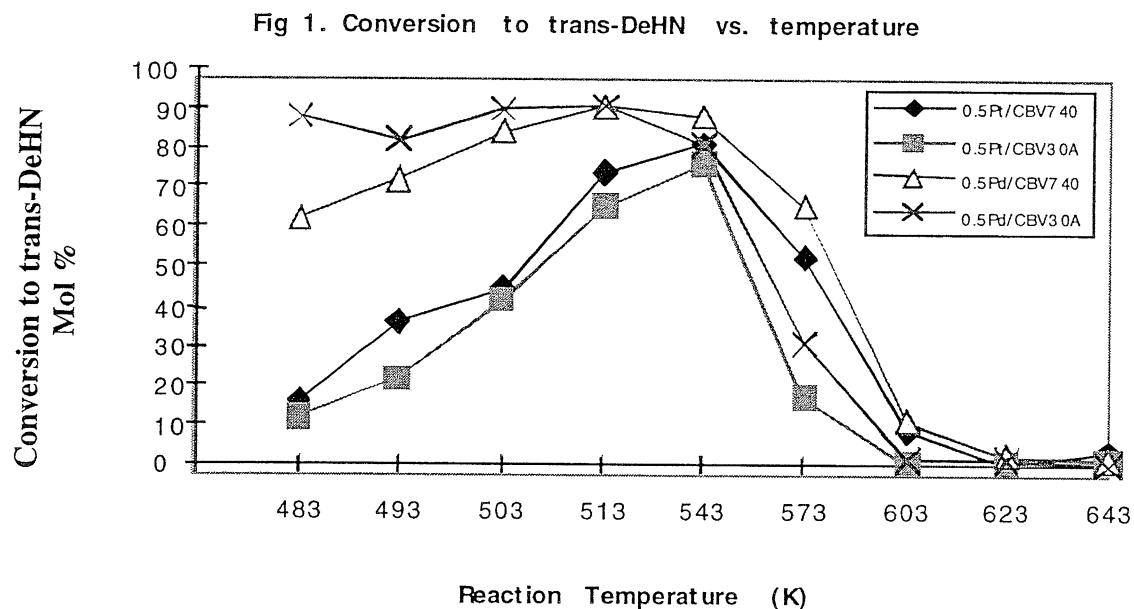


**Figure 7.1** Conversion to trans-DeHN vs. temperature.

Figure 7.2 shows that almost 100 % selectivity was achieved when the temperature was between 483 and 513 K. The selectivity decreased sharply as the temperature rose above 573 K. The GC/MS and GC analysis indicated that skeletal isomerization and hydrocracking reactions took place above 543 K. Figure 7.2 also reveals that the type of noble metal and support had a significant impact on the selectivity in the intermediate temperature range from 531 to 603 K, but made almost no difference at low (<513K) or high (>603 K) temperatures.

Fig. 2 Selectivity vs temperature

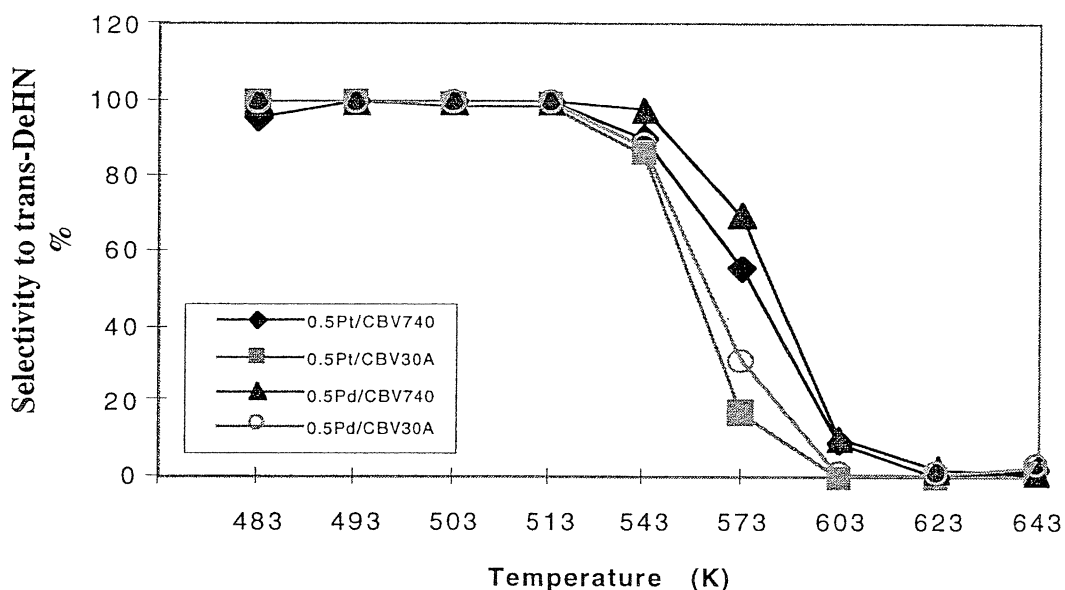


Figure 7.2 Selectivity vs temperature.

Based on the information given in Figs. 7.1 and 7.2, the optimum temperature range for achieving good selectivity and high conversion is 503-543 K for the two zeolite-supported Pd catalysts and 513-543 K for the two Pt-loaded catalysts. At 513 K, nearly 90 % conversion and 100 % selectivity were achieved by using the two Pd-loaded catalysts.

#### *Effect of Hydrogen Pressure on Conformational Isomerization of cis-DeHN*

Although the conformational isomerization of cis-DeHN is greatly affected by reaction temperature, from Scheme 1, hydrogen pressure also plays a key role, from the reduction of the metal oxide to the dehydrogenation and hydrogenation reactions. First, the reduction of catalyst precursors requires hydrogen and thus will be influenced by the initial hydrogen pressure applied. On the other hand, because conformational isomerization, as indicated in Scheme 1, involves hydrogenating and dehydrogenating procedures, the whole isomerization process will be affected by the pressure of hydrogen. At the beginning of isomerization reactions, an increase in the hydrogen partial pressure will reduce the equilibrium concentration of the dehydrogenated intermediates from cycloalkanes. However, with an ongoing reaction, an increased hydrogenation pressure will be beneficial in the hydrogenation of isomerized cycloalkene intermediates. [19] Therefore, in order to determine the impact of initial hydrogen pressure in

the conformational isomerization of cis-DeHN, a reaction temperature of 240 °C (513 K) was selected with a pressure range of 200 to 1000 psig. The results obtained are shown in Figs. 7.3 and 7.4.

As seen in Fig. 7.3, conversion to trans-DeHN exhibits a generally increasing trend with the initial hydrogen pressure. In addition, the initial pressure has a greater impact on conversion in the lower range, 200-500 psig. In this range, the two zeolite-supported Pd catalysts appear more active than the two Pt-containing catalysts. However, when the initial hydrogen pressure is above 500 psig, the conversion difference between Pt and Pd, with the same supports, becomes smaller. It is interesting to note that the two Pd-loaded catalysts give a higher conversion than do their respective Pt catalysts. One possible explanation is the difference between the atomic numbers of Pt and Pd. However, although Pt can provide more active hydrogenation/dehydrogenation centers, the observed difference in conversion between Pt and Pd does not jive with the difference in number of active sites at the relatively low temperature of 240 °C. The results also indicate that 0.5Pt/CBV740 is slightly more active than 0.5Pt/CBV30A, whereas 0.5Pd/CBV30A is more active than 0.5Pd/CBV740 over the whole pressure range discussed.

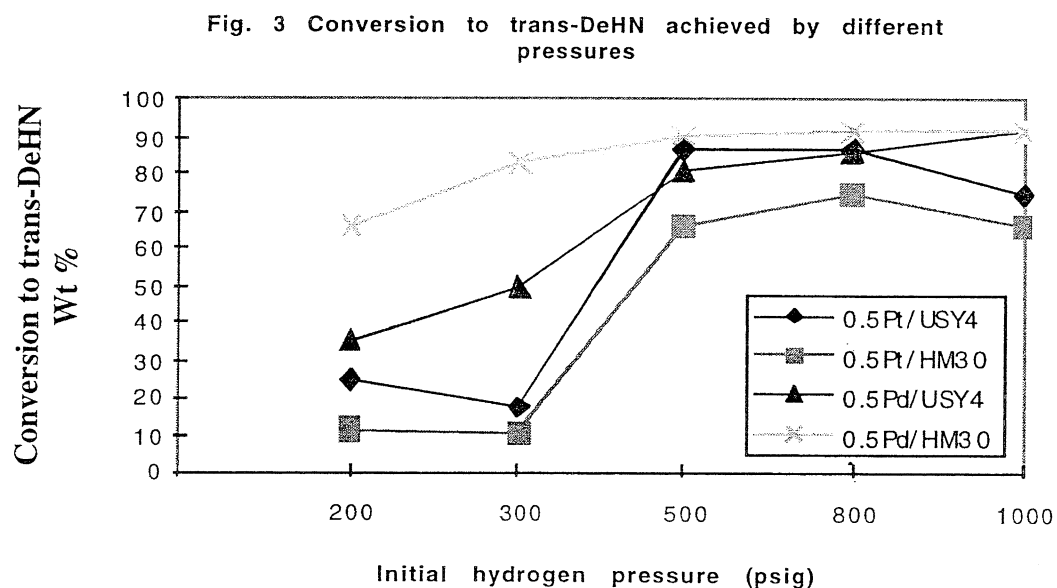


**Figure 7.3** Conversion to trans-DeHN achieved by different pressures.



According to Fig. 7.4, in the lower pressure range, 200-500 psig, the selectivity to trans-DeHN shows an increasing trend with initial hydrogen pressure; however, when the pressure is higher than 500 psig, little difference in selectivity among the catalysts is evident. When the pressure is lower than 500 psig, the two Pd-loaded catalysts display a higher selectivity. Moreover, the catalyst supports CBV740 and CBV30A have little influence on the selectivity to trans-DeHN over the whole pressure range.

Fig. 4 Selectivity to trans-DeHN vs. pressure change

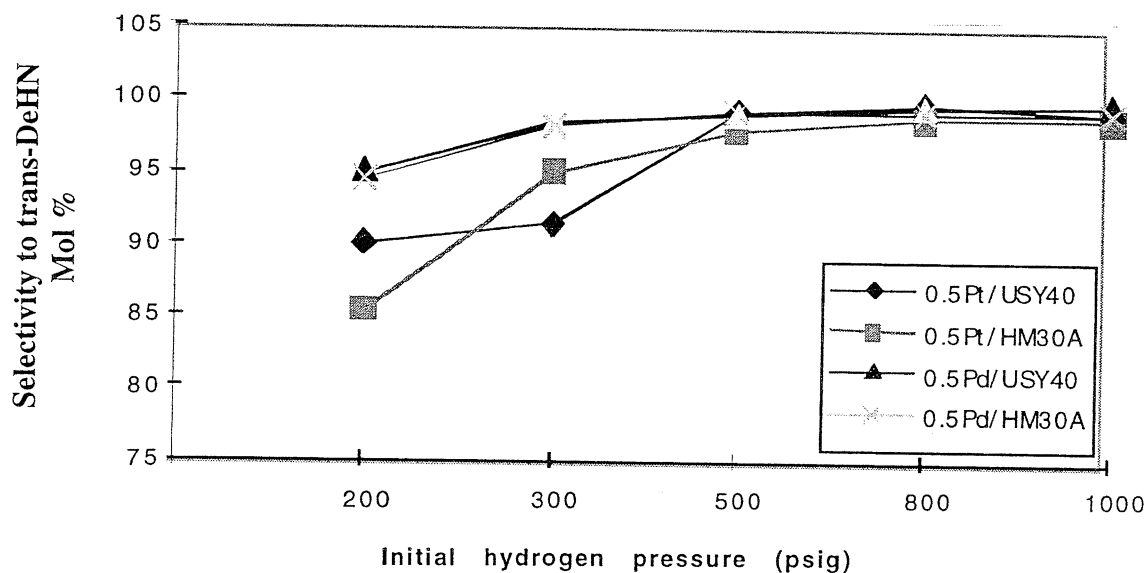


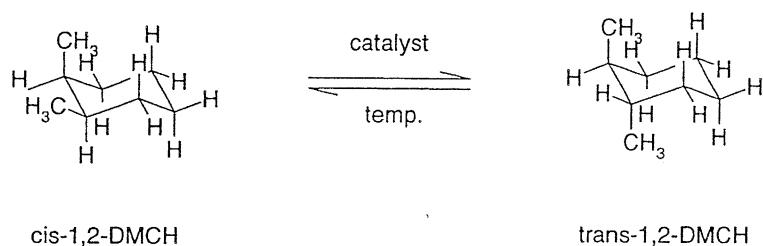
Figure 7.4 Selectivity to trans-DeHN versus pressure.

As shown in Figs. 7.3 and 7.4, in order to achieve both good selectivity and high conversion, the optimum pressure range should be 500 to 800 psig for the four zeolite-supported catalysts.

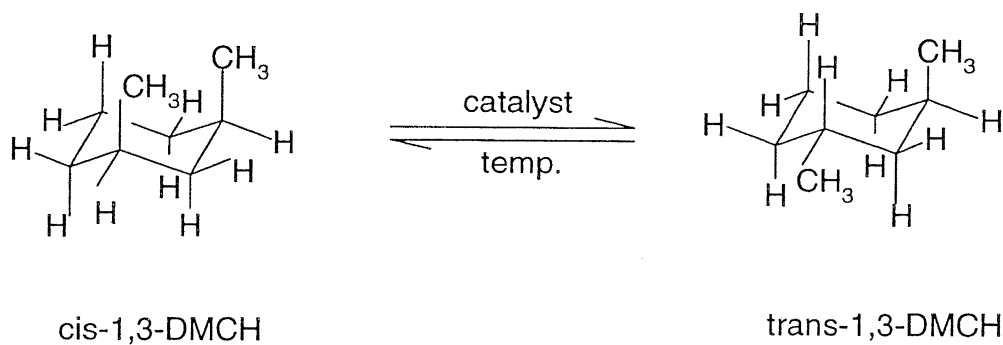
In summary, the conformational isomerization of cis-DeHN can be accomplished with the use of zeolite-supported noble-metal catalysts. The isomerization yields can be optimized both through the selection of an appropriate support and highly efficient metal and through the adjustment of operating conditions such as reaction temperature and initial hydrogen pressure. It is evident that zeolite-supported metal catalysts can promote the conversion of cis-DeHN into trans-DeHN with high conversion (90 %) and good selectivity (100 %). Therefore, catalytic conformational isomerization is an effective method for increasing the amounts of the more thermally stable components in jet fuels.

### Conformational Isomerization of cis-DMCHs

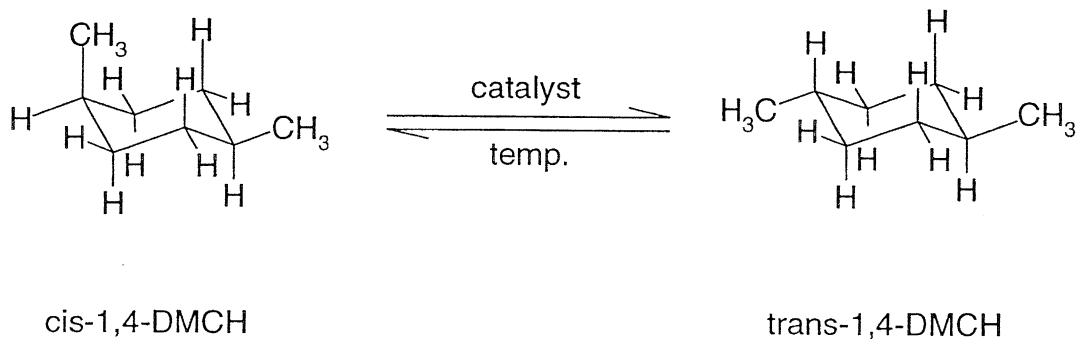
In order to understand better the effect of configurational structure on the thermodynamic stability of model compounds, the general schemes for the conversion of cis-DMCHs (dimethylcyclohexanes) to their respective trans-isomers are described as below.



Scheme 3. Conversion from cis-1,2-DMCH to trans-1,2-DMCH.



Scheme 4. Conversion from cis-1,3-DMCH to trans-1,3-DMCH.



Scheme 5. Conversion from cis-1,4-DMCH to trans-1,4-DMCH.

Compared with the cis-decalin discussed previously, the three cis-DMCHs are less thermally and chemically stable. Therefore, activation energies for conformational isomerization will be lower than that for cis-decalin. Consequently, there exists competition, to some extent, between skeletal and conformational isomerization in a relatively low-temperature range. However, the reaction temperature should not be lower than 220 °C in order to overcome the activation energies of the three cis-DMCHs during conformational isomerization. Furthermore, based on the above three schemes, the steric hindrance between cis- and trans-DeHN is much larger than that between the corresponding isomers of DMCHs. Therefore, the conversion from cis-DeHN to trans-DeHN will be more sensitive to the channel structures and pore sizes of the zeolites.

In this study, 0.5Pd/CBV740 and 0.5Pd/CBV30A were used for the conformational isomerization of the cis-DMCHs.

#### *Conformational Isomerization of cis-1,4-DMCH*

Table 7.4 lists the results for the conversion of cis-1,4-DMCH to trans-1,4-DMCH, in which the effects of reaction temperature, residence time, and initial hydrogen pressure are included. Selectivities as high as 100 % along with conversions of 76 % were achieved.

**Table 7.4** Conformational isomerization of cis-1,4-DMCH over 0.5Pd/USY40 and 0.5Pd/HM30A.

Catalyst	Temp (°C)	Press. (psig) (H <sub>2</sub> )	Time (min)	Conv. to trans (mol-%)	Selectivity (mol-%)
0.5Pd/USY40	230	500	60	48.31	100
0.5Pd/USY40	240	500	60	50.83	100
0.5Pd/HM30A	240	500	60	72.58	100
0.5Pd/USY40	250	500	60	67.51	97.87
0.5Pd/HM30A	250	500	60	66.75	85.15
0.5Pd/USY40	260	500	60	60.76	75.56
0.5Pd/USY40	240	500	120	72.15	98.82
0.5Pd/HM30A	240	500	120	68.67	87.61
0.5Pd/USY40	240	1000	60	76.41	96.98
0.5Pd/HM30A	240	1000	60	74.42	100

As seen from Table 7.4, with an initial hydrogen pressure of 500 psi and residence time of 60 min, the optimum temperature range was 230 – 250 °C for 0.5Pd/USY40, and 240 – 250 °C for 0.5Pd/HM30A. The temperature used for conformational isomerization of cis-1,4-DMCH is

detrimental if it exceeds 260 °C with the two Pd-loaded catalysts used. Based on the above results, when the residence time was extended from 60 min to 120 min at 240 °C, conversion to trans-1,4-DMCH was greatly enhanced for 0.5Pd/USY40 with a small gain in selectivity. However, under the same conditions with the HM30A-supported catalyst, both conversion and, particularly, selectivity to trans-1,4-DMCH were reduced. Therefore, a longer residence time favors isomerization reactions using 0.5Pd/USY40, but not 0.5Pd/HM30A. Furthermore, the effect of initial hydrogen pressure on the conformational isomerization of cis-1,4-DMCH was investigated over the same reaction-temperature range. As shown, by increasing the pressure from 500 to 1000 psig with a 60-min residence time, the conversion was improved, particularly for 0.5Pd/USY40, without sacrificing selectivity. Thus, conformational isomerization catalyzed by Pd-loaded USY40 can be optimized through an increase of residence time or by raising the initial hydrogen pressure. In contrast, a short residence time and low pressure are conducive to the conformational isomerization of cis-1,4-DMCH, using 0.5Pd/HM30A.

#### *Conformational Isomerization of cis-1,3-DMCH*

The conformational isomerization of cis-1,3-DMCH was carried out using the two Pd-containing catalysts with the reaction temperature ranging from 230 to 260 °C. The results are summarized in Table 7.5.

**Table 7.5** Conformational Isomerization of cis-1,3-DMCH over 0.5Pd/USY40 and 0.5Pd/HM30A.

Catalyst comp.	Temp. (°C)	Pressure (psig)	Time (min)	Conv. to trans (mol-%)	Selectivity (mol-%)
0.5Pd/USY40	230	500	60	5.08	100
0.5Pd/HM30A	230	500	60	2.30	100
0.5Pd/USY40	260	500	60	16.75	47.30
0.5Pd/HM30A	260	500	60	14.43	30.85

As shown in Table 7.5, although 100 % selectivity was achieved at lower temperatures (e.g., 230 °C), little conversion (2-5 %) was observed. However, when the temperature was raised to 260 °C, a higher conversion of cis-1,3-DMCH (14-17 %) was achieved. As indicated, relatively high temperatures seemed to favor conversion to trans-1,3-DMCH, but the selectivity to trans-1,3-DMCH was reduced to 30-50 %. Moreover, both higher conversion and selectivity were obtained using a CBV30A-supported Pd catalyst. Thus, conversion to trans-1,3-DMCH can be

optimized by the selection of an appropriate supported catalyst and the adjustment of reaction temperature and initial hydrogen pressure.

#### *Conformational Isomerization of cis-1,2-DMCH*

The conversion of cis-1,2-DMCH was studied by applying the same two catalysts used for the isomerization of cis-1,3-DMCH and cis-1,4-DMCH. The investigation focused on the impact caused by reaction temperature and residence time. The results from the conformational isomerization of cis-1,2-DMCH are listed in Table 7.6, where a conversion as high as 74 %, with 93 % selectivity, was obtained.

**Table 7.6** Conformational isomerization of cis-1,2-DMCH over Pd-loaded catalysts.

Catalyst comp.	Temp. (°C)	Time (min)	Pressure (psig)	Conv. to trans (mol-%)	Selectivity (mol-%)
0.5PdUSY40	200	60	500	10.78	100
0.5Pd/HM30A	200	60	500	2.73	100
0.5Pd/USY40	220	60	500	19.01	91.84
		120	500	62.58	79.62
0.5Pd/HM30A	220	60	500	54.15	100
		120	500	74.00	93.39
0.5Pd/USY40	230	60	500	38.57	70.73
0.5Pd/HM30A	230	60	500	71.10	90.51
0.5Pd/HM30A	260	60	500	25.30	27.94

According to Table 7.6, when 0.5Pd/USY40 and 0.5Pd/HM30A were used for the cis-1,2-DMCH conformational isomerization with a 500-psig initial hydrogen pressure and 60-min residence time, the optimum temperature range was 220 – 230 °C. Moreover, under such reaction conditions the highest yield of trans-1,2-DMCH was obtained using Pd-loaded HM30A at 220 °C. With a 60-min residence time, highest conversion (74 %) and good selectivity (93 %) were observed in the conversion of cis-1,2-DMCH to trans-DMCH.

When the residence time was extended from 60 to 120 min at 220 °C, the conversion to trans-1,2-DMCH increased dramatically from 19 to 63 mol%, but the selectivity decreased from 92 to 80 mol% using 0.5Pd/USY40. In regard to cis-1,2-DMCH isomerization catalyzed by 0.5Pd/HM30A, a higher conversion and lower selectivity to trans-1,2-DMCH were also observed with an increased residence time.

As shown in Table 7.6, with a 60-min residence time, higher conversion and lower selectivity to trans-1,2-DMCH were achieved at 230 °C than at 220 °C for both 0.5Pd/USY40 and 0.5Pd/HM30A.

Based on the above discussion, the conversion and selectivity to trans-1,2-DMCH can be optimized through the adjustment of reaction temperatures and residence times used in the conformational isomerization of cis-1,2-DMCH with the USY40- and HM30A-supported Pd catalysts.

In summary, the conformational isomerization of the cis-DMCHs undoubtedly requires the use of catalysts. As shown, noble-metal-loaded zeolite bifunctional catalysts can efficiently promote these isomerization reactions. Although the selection of the acidic support is very important, reaction temperature, initial hydrogen pressure, and residence time also have a large impact on both conversion and selectivity in the isomerization.

#### **7.4 Conclusions**

Based upon the above results and discussion, zeolite-supported catalysts can be utilized to isomerize conformationally cycloalkanes such as cis-DeHN, cis-1,2-DMCH, cis-1,3-DMCH, and cis-1,4-DMCH with high conversion and good selectivity through both the application of appropriate bifunctional catalysts and the adjustment of reaction conditions. Therefore, catalytic conformational isomerization of cycloalkanes is an excellent method for increasing the amounts of the more thermally stable components in jet fuels.

## 8.0 CARBON SKELETAL ISOMERIZATION

### 8.1 Introduction

Advanced jet fuels for future high-Mach aircraft are required to be thermally stable at temperatures up to 900 °F. [20] However, at present the available jet fuels do not meet such demanding requirements. [21] There are strong indications that a relationship between the composition and thermal stability of jet fuels exists. [20-23] Coal-derived jet fuels, which are rich in alkylcycloalkanes, decalins, and tetralins generally show higher thermal stability than petroleum-based jet fuels, which are composed mostly of long-chain alkanes. [20,24] Based on previous research [20,21,25,26], cyclic hydrocarbons are more thermally stable than chain hydrocarbons with the same carbon number whereas methylcyclopentane (MCP), for example, is more stable than cyclohexane in the temperature range of 400-500 °C. Therefore, in order to improve the thermal stability of jet fuels, there is a need to enhance the contents of those more thermally stable components in jet fuels. One convenient and effective way is isomerization. Hydrocarbon isomerization includes skeletal isomerization which involves carbon-carbon  $\sigma$ -bond rupture and conformational isomerization in which no carbon-carbon  $\sigma$ -bond cleavage occurs and only configurational change is observed.

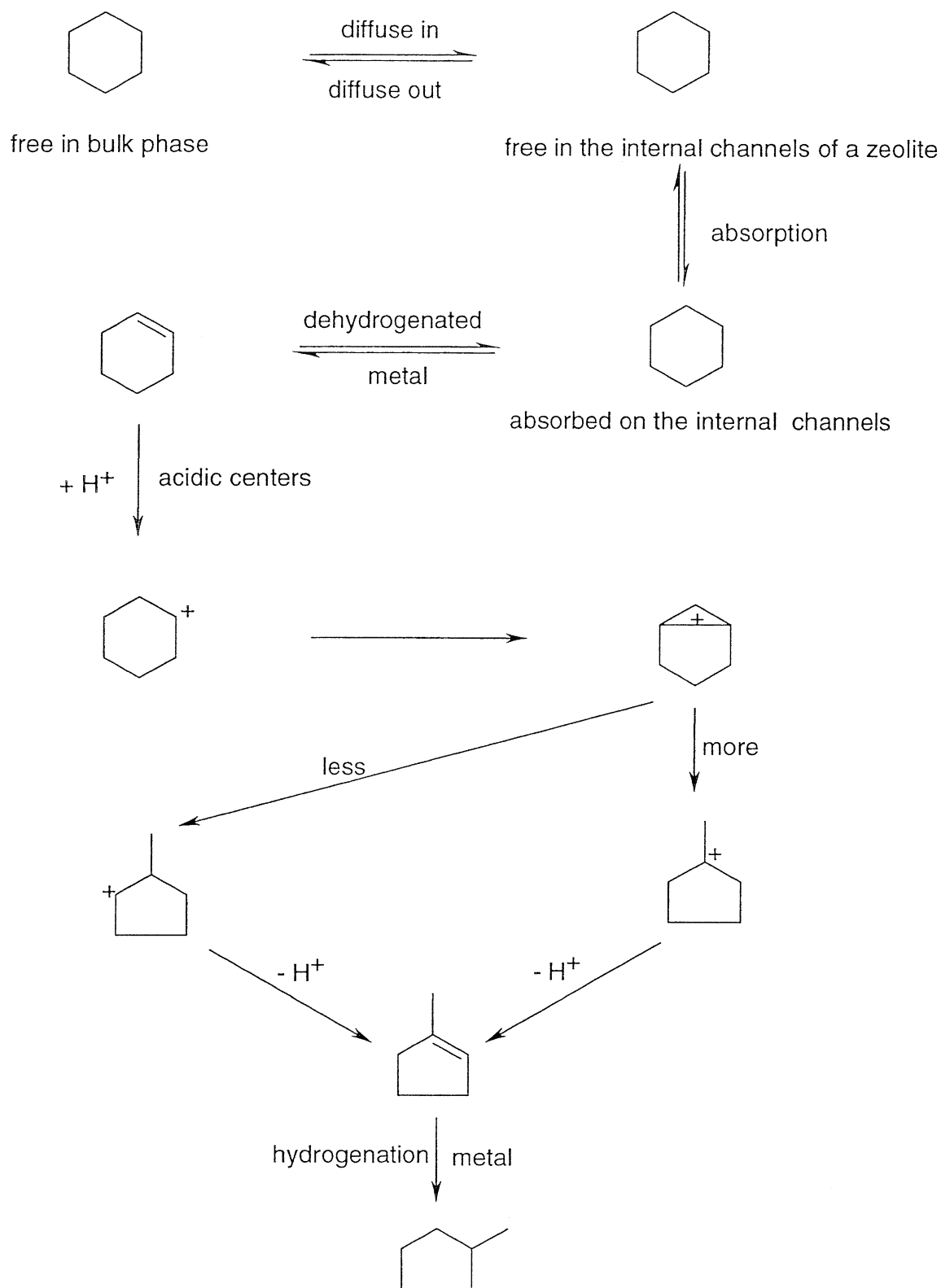
This final report will focus on the hydrocarbon skeletal isomerization. For simplicity, the model compound cyclohexane (CH) has been used in this study. Commonly, isomerization is achieved with the help of catalysts. The most-often used and widely studied catalysts in industry and research laboratories are bifunctional zeolite-supported catalysts. These catalysts can provide two types of catalytic sites which facilitate hydrogenating or dehydrogenating on the surface of active metals and isomerization on the acidic supports. It has been widely accepted that the skeletal isomerization of cyclohexane proceeds through a bifunctional mechanism. [27] For a zeolite-supported metal catalyst, the loaded metal provides hydrogenation/dehydrogenation sites, and the zeolite donates acidic centers where isomerization reactions take place. As indicated in Scheme 1, cyclohexane molecules first diffuse into the internal channels of a zeolite from the bulk phase. Here, the molecules are absorbed by the active metal sites on the catalyst surface and are subsequently dehydrogenated to form cyclohexene. Cyclohexene undergoes carbon skeletal isomerization on the acidic centers to form methylcyclopentene through the rearrangement of the

$\sigma$  bonds. Methylcyclopentene is then hydrogenated to methylcyclopentane by the active metals. Finally, methylcyclopentane diffuses out of the zeolite and returns to the bulk phase.

Although the above mechanism has been accepted as the main reaction pathway for most isomerization reactions, a new type of mechanism, called “hydrogen spillover”, has been introduced to explain the product distribution of cyclohexane isomerization catalyzed by H-ZSM-5 supported Pt catalysts. [29] In this mechanism, the step “activation of molecular gas-phase hydrogen on metal and the formation of spillover hydrogen” is considered the key factor in controlling the reaction directions. However, in this final report, the results will be explained according to the bifunctional catalytic mechanism in Scheme 1. Therefore, skeletal-isomerization reactions of hydrocarbons are not only affected by temperature but also influenced by the hydrogen pressure used. In addition, because this type of reaction is kinetically reversible, the residence time may have some impact on the product distribution. As expected, conversion and selectivity to desired isomers will depend on the catalysts as well as on the reaction conditions used.

This final report presents the results of the skeletal isomerization of the model-compound cyclohexane using the six noble-metal-loaded zeolite catalysts, 0.5Pt/LZ-Y62, 0.5Pd/LZ-Y62, 0.5Pt/CBV30A, 0.5Pd/CBV30A, 0.5Pt/CBV740, and 0.5Pd/CBV740, under various reaction conditions.





Scheme 1. Reaction pathways of cyclohexane isomerization

## 8.2 Experimental

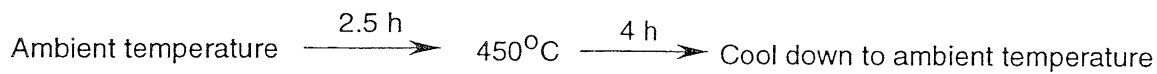
The catalysts used are listed in Table 8.1. They were prepared by incipient-wetness impregnation. After impregnation, the catalyst precursors were dried in vacuum at 120 °C for 8 h and then calcined under air in a Muffle furnace using the temperature program described in Scheme 2. Aldrich reagent-grade cyclohexane was employed in this study. The reduction of the corresponding catalyst precursors was carried out *in situ*, where typically cyclohexane and a catalyst precursor were charged into a 25-ml horizontal microreactor. The reactor was closed and purged six times with 1000-psig UHP hydrogen and finally pressurized to the desired value. It was then placed in a fluidized sand bath, preheated to the designated temperature, and removed after a specified residence time in the sand bath. Subsequently, the reactor was quenched by immersion into a cold-water bath and then air dried. The liquid products were separated from the used catalyst by filtration. The liquids obtained were analyzed on a Perkin-Elmer 8500 GC equipped with a FID detector and operated in split mode; the analysis program is shown in Table 8.2. The characterization of products was carried out by GC/MS.

**Table 8.1** Typical properties of zeolites used.

Trade name (other)	Cation form	SiO <sub>2</sub> /Al <sub>2</sub> O <sub>3</sub> (molar ratio)	Na <sub>2</sub> O (wt-%)	Surface area (m <sup>2</sup> /g)	Provider
LZ-Y62	ammonium	5	NA	NA	Aldrich
CBV740 (USY40)	hydrogen	40	0.03	750	Zeolyst
CBV30A (HM30A)	ammonium	35	0.02	600	PQ

**Table 8.2** GC analysis program used for product analysis.

Sample injected (μl)	Initial temp. (°C)	Isothermal (min)	Ramp rate (°C/min)	End temp. (°C)	Isothermal (min)
0.03	40	6	4	120	5



Scheme 2. Temperature program used for calcination.

### 8.3 Results and Discussion

#### Effect of Temperature on CH Conversion Using Different Noble-Metal-Loaded LZ-Y62 or CBV30A Catalysts

According to the Arrhenius equation,  $k=A\exp(-E_a/RT)$ , and  $K_p=\exp(-\Delta G^0/RT)$ , skeletal isomerization will be affected by reaction temperature both kinetically and thermodynamically. In order to elucidate the impact of temperature on conversion and selectivity in cyclohexane isomerization, 0.5Pt/LZ-Y62, 0.5Pt/CBV30A, 0.5Pd/LZ-Y62, and 0.5Pd/CBV30A were tested at 275, 300, 330, 350, and 370 °C with an initial hydrogen pressure of 1000 psig, as specified in Table 8.3.

**Table 8.3** Reaction conditions used for the effects of pressure.

Reaction	Conditions	Temperature (°C)
Initial H <sub>2</sub> pressure (psig)	1000	275
Residence time (min)	60	300
Wt. of CH (g)	3.20	330
Wt. of catalyst precursor (g)	0.15	350
CH/catalyst precursor (g/g)	21.33	370

Because almost no reaction was observed at temperatures as low as 330 °C with the two LZ-Y62 supported noble-metal catalysts, the results shown in Table 8.4 were obtained at 350 and 370 °C. Moreover, although no tests were conducted for Pt- or Pd-loaded LZ-Y62 between 330 and 350 °C, a very low conversion and high selectivity would be expected in this temperature range.

**Table 8.4** Skeletal isomerization of cyclohexane over 0.5Pt/LZ-Y62 and 0.5Pd/LZ-Y62.

Catalyst composition	Temp. (°C)	Conv. of CH (mol%)	Select. to MCP (mol%)
0.5Pt/LZ-Y62	350	6.62	97.73
	370	18.61	95.65
0.5Pd/LZ-Y62	350	3.74	98.66
	370	8.44	50.83

The results obtained using CBV30A-supported catalysts are shown in Figs. 8.1 and 8.2. Because LZ-Y62 and CBV30A have quite different  $\text{SiO}_2/\text{Al}_2\text{O}_3$  ratios (5 and 35, respectively), it is hard to compare the isomerization results obtained using the LZ-Y62- and CBV30A-supported catalysts. The  $\text{SiO}_2/\text{Al}_2\text{O}_3$  ratio influences the activity, selectivity, and stability of a catalyst. [27] Because conversion is negligible when the reaction temperature is as low as 330 °C, it is difficult to determine the selectivity of the two LZ-Y62 loaded catalysts. When the temperature was raised to 350 °C, the conversion of cyclohexane was 6.62 mol% and the selectivity as high as 97.73 mol% using 0.5Pt/LZ-Y62. As the temperature was increased to 370 °C, the conversion was slightly higher without sacrificing the selectivity. As seen from Table 8.3, 0.5Pt/LZ-Y62 was more active and selective during skeletal isomerization of cyclohexane, which may be attributed to more active Pt centers present at relatively high temperatures. Although isomerization of cyclohexane can be achieved using LZ-Y62 supported noble-metal catalysts at higher temperatures, the conversion will be very low. Therefore, some modifications should be made to enhance the catalytic properties of LZ-Y62.

As shown in Fig. 8.1, when the reaction temperature was increased from 275 to 330 °C, the conversion of cyclohexane increased almost linearly using the two noble-metal-loaded CBV30A catalysts. However, for temperatures above 330 °C, there was little impact on the CH conversion. Considering the entire temperature range of 275-370 °C, the CH conversion showed little variation with the noble metal used.

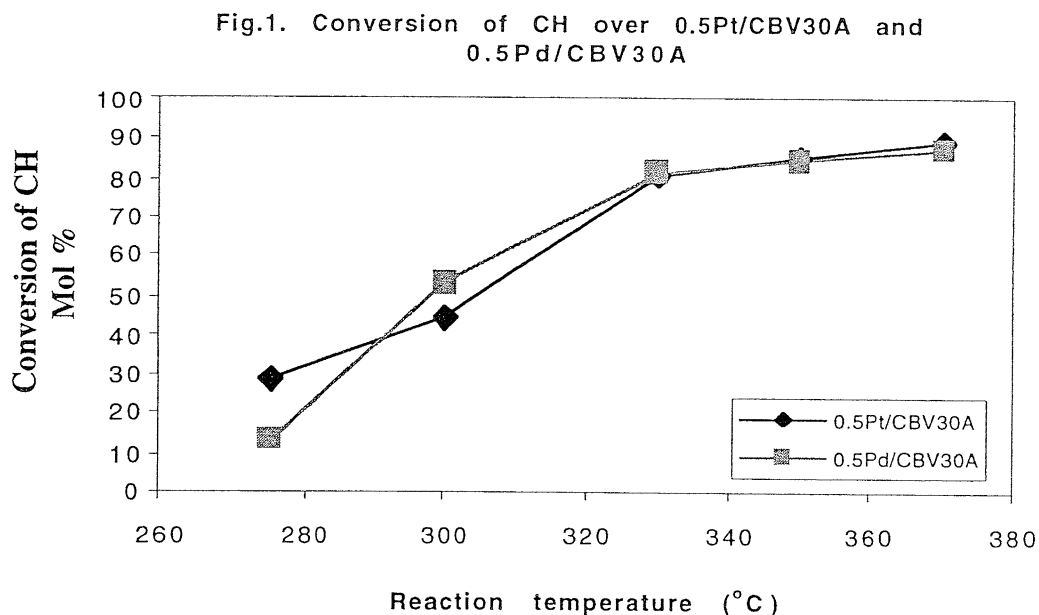


**Figure 8.1** Conversion of CH over 0.5Pt/CBV30A and 0.5Pd/CBV30A.

As indicated in Fig. 8.2, when the temperature increased from 300 to 370 °C, the selectivity to methylcyclopentane decreased. With selectivity decreasing, more by-products from hydrocracking were formed. When the temperature was not higher than 300 °C, 100 % selectivity was obtained with both 0.5Pt/CBV30A and 0.5Pd/CBV30A, indicating that no side reactions had taken place. Fig. 8.2 also shows that selectivity was little affected by the different noble metals loaded onto CBV30A.

In summary, conversion to methylcyclopentane can be optimized through the adjustment of reaction temperature; 85% conversion and 95% selectivity were obtained at 330 °C using 0.5Pd/CBV30A. For the two CBV30A-supported noble-metal catalysts, based on the experimental results, the optimum range of temperature is between 300 and 330 °C. However, with respect to LZ-Y62 containing catalysts, the temperature should not be lower than 350 °C.

Fig. 2. Selectivity to MCP over 0.5Pt/CBV30A and 0.5Pd/CBV30A

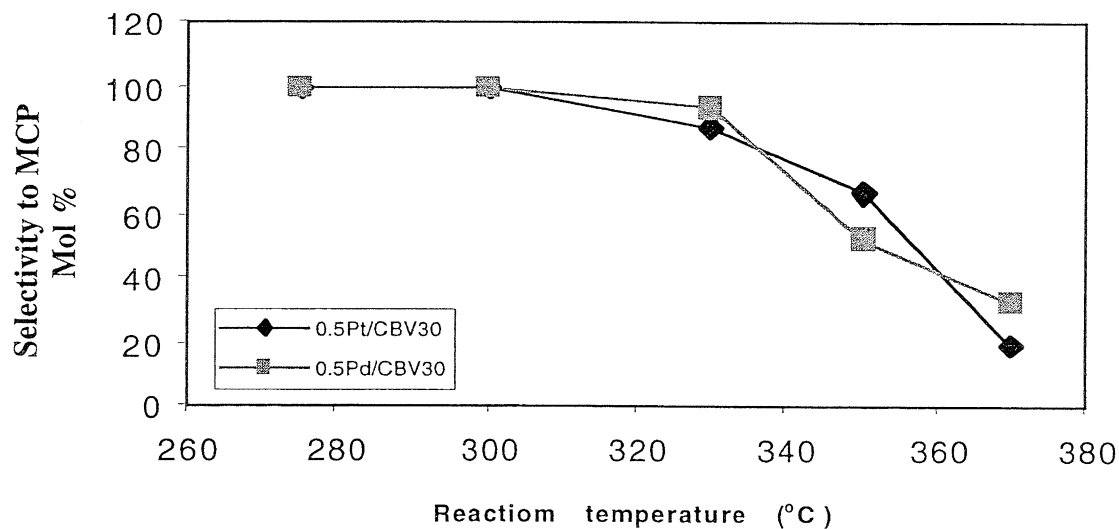


Figure 8.2 Selectivity to MCP over 0.5Pt/CBV30A and 0.5Pd/CBV30A.

#### Effect of Initial Hydrogen Pressure on Skeletal Isomerization of Cyclohexane

##### *Effect of H<sub>2</sub> Pressure Using 0.5Pt/CBV30A and 0.5Pd/CBV30A at 370 and 300 °C*

In this section, the effect of initial hydrogen pressure on CH skeletal isomerization was investigated using the two CBV30A-supported noble-metal catalysts. The reaction temperatures used were 370 and 300 °C. The reaction conditions for 370 °C are listed in Table 8.5.

**Table 8.5** Reaction conditions used at 370 °C.

Reaction	Conditions	Initial H <sub>2</sub> pressure (psig)
Temp. (°C)	370	200
Residence time (min)	60	300
Wt. of CH (g)	3.20	500
Wt. of catalyst precursor (g)	0.15	800
CH/catalyst precursor (g/g)	21.3	1000

In order to elucidate the effect of hydrogen pressure on CH skeletal isomerization using the two CBV30A-supported noble-metal catalysts, a reaction temperature of 370 °C was used first. The results are shown in Table 8.6.

**Table 8.6** Cyclohexane isomerization by pressure change.

Catalyst	H <sub>2</sub> pressure (psig)	Conv. of CH (%)	Select. to MCP (%)
0.5Pt/CBV30A	200	78.35	84.28
	300	86.01	68.59
	500	88.67	44.30
	800	92.75	12.69
	1000	89.15	19.82
0.5Pd/CBV30A	200	76.76	87.87
	300	83.88	73.49
	500	89.53	44.10
	800	91.74	14.74
	1000	87.26	32.75

According to the results in Table 8.6, when the pressure increased in the range of 200-800 psig, the conversion increased with both 0.5Pt/CBV30A and 0.5Pd/CBV30A, but the selectivity decreased. However, when the pressure was raised to 1000 psig, conversion decreased and selectivity increased. Such a phenomenon could be explained by the function of hydrogen during the dehydrogenation/hydrogenation process in isomerization. When the pressure is between 200 and 800 psig, dehydrogenation is inhibited, resulting in a lower concentration of the intermediate cyclohexane; when the pressure is raised to 1000 psig, the hydrogenation of the isomerized intermediate (methylcyclopentene) is favored, which overcomes the side effect of pressure on dehydrogenation. Overall, at 370 °C, hydrocracking of cyclohexane is favored by increased H<sub>2</sub> pressure, which leads to a higher conversion of cyclohexane but to a lower selectivity. Furthermore, in order to clarify the role of hydrogen pressure at lower reaction temperatures with

the two noble-metal-loaded CBV30A catalysts, a CH skeletal isomerization was conducted at 300 °C; the reaction conditions used are listed in Table 8.7.

**Table 8.7** Reaction conditions used at 300 °C.

Reaction	Conditions	H <sub>2</sub> pressure (psig)
Temperature (°C)	300	500
Residence time (min)	60	
Wt. of cyclohexane (g)	3.20	
Wt. of catalyst precursor (g)	0.15	1000
CH/catalyst precursor (g)	21.3	

Under the above reaction conditions, the CH isomerization results obtained with 0.5Pt/CBV30A and 0.5Pd/CBV30A are shown in Table 8.8.

**Table 8.8** CH isomerization over Pt- or Pd-loaded CBV30A with pressure change at 300 °C.

Catalyst	H <sub>2</sub> pressure (psig)	Conv. of CH (%)	Select. to MCP (%)
0.5Pt/CBV30A	500	58.95	100
	1000	45.03	100
0.5Pd/CBV30A	500	68.36	100
	1000	53.25	100

At 300 °C, the initial hydrogen pressure had no influence on the selectivity (all were 100 mol%), but did have an effect on the conversion of cyclohexane. Such a phenomenon could be explained by the effect of hydrogen pressure during the dehydrogenation/hydrogenation process. High H<sub>2</sub> pressure does not favor the dehydrogenation of cyclohexane on the metal surface, which reduces the concentration of cyclohexene. Thus, higher conversion of cyclohexane was observed at 500 psig rather than at 1000 psig with both Pt- and Pd-loaded CBV30A catalysts.



*Effect of H<sub>2</sub> Pressure with 0.5Pt/LZ-Y62 and 0.5Pd/LZ-Y62 at 370 °C*

In order to obtain some information concerning the effect of H<sub>2</sub> pressure on CH skeletal isomerization using the two noble-metal catalysts containing LZ-Y62 with a low SiO<sub>2</sub>/Al<sub>2</sub>O<sub>3</sub> ratio, experiments were conducted under the reaction conditions listed in Table 8.9.

**Table 8.9** Reaction conditions used at 370 °C with different H<sub>2</sub> pressures.

Reaction	Conditions	Initial H <sub>2</sub> pressure (psig)
Temperature (°C)	370	200
Residence time (min)	60	300
Wt. of CH (g)	3.20	500
Wt. of catalyst precursor (g)	0.15	800
CH/catalyst precursor (g/g)	21.3	1000

At 370 °C with 0.5Pt/LZ-Y62 and 0.5Pd/LZ-Y62, the CH isomerization results using different pressures are described in Table 8.10. The conversion decreased with increasing hydrogen pressure but the selectivity showed little variation over the whole pressure range with the LZ-Y supported Pt catalyst. In contrast, when cyclohexane isomerization was catalyzed by 0.5Pd/LZ-Y62, the conversion first increased with rising pressure in the range 200 to 500 psig. It then decreased at pressures above 500 psig. The selectivity was less affected by pressure, except at 1000 psig. Moreover, the type of noble metal loaded had a strong influence on both conversion and selectivity. The above results can also be explained by the role of H<sub>2</sub> pressure during the hydrogenation/dehydrogenation step, different atomic numbers, and activity toward dehydrogenation/hydrogenation of Pt and Pd.

**Table 8.10** CH isomerization over Pt- or Pd-loaded LZ-Y62 at 370 °C with pressure change.

catalyst	H <sub>2</sub> pressure	Conv. of CH (9%)	Select. to MCP (%)
0.5Pt/LZ-Y62	200	59.88	98.11
	300	54.44	100
	500	40.64	100

0.5Pd/LZ-Y62	800	30.06	100
	1000	18.61	95.65
	200	23.33	91.94
	300	30.65	97.29
	500	33.95	100
	800	20.96	100
	1000	8.44	50.83

*Effect of H<sub>2</sub> Pressure with 0.5Pt/CBV740 and 0.5Pd/CBV740*

In order to clarify further the effect of initial hydrogen pressure on the skeletal isomerization of cyclohexane catalyzed by 0.5Pt/CBV470 or 0.5Pd/CBV740, experiments were performed at 330 and 370 °C. Reaction conditions are shown in Table 8.11, and the results achieved are shown in Figs. 8.3 and 8.4.

**Table 8.11** Reaction conditions used with 0.5Pt/CBV740 and 0.5Pd/CBV740.

Reaction	Conditions	Initial H <sub>2</sub> pressure (psig)
Temp. (°C)	330 (or 370)	200
Residence time (min)	60	300
Wt. of CH (g)	3.20	500
Wt. of catalyst precursor (g)	0.15	800
CH/catalyst precursor (g/g)	21.3	1000

When the reaction temperature was 330 °C, as shown in Figs. 8.3 and 8.4, the highest conversion was observed at 300 psig along with the lowest selectivity. When the two USY40-supported catalysts were used, both conversion and selectivity were less affected when the initial hydrogen pressure was higher than 500 psig. In addition, the conversion was more affected by

the type of noble metal, benefitting particularly from the Pt-loaded catalyst in the range of 200 – 500 psig. It is noteworthy that the particular noble metal used had little effect on the selectivity.

**Fig. 3 Conversion vs. pressure over 0.5Pt/CBV740  
and 0.5Pd/CBV740 at 330 °C**

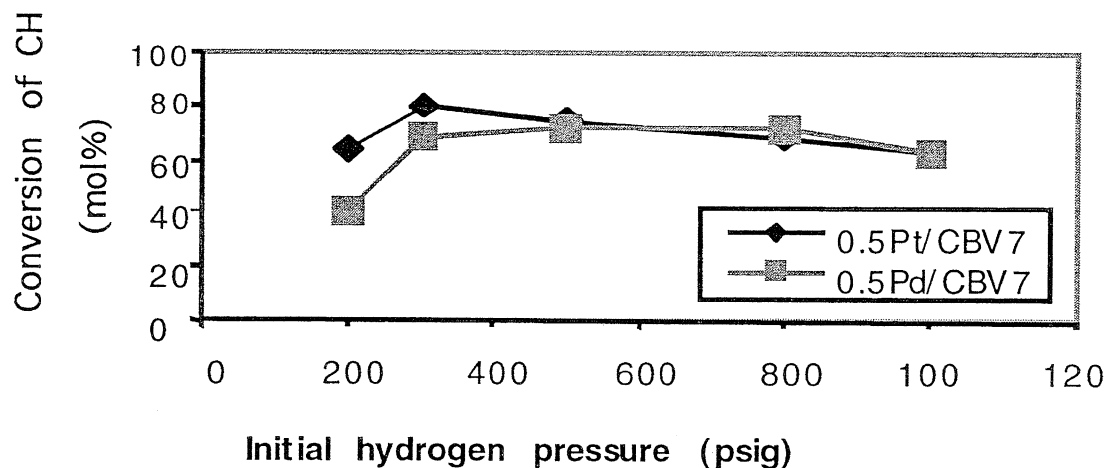


**Figure 8.3** Conversion vs pressure over 0.5Pt/CBV740 and 0.5Pd/CBV740 at 330 °C.

**Fig. 4 Selectivity vs. pressure over 0.5Pt/CBV740  
& 0.5Pd/CBV740 at 330 °C**

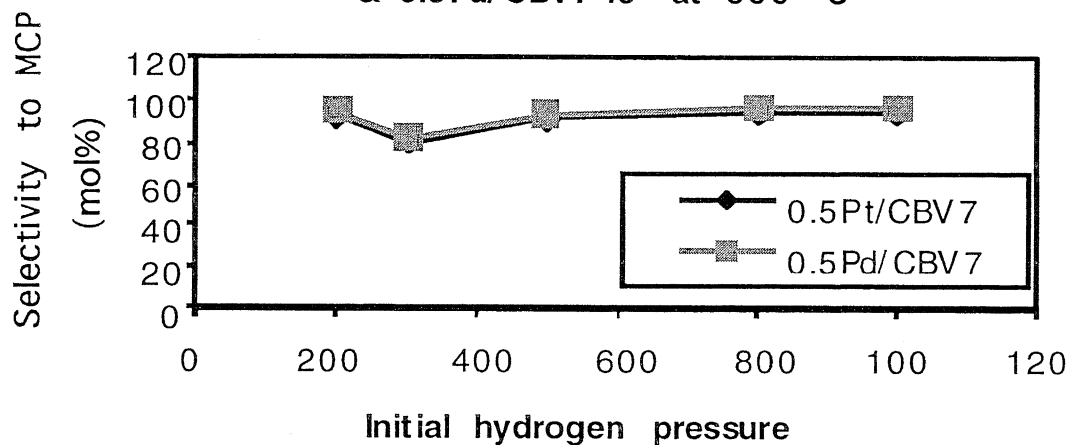


**Figure 8.4** Selectivity vs pressure over 0.5Pt/CVB740 and 0.5Pd/CBV740 at 330 °C.

According to Fig. 8.5, at temperatures below 370 °C, when the pressure was in the range of 200-500 psig, the conversion of cyclohexane exhibited an increasing trend with pressure; however, when the pressure was higher than 500 psig, the conversion was minimally affected.

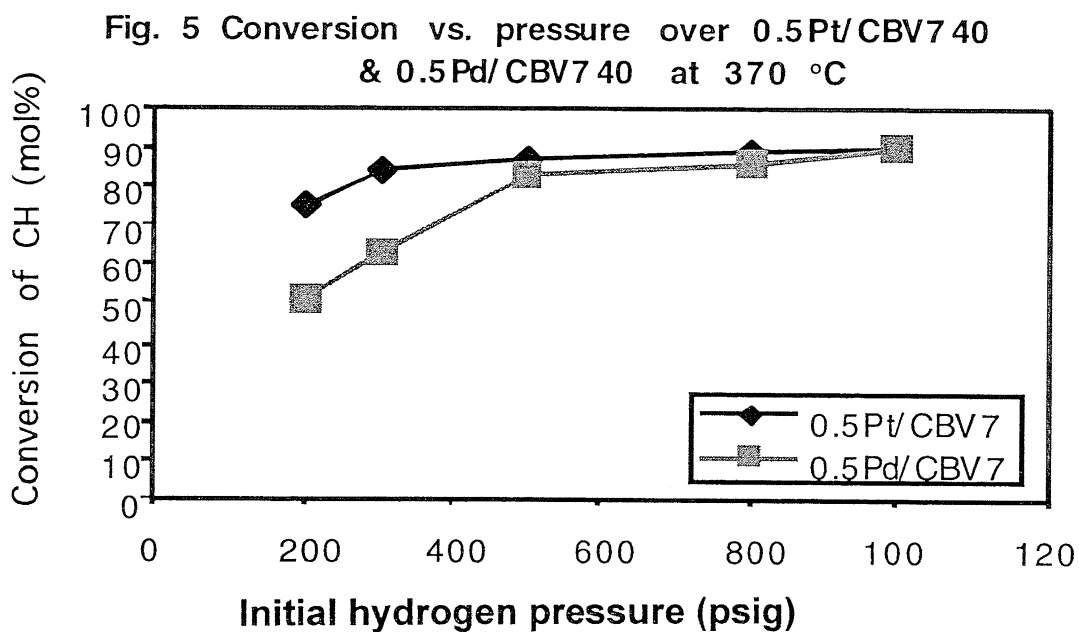


**Figure 8.5** Conversion vs pressure over 0.5Pt/CBV740 and 0.5Pd/CBV740 at 370 °C.

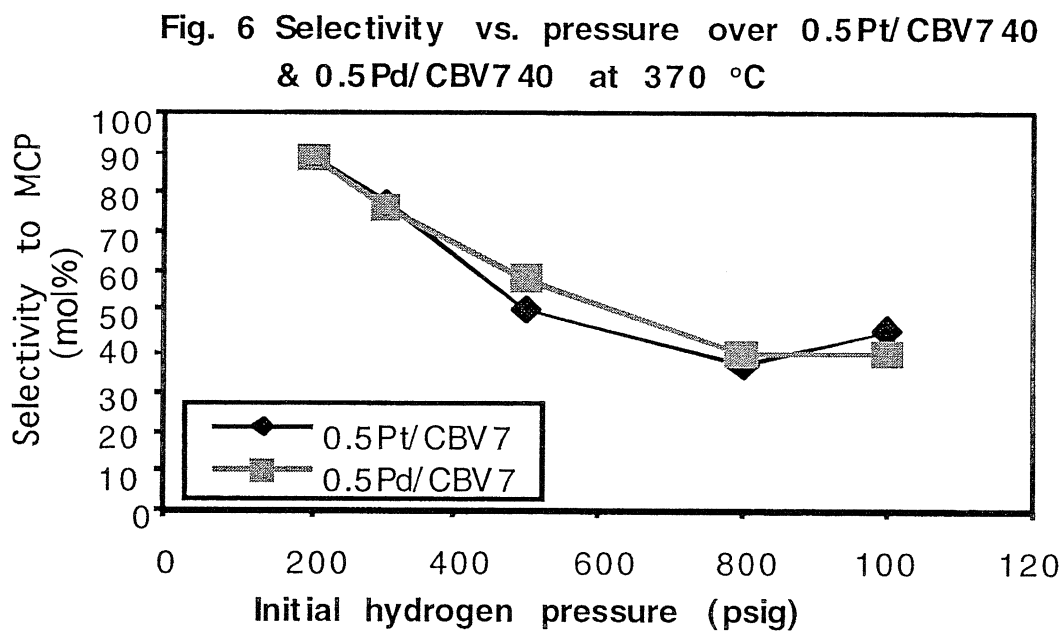


**Figure 8.6** Selectivity vs pressure over 0.5Pt/CBV740 and 0.5Pd/CBV740 at 370 °C.

As shown in Fig. 8.6, the selectivity to methylcyclopentane decreased as pressure increased, indicating that more by-products were formed from hydrocracking reactions. At 370 °C, the

optimum pressure range for cyclohexane isomerization is 300 to 500 psig. Comparing the results obtained at 330 °C and 370 °C, the skeletal isomerization of cyclohexane, especially the selectivity to methylcyclopentane, was more influenced by initial hydrogen pressure at 370 °C since hydrocracking is favored by higher pressures. However, at 330 °C, hydrogen pressure had little influence on conversion and selectivity. Overall, at both 330 °C and 370 °C, the particular noble metal used made little difference in the isomerization of cyclohexane.

#### Effect of Cyclohexane and Catalyst-Precursor Loading

In order to determine the effect of the amount of CH and catalyst precursor used in the isomerization, the precursors of 0.5Pt/CBV30A and 0.5Pd/CBV30A were studied. The reaction conditions are listed in Table 8.12.

**Table 8.12** Reaction conditions used for different feedstock loadings.

Reaction	Conditions	CH/catalyst precursor (g/g)	
Temperature (°C)	300	CH	catalyst precursor
		2.14	0.10
H <sub>2</sub> pressure (psig)	1000	3.20	0.15
Residence time (min)	60		

Under the above reaction conditions, the CH isomerization was carried out using the two CBV30A-supported catalysts; the results obtained are shown in Table 8.13.

**Table 8.13** Isomerization results for cyclohexane using 0.5Pt/CBV30A and 0.5Pd/CBV30A.

Catalyst	Wt. of cat. precursor (g)	Conv. of CH (%)	Select. to MCP (%)
0.5Pt/CBV30A	0.10	48.72	100
	0.15	45.03	100
0.5Pd/CBV30A	0.10	56.91	100
	0.15	53.25	100

The weight of cyclohexane and catalyst precursor charged into a reactor had little influence on conversion and selectivity; this can be attributed to the equal loading ratios of cyclohexane to the catalyst precursor used (all were 21.3 g/g). If the loading ratios of cyclohexane to catalyst precursor are different, the results for cyclohexane isomerization using the same catalyst could change.

Although the effect of noble-metal type is not discussed in a separate section, it is included in the above description of pressure, temperature, and other factors. Briefly, when zeolites with high  $\text{SiO}_2/\text{Al}_2\text{O}_3$  molar ratios such as CBV740 and CBV30A were used as the support material in a bifunctional catalyst, the catalytic properties were little affected by the type of noble metal at relatively high temperatures, but were greatly affected at lower reaction temperatures.

## 8.4 Conclusions

According to the experimental results obtained, both CBV740- and CBV30A-supported noble-metal catalysts can be effective in cyclohexane skeletal isomerization. Reduced conversion of cyclohexane is observed with LZ-Y62 supported catalysts until the reaction temperature is raised to 370 °C, which can be explained by the relatively weak acidic strength of the zeolite with its lower  $\text{SiO}_2/\text{Al}_2\text{O}_3$  ratio. As shown in the study, because carbon skeletal isomerization involves the carbon-carbon  $\sigma$ -bond cleavage, a relatively high temperature is generally required for this group of isomerization reactions which are catalyzed by zeolite-containing catalysts. For example, conversion of cyclohexane is observed at temperatures of at least 275 °C. High conversion and good selectivity have been achieved conclusively using CBV30A- or CBV740-supported noble-metal catalysts. Optimum isomerization of cyclohexane can be obtained by selecting a suitable acidic support and adjusting the reaction conditions such as temperature, initial hydrogen pressure, residence time, and the loading ratio of cyclohexane to catalyst precursor for the six catalysts discussed.

In summary, the carbon skeletal isomerization of the model-compound cyclohexane has been successfully accomplished with the use of a bifunctional zeolite-supported noble-metal catalyst. Therefore, catalytic carbon skeletal isomerization is an effective method to upgrade the composition of jet fuels.

## 9.0 REFERENCES

1. Department of Energy Coal Sample Bank; Penn State University, Dec. 1995.
2. Reddy, K. M., Wei, B., and Song, C., High-Temperature Simulated Distillation GC Analysis of Petroleum Resids and Their Products from Catalytic Upgrading over a Co-Mo/Al<sub>2</sub>O<sub>3</sub> Catalyst, *Catal. Today*, in press.
3. Edwards, T., *ACS Petroleum Chemistry Division Preprints*, **41**(2), 481-487 (1996).
4. Edwards, T. and Atria, J.V., *ACS Petroleum Chemistry Division Preprints*, **40**(4), 649-654 (1995).
5. Song, C., Eser, S., Schobert, H.H., and Hatcher, P.G., *Energy & Fuels*, **7**, 234-243 (1993).
6. Lai, W-C, Song, C., Schobert, H.H., and Arumugam, R., *ACS Fuel Chemistry Division Preprints*, **37**(4), 1671-1680 (1992).
7. Song, H. and Hatcher, P.G., *ACS Fuel Chemistry Division Preprints*, **37**(2), 529-539 (1992).
8. Lai, W-C and Song, C., *Fuel*, **74**, 1436-1451 (1995).
9. Gregory, R. in: Schobert, H.H., Eser, S., Song, C., Hatcher, P.G., Boehman, A. and Coleman, M.M., Technical Progress Report, Jan-Mar 1997, Prepared for U.S DoE, Contract No. DE-FG22-92PC92104, pp. 49-66.
10. Schobert, H.H. et al., (1997), Advanced Thermally Stable Jet Fuel, Task 5. Exploratory Studies on the Direct Conversion of Coal to High-Quality Jet Fuels, by: S.C. Martin, Technical Progress Report 92PC92104-TPR-19, p. 19-22.
11. Schobert, H.H. et al., (1997), Advanced Thermally Stable Jet Fuel, Task 5. Exploratory Studies on the Direct Conversion of Coal to High-Quality Jet Fuels, by: S.C. Martin, Technical Progress Report 92PC92104-TPR-20, p. 33-41.
12. Hossain, T., Zaman, N., Jahan, S.T., Podder, J., and Rashid, M.A., *J. Mech. Eng. Res. & Dev.*, **16**, 47-51 (1994).
13. ASTM D2639, Standard Test Method for Plastic Properties of Coal by the Constant-Torque Gieseler Plastometer, (1997), American Society for Testing and Materials Annual Book of Standards, Section 5, p. 261-266.
14. Lai, W-C and Song, C., *Fuel Processing Technology*, **48**, 1(1996).
15. Song C., Eser S., Schobert, H. H., and Hatcher, P. G., *Energy & Fuels*, **7**, 234 (1993).
16. Lai, W-C and Song, C., *Catalysis Today*, **31**, 171(1996).
17. Siegel, S. and Smith, G. V., *J. Am. Chem. Soc.*, **82**, 6082 (1960).

18. Siegel, S., Thomas, P. A., and Holt, T. J., *J. Catal.*, **4**, 73 (1965).
19. *Zeolite Chemistry and Catalysis*, J. A. Rabo (ed.), 596, ACS (1976).
20. Lai, W.-C. and Song, C., *Fuel Processing Technology*, **48**, 1(1996).
21. Song, C., Eser, S., Schobert, H. H., and Hatcher, P. G., *Energy & Fuels*, **7** (2), 235 (1993).
22. Yu, J. and Eser, S., *Industrial & Engineering Chemistry Research*, **37**, (12), 4601 (1998).
23. Yu, J. and Eser, S., *Industrial & Engineering Chemistry Research*, **37** (12), 4591 (1998).
24. Song, C., Lai, W.-C., and Schobert, H. H., *Industrial & Engineering Chemistry Research*, **33** (3), 548 (1994).
25. Song, C., Lai, W.-C., and Schobert, H. H., *Industrial & Engineering Chemistry Research*, **33** (3), 534 (1994).
26. Lai, W.-C. and Song, C., *Catalysis Today*, **31**, 171 (1996).
27. Minachev, K. M. and Isakov, Y. I., *Zeolite Chemistry and Catalysis*, ed. by J. A. Rabo, *ACS Monograph* **171**, ACS, 552 (1976).
29. Rosesner, F. et al., *New Aspects of Spillover Effect in Catalysis* 77, ed. by T. Inui et al., Elsevier 1997, 151.







